Nanoparticle-Peptide Therapeutics to Treat and Prevent the Progression of Post Traumatic Osteoarthritis

By

MARCUS ADAM DELONEY
DISSERTATION

Submitted in partial satisfaction of the requirements for the degree of

DOCTOR OF PHILOSOPHY

in

Biomedical Engineering

in the

OFFICE OF GRADUATE STUDIES

of the

UNIVERSITY OF CALIFORNIA

DAVIS

Approved:

Alyssa Panitch, Chair

Blaine A. Christiansen

J. Kent Leach

Committee in Charge

2021

To my mother for fostering and cultivating my scientific mind

ACKNOWLEDGEMENTS

Nothing in my life has been a solitary effort, and that includes my doctoral studies. I would first like to thank my family for always encouraging and supporting me. To my mother, Monica Deloney, for nurturing my love of science and education, and my Aunt Kathy and Uncle Jim for showing me what's possible with hard work and dedication. To my siblings for always listening to me when I needed to talk. To my cousins who were always there for a laugh when I needed it the most. And lastly to my husband, Brandon Oselio, for keeping me sane and always uplifting me. This would not have been possible without all of your unfettered encouragement.

Thank you to my amazingly supportive advisor Prof. Alyssa Panitch for all she has helped me through over the years and allowing me to re-join her lab after leaving for a short stent. Her continued faith in me as a scientist gave me confidence when I had none of my own, and for that I will be forever grateful. I would also like to acknowledge and thank my co-advisor, committee, and academic mentors. Prof. Christiansen, your mentorship expanded my eyes into orthopedics and my enthusiasm to collaborate with physicians, especially within the operating room. Prof. Leach, thank you for challenging me and offering your insights as a fellow chemical turned biomedical engineer. Additionally, thank you to all of my mentors from the Clinical and Translation Science Center. There are entirely too many to list, but my sincerest thank you to all of you. The numerous courses, seminars, individual meetings gave me immeasurable constructive feedback to significantly improve my presentation skills as well as thought process as a scientist. Being one of your scholars is one of the highest honors and most memorable experiences I received during my studies.

To my mom, thank you the most. Raising me could not have been easy, let alone as a single mother. You have sacrificed more that I will ever know to get me to where I am today. You've always been the first person I turn to when something (good, bad, or otherwise) happens, and you've always been there for me. From changing jobs to ensure I went to a better school, to wearing maize & blue when we all know you bleed green (though, hopefully

not anymore). You've been my rock and I would not be where I am today without your love and encouragement.

Brandon, thank you for supporting and inspiring me. Seeing your passion for knowledge was and is motivating. You opened my eyes to the idea of graduate school and I doubt I would be where I am today without you. Your partnership is more than I could have ever asked for and look forward to our future together.

To my family and tribe of parents, there are way too many of you and I wouldn't have it any other way. First my sister, Erin, thank you for pushing me to be creative and inspire me to think outside the equation. You showed me that just because I'm an engineer does not give me license to use stock images nor comic sans. Your guidance significantly improved my scientific communication and lead me to a love of graphic design that will forever influence my personal and profession outlook. For my brother, Matt, thank you for being strong and head-fast. Showing me to stand my ground for what I know and when to admit I need help. It was a tough pill to swallow, but without learning that lesson I would have never made it through graduate school. For my second mothers: my aunts, you showed me the world outside of my own and opened my mind to accept different ideologies and thought patterns than my own. Kathleen and Marnie, you specifically fostered this in me from a young age. Inviting me to your families and treating me as your own son, giving me experiences I would not have otherwise received - thank you. And to my cousins, you're obnoxious, crude, invasive, and I love you all. Our daily chats got me through some of my darkest times and I know we have each other always.

Thank you to the biomedical engineering student association (BESA) and all of the BESA graduate students – graduate school would not have been the same without you. A special thank you to Christal Wintersmith for answer all of my silly questions and for always looking out for my personal well-being. Thank you to Dr. Vasilios Morikis, Dr. Jenna Foster, Dr. Oybek Kholiov, Rachel Mizenko, and Hanna Koster. I will forever remember our adventures outside of lab, and look forward to what comes next. Thank you to all past, present, and

future members of the Panitch and Christiansen Lab. Specifically Tima Dehghani, Alena Casella, Hark Sodhi, Michael Nyguen, Dr. Vanessa Dartora, Dr. Nelda Vázques Portalatín, Dr. Hailey Cunningham, Dr. Allison Hsia, Dr. Armaun Emani and Kristin Biris. You all made coming lab fun and I will miss working with you all.

I would like to thank the Designated Emphasis in Biotechnology and FUTURE program at UC Davis for all they taught me about networking and the professional world. Finally I would like to thank the Clinical Translational Science Center for their financial support as well as training and mentoring during my Ph.D.

This would not have been possible without the love, support, and encouragement of all of you. Thank you all.

TABLE OF CONTENTS

LIST OF FIGURES

Figure

LIST OF TABLES

Table

LIST OF ABBREVIATIONS

AAc Acrylic Acid

ACI Autologous Chondrocyte Implantation

ACL Anterior Cruciate Ligament

ACN Acetonitrile

AD Aggrecan Depleted

ADAMTS A Disintegrin and Metalloproteinase with Thrombospondin Motifs

AMPS 2-acrylamido-2-methyl-1-propanesulfonic acid

API Active Pharmaceutical Ingredient

BAC N, N′-bis (acryloyl) cystamine

CMGI Center for Molecular and Genomic Imaging

COX-2 Cyclooxygenase-2 Enzyme

CPP Cell-Penetrating Peptides

CrmA DNA-Cytokine response modifier A

CS Chondroitin Sulfate

DCM Dichloromethane

DDS Drug Delivery System

DIPEA N-Diisopropylethylamine

DLS Dynamic Light Scattering

DMEM Dulbecco's Modified Eagle Media

DMF Dimethylformamide

DMSO Dimethyl Sulfoxide

DTT Dithiothreitol

ECM Extracellular Matrix

ELISA Enzyme-Linked Immunosorbent Assay

EtOH Ethanol

FBS Fetal Bovine Serum

FDA Food and Drug Administration

FL Fluorescein o-Acrylate

FPLC Fast-Protein Liquid Chromatography

GAG Glycosaminoglycan

GAH GAHWQFNALTVRGSG HA-binding Peptide

GSH Glutathione

HA Hyaluronic Acid

HBSS Hank's Balanced Salt Solution

HepG2 Hepatocellular Carcinoma

hNP Hollow Nanoparticle

HPLC High-Performance Liquid Chromatography

IA Intra-Articular

IC Inorganic Cores

IGD Interglobular Domain

IL-1β Interleuken-1 Beta

IL-6 Interleuken-6

IVIS In Vivo Image System

KAFAK KAFAKLAARLYRKALARQLGVAA MK2i Peptide

KPS Potassium Persulfate

KS Keratin Sulfate

LCST Lower Critical Solution Temperature

LDD Localized Drug Delivery

MBA N, N′-methylene-bis-diacrylaminde

MACI Matrix-Induced ACI

MALDI-TOF Matrix Assisted Laser Desorption/Ionization - Time of Flight

MAPKAP2 Mitogen Activated Protein Kinase Activated Protein Kinase 2

MK2 MAPKAP2

MK2i MK2 inhibitor

MMP Matrix Metalloprotease

NaOH Sodium Hydroxide

NIACLR Non-Invasive ACL Rupture

NIPAm N-Isopropylacrylamide

NP Nanoparticle

NSAID Non-Steroidal Anti-Inflammatory Drug

pd-NP Pre-Dialysis Nanoparticle

pNIPAm Poly(N-Isopropylacrylamide)

PC Polymer Cores

PDI Polydispersity Index

PEG PLGA-poly(ethylene glycol)

PLGA poly(lactic-co-glycolic acid)

PNP Polymeric Nanoparticle

PRP Platelet-Rich Plasma

PTOA Post Traumatic Osteoarthritis

OA Osteoarthritis

RBITC Rhodamine B Isothiocyanate

ROS Reactive Oxidative Species

SDD Systemic Drug Delivery

SDS Sodium Dodecyl Sulfate

sNP Solid Nanoparticle

TEM Transmission Electron Microscopy

TFA Trifluoroacetic Acid

TFF Transverse Flow Filtration

THF Tetrahydrofuran

TIPS Triisopropylsilane

TNF-α Tumor Necrosis Factor-Alpha

tNP Thermoresponsive NP

TRE Total Radiance Emission

UCST Upper Critical Solution Temperature

YARA YARAAARQARAKALARQLGVAA MK2i Peptide

ABSTRACT

Nanoparticle-Peptide Therapeutics to Treat and Prevent the Progression of Post Traumatic Osteoarthritis

by

Marcus Adam Deloney

Chair: Alyssa Panitch

Post traumatic osteoarthritis (PTOA) is the result of a joint trauma or injury and accounts for 12.5% of all OA cases. Following joint trauma, inflammatory cytokines are produced and stimulate the secretion of catabolic enzymes that degrade articular cartilage. The degraded articular cartilage further stimulates catabolic enzyme and inflammatory cytokine expression. These lead to the development of the inflammatory cycle associated with PTOA. We hypothesized that inhibiting inflammation and treating the damaged cartilage may prevent the progression of PTOA and restore functionality to osteoarthritic cartilage using nanoparticle-peptide therapeutics.

The first study developed polymeric core-shell nanoparticles composed of N-isopropyl acrylamide (NIPAm), N, N′-bis (acryloyl) cystamine (BAC), 2-acrylamido-2-methyl-1-propane sulfonic acid (AMPS), and acrylic acid (AAc) (poly(NIPAm-co-AMPS-BAC-AAc)) by exploiting the thermoresponsive behavior of NIPAm. NIPAm has a lower critical solution temperature (LCST) of 32°C. Below the LCST, NIPAm is hydrophilic and causes the particle to swell, and above the LCST is hydrophobic and causes the particle to constrict. Poly(NIPAm-co-AMPS-BAC-AAc) shells were crosslinked around the hydrophobically stabilized non-crosslinked poly(NIPAm) (pNIPAm) cores above the LCST of NIPAm. Removal of the cores via diffusion resulted in thermoresponsive, degradable nanoparticles with low density, termed hollow, cores. The hollow nanoparticles (hNPs) encapsulated more of

the anti-inflammatory MK2 inhibiting (MK2i) peptide than solid nanoparticles, and loaded roughly 2.5 times more MK2i below the LCST of NIPAm than above it. These hNPs loaded with MK2i inhibited IL-6 production in stimulated bovine chondrocytes *in vitro*. The hNPs were also retained within the joint space of rats for 7 days. These results show the ability of MK2i loaded hNPs to inhibit inflammation and show that the drug-loaded hNPS have potential as a therapeutic to treat PTOA.

We also showed the ability of hNPs to be conjugated with the hyaluronic acid (HA) binding peptide GAHWQFNALTVRGSG (GAH). AAc served as the carboxylate anchor within the shell of the hNP and allowed for GAH conjugation. hNPs conjugated with roughly 19 GAH, termed 19 GAH-hNP, bound to HA in solution and resulted in a 94.0% increase in dynamic viscosity compared to the HA solution treated with unconjugated hNPs. Bovine cartilage explants were treated with trypsin to remove aggrecan and served as an *ex vivo* model for OA. The aggrecan-depleted (AD) explants treated with 0.10 mg of unconjugated hNPs had a muted effect on restoring compressive strength and suppression of CS release, likely due to reduced HA interactions. While the AD explants treated with 0.10 mg of 19 GAH-hNP restored the compressive strength to healthy levels 6 days after a single treatment and inhibited degradation of the ECM of cartilage. Based on these results, treatment with 19 GAH-hNP may be able to prevent the development of PTOA.

Finally, the MK2i loaded hNP (hNP+MK2i) and hNPs were tested in a small animal *in vivo* study. Previous research developed a physiologically relevant non-invasive ACL rupture (NIACLR) model using a tibial compression to tear the ACL. We attempted to utilize this model to test the efficacy of our hNP+MK2i therapeutic to inhibit the progression of PTOA *in vivo*. However, only 9 of the 28 rats that underwent tibial compression resulted in a complete ACL tear, and we were not able to quantify the efficacy of our hNP+MK2i therapeutic.

These data presented here suggests the use of nanoparticle-peptide therapeutics may be a translatable platform to inhibit the progression of PTOA.

CHAPTER I

Introduction

1.1 Background & Significance

Osteoarthritis (OA) is a growing and impactful disease that currently afflicts 1 out of every 10 persons in the United States, and is projected to increase to 1 out of 3 by the year 2030[1]. Post traumatic osteoarthritis (PTOA) specifically accounts for 12.5% of all OA cases and is expected to increase with the increasing aging population[1]. Patients suffering from OA experience loss of mobility, joint swelling, and pain — all affecting the patient's quality of life. Within the U.S., OA currently costs $185 billion annually[2], and is projected to increase over the next decade[3].

OA is characterized by inflammation of the joint and degradation of articular cartilage. Cartilage is a unique tissue composed of a single cell type, chondrocytes, and is aneural, avascular, and alymphatic with extremely low cell density[4]. Since there are no nerves within cartilage, the patient is typically unaware of its damage until there is significant bone remodeling, increased intraosseous pressure, microfractures, meniscal injury, and/or synovitis[5]. Damaged cartilage is slow to heal, if it heals at all, due to it having no blood supply and low cell density[4]. Due to the unique composition of articular cartilage and limited to no capacity to regenerate on its own, it is imperative to protect as much of the native cartilage as possible to maintain functionality. Within this body of work we use nanoparticle-peptide therapeutics to prevent the inflammation and degradation of articular cartilage that is associated with PTOA.

1.2 Articular Cartilage Structure & Function

Articular cartilage is a smooth, white tissue that covers the ends of bones where they come together to form joints and allows for the relative movement of the opposing joint surfaces with minimal wear and tear[6]. It distributes the joint load over a wide area, and decreases the stresses sustained by contacting joining surfaces and minimizing peak stresses felt by the bones[7]. The composition of extracellular matrix (ECM) of articular cartilage is: collagen (15-22% wet weight), proteoglycans (4-7% wet weight), water (60-85%), and electrolytes[6]. Notably, chondrocytes account for only 5% of the wet weight of articular cartilage; however, they are responsible for the maintenance and stability of its ECM[8,9] Figure 1.1. Collagen forms interweaving fibrils within articular cartilage and provides tensile strength by crosslinking and stabilizing the matrix[10]. The most common proteoglycan is aggrecan which is composed of a core protein with covalently bound glycosaminoglycans (GAGs) chains branched off of it. The GAG chains, comprised of chondroitin sulfate (CS) and keratin sulfate (KS), give aggrecan an anionic charge which creates an osmotic gradient within articular cartilage that allows for water retention and provides the tissue with its compressive strength[11]. The interactions between collagen and proteoglycans control the biology and provide the mechanical properties of articular cartilage[10–12].

1.2.1 Collagen

Collagen type II accounts for roughly 95% of the collagen within cartilage, the balance being collagen type: XI (3%), VI (0-1%), IX (1%), X(1%)[10]. Collagen type II is composed of three alpha-1 (II) helical polypeptide fibrils which give articular cartilage tensile strength, accounting for 45 - 70% of the dry weight of cartilage, and has a high degree of structural organization[6]. Collagen type VI, while less than 1% of collagen found, is responsible for anchoring chondrocytes to the ECM[13]. Moreover, collagen type VI is believed to transmit mechanical and osmotic signals from the ECM to chondrocytes[14]. Collagens type IX and XI allow for specific covalent bonds to form the fibrillar matrix, and collagen type X is

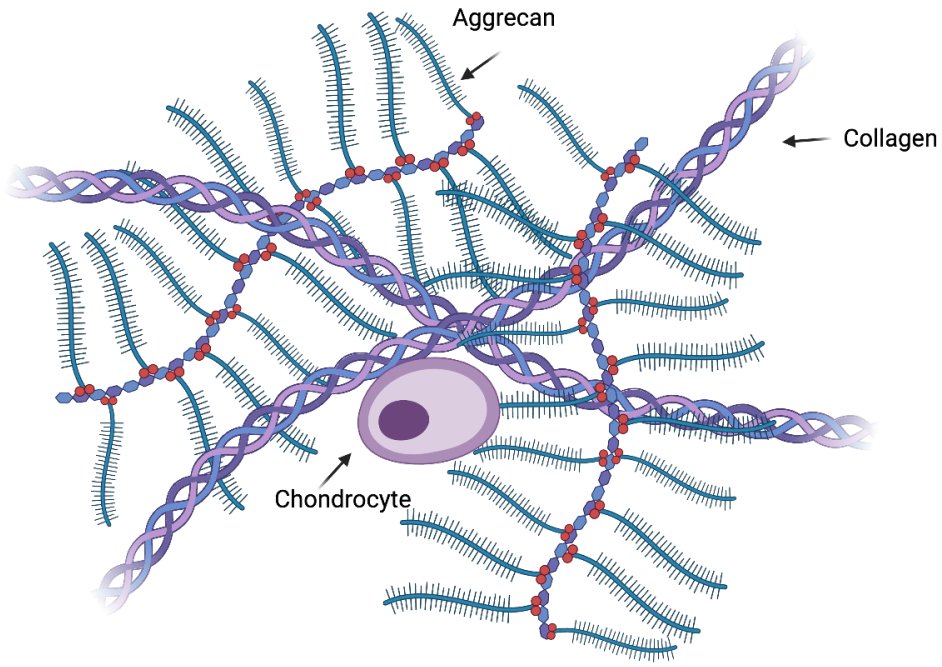

Figure 1.1: Animation of the extracellular matrix of articular cartilage with aggrecan, chondrocytes, and collagen. Image created with Biorender.com

found near the growth plates and believed to be responsible for ossification[10,15]. The tensile strength of cartilage is afforded by the crosslinks between the alpha chains of the various collagen monomers within the ECM[6].

1.2.2 Proteoglycans

Aggrecan is the most abundant proteoglycan within articular cartilage and is composed of three modular domains: G1, G2, and G3. The G1 domain of aggrecan consists of three regions: A, B, and B′, with the A region being responsible for interaction with the link protein[8,9,11,16,17]. The G1 and G2 domain of aggrecan are separated by an interglobular domain (IGD) which is susceptible to proteolytic cleavage by several known proteases, including

matrix metalloproteases (MMPs) and aggrecanses[18]. The G2 domain of aggrecan has two regions: B and B′ and is followed by the glycosaminoglycan (GAG) domain composed of the keratin sulfate (KS) and chondroitin sulfate (CS) regions[11,17]. The GAG domain begins with the KS region followed by the CS region, with roughly 60 KS and 100 CS per aggrecan that together provide aggrecan with its anionic charge[17]. The GAG domain is followed by the G3 domain and the C-terminus of aggrecan. The G3 is believed to be responsible for modulating aggrecan production and its secretion from chondrocytes[11,17,19]. Aggrecan binds to hyaluronic acid (HA) through the link protein, with the A domain of the link protein interacting with the A domain within G1 region of aggrecan, and the B and B′ domain of the link protein interacting with HA[20,21]. Multiple aggrecan molecules are bound to a single central hyaluronic acid filament via the link protein and their collective negative charge attracts counter sodium ions that generate an osmotic imbalance[17]. This osmotic imbalance draws water into the ECM, allowing it to swell and expand, and affords cartilage compressive strength[9,11,17]. The interaction of aggrecan with HA via the link protein allows for its aggregation and anchors it within the cartilage matrix[11,16,17]. Collagen provides cartilage with stiffness, and thus limits the over expansion due to aggrecan-induced swelling[10,22]. The interplay between the proteoglycans and collagen are crucial for healthy cartilage.

1.2.3 Synovial Fluid and Surrounding Tissue

The synovial cavity is filled with synovial fluid and the synovium. The synovial fluid (SF) acts as a biological lubricant and medium through which nourishment and cytokines diffuse through to the cartilage. The SF contains HA and other biomacromolecules, such as lubricin and superficial zone protein, that provide low friction and low ware properties[23]. The SF maintains the homeostasis of the joint and disruption of the synovial membrane leads to joint inflammation[24]. Furthermore, the infrapatellar fat pad (IFP) is adipose tissue near the synovium. The IFP helps in stabilizing the patella during by filling the gaps between joint tissues[24]. Disruption to the IFP and/ or SF have been shown to cause inflammation and

have a high likelihood of progressing to OA[23,24].

1.3 Osteoarthritis & Post Traumatic Osteoarthritis

Osteoarthritis (OA) is the most common degenerative joint disease characterized by inflammation of the joint and degradation of ECM molecules of articular cartilage[4,25,26]. The breakdown of the ECM leads to lesions on the surface of the articular cartilage and progressing to subchondral bone Figure 1.2. This causes the breakdown of the cartilage itself, and results in pain and loss of mobility[4,25,26]. Risk factors such as: trauma, sex, obesity, age, overuse, genetics, and anatomic factors, are believed to contribute to the likelihood of a person developing OA[26]. Post traumatic osteoarthritis (PTOA) is OA that is the result of a joint trauma or injury that substantially disrupts the joint, such as dislocation and/ or tears in the meniscus, anterior, or posterior cruciate ligaments[1,4]. Within this body of work, we specifically examine PTOA, which accounts for 12.5% of all reported cases of OA[1] due to its distinct genesis point and well developed small animal models[27–29].

1.3.1 Pathology of Post Traumatic Osteoarthritis

Following injury to articular cartilage, inflammatory cytokines, such as interleukin-1-beta (IL-1β), interleukin-6 (IL-6), and transcription necrosis factor-alpha (TNF-α), are expressed by chondrocytes and stimulate the secretion of catabolic enzymes that in turn degrade the ECM components of cartilage[4,30]. Aggrecan is degraded in the early stages of OA by aggrecanases, which are members of the ADAMTS (a disintegrin and metalloproteinase with thrombospondin motifs) family[11,31,32]. The most prominent aggrecanases are ADAMTS-4 and -5, commonly called aggrecanase 1 and aggrecanase 2, respectively[11,31,32]. Aggrecan is cleaved within its interglobular domain (IGD), and its degradation exposes HA to degradation by hyaluronidases[33]. The degraded articular cartilage fragments further upregulate cytokine and metalloprotease (MMP) activity[30,34]. Collagen is believed to be degraded in late stage OA and is irreversibly cleaved by collagenases, such as MMP-1, -8, and -13[34–37].

MMP-13 is the predominate collagenase expressed by chondrocytes during the progression of OA and has a high affinity for collagen type II[34–38]. Synovial macrophages phagocytose degraded cartilage fragments. This causes the release of TNF-α, IL-6, and IL-1β, which further stimulate catabolic enzyme production and perpetuate osteoarthritis[4,39,40].

1.3.2 Current Treatments for PTOA & OA

Currently no FDA approved therapeutic exists to treat and prevent OA. There are, however, several surgical and non-surgical options to treat the effects of OA, depending on the disease severity. Non-surgical methods that do not disrupt the joint capsule, such as lifestyle adaptations, exercise, and physical therapy[41], are preferred since any disturbance to the joint capsule may initiate inflammation and increase the chance of developing PTOA[42,43]. Non-surgical pharmaceutical options to treat OA are divided into supplements and injections. Common supplements to treat OA include: non-steroidal anti-inflammatory drugs (NSAIDs), painkillers (primarily opioids), and topical creams; and common injections include: corticosteroids, viscosupplements, platelet-rich plasma (PRP), and glucosteroids[44,45]. Overuse of NSAIDs are linked to increased cardovascular[46], kidneys[47], and gastrointestinal tract complications[44,48,49]. Opioids, as well as topical creams, only address the pain associated with trauma and not the underlying causes of inflammation, and opioids are linked to severe cases of addiction[44,50]. Intra-articular injections of corticosteroids and glucosteroids address localized inflammation, but result in chondrocyte death[50]. Viscosupplements, commonly used once the patient complains of pain, aim to increase mobility and reduce discomfort. However, viscosupplements only delay surgical intervention and have conflicting evidence of efficacy[44,51]. PRP contain growth factors that promote cartilage health and regeneration. However, their effectiveness is under debate amongst the medical community due to limited availability and a lack of data on their effectivness[44,52]. While intra-articular injections disrupt the joint capsule, they allow for localized delivery directly into the joint. The current therapies to treat OA focus on symptoms and inflammation, while not treating the dam-

age to articular cartilage. Addressing the damage to articular cartilage itself and inhibiting further inflammation is key to creating a therapeutic to prevent the progression of OA.

Current surgical measures to repair osteoarthritic joints include: osteotomy, mosaicplasty, microfracture, autologous chondrocyte implantations (ACI), matrix-induced autologous chondrocyte implantation (MACI), and total knee replacement[53]. These surgical techniques disrupt the joint capsule, cause inflammation, and increased chances of developing PTOA[42,43]. While surgical intervention relieves patient pain, it does not protect cartilage from further degeneration. There is a necessity for a therapeutic to address joint damage without significantly stimulating inflammation.

1.3.3 Drug Delivery Systems

Drug delivery of active pharmaceutical ingredients (APIs) are split into two categories: systemic and localized. Systemic drug delivery (SDD) allows for therapeutic circulation throughout the entire body and is convenient as well as widely accepted by patients[54,55]. However, SDD requires more frequent dosing to maintain therapeutic concentrations *in vivo* and continual systemic exposure increases the chances of off-target side effects[56]. This has increased the interest in treatments utilizing localized drug delivery (LDD). LDD can increase drug concentrations within the desired tissue, while reducing the systemic concentration and overall amount of drug required which decreases the likelihood of off-target side effects[57]. Moreover, LDD limits the metabolism of the API by the liver and kidney and allows for a relative increase in the drug's half-life compared to SDD[57]. However, many APIs administered via SDD and LDD suffer from poor stability, low solubility, and rapid clearance within the body[58]. Nanoparticles are used to overcome these limitations by increasing the solubility and stability of APIs, and allow for their controlled release *in vivo*[59].

Nanoparticles used as a drug delivery system (DDS) aim to regulate particle size, surface characteristics, and the release of API to elicit a site specific therapeutic response with tailorable release profile[60]. Lipid, inorganic, and polymeric nanoparticles have been engi-

neered for optimized API administration to overcome conventional delivery limitations, such as biodistribution and intracellular trafficking[61]. The benefits and current areas of improvement for each are listed in Table 1.1.

The application of the nanoparticle significantly impacts the base material used. Lipid nanoparticles (LNPs) are the most common FDA-approved NPs[59,62]. The most well-known LNP is the SARS-CoV-2 mRNA vaccine given emergency use authorization by the FDA[63]. LNPs offer numerous advantages including easy formulation, self-assembly, biocompatibility, high bioavailability, and tunable physiochemical properties[64]. LNPs are near neutral at physiological pH, making them an ideal platform for nucleic acid encapsulation and delivery[65,66]. However, LNPs have low encapsulation efficiencies and biodistribution that leads to high uptake within the liver and spleen[64,67].

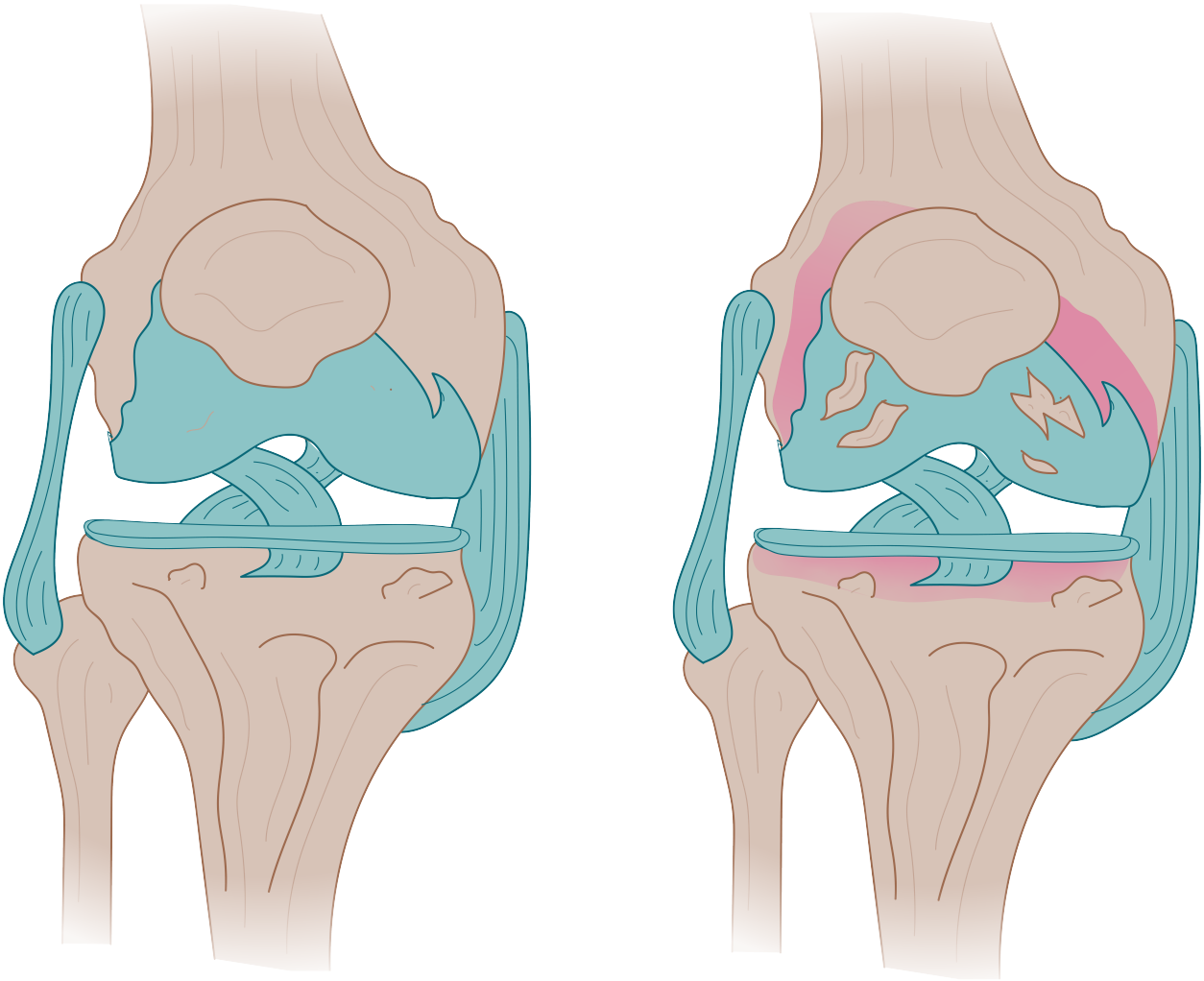

Figure 1.2: Animation of healthy vs osteoarthritic knee. Damage to the surface of the articular cartilage progresses to the subchondral bone. Image created with Biorender.com

Table 1.1: Summary of NPs used for drug delivery applications

Type of Nanoparticle	Advantage	Applications	Current Limitations
Lipid NPs	Easy formulation, self-assembly, biocompatibility, high bioavailability, and tunable physiochemical properties[64]; Neutral pH is ideal for nucleic acid encapsulation and delivery[65,66]	Nucleic acids for vaccines[63,64,67]; small molecule anti-cancer; anti-fungal, macular degeneration drugs[59,62,68]	Low encapsulation efficacy[64]; low biodistribution[67]; distribution requires extremely cold storage[63]
Inorganic - Gold NPs	Controlled size, structure, and geometry[61,69,70]	Antibodies for cancer treatment[71,72]; peptides for antisense gene regulation[73,74]; nucleic acids for cancer cell treatment[75,76]	Low bioavailability, low non-immunogenicity[59,61,69,77]; Not widely researched for clinical translation[78]
Inorganic - Iron Oxide NPs	Highly tunable with magnetic core and allows for easy surface modification with biocompatible coatings and API conjugation[79–81]	Anti-HER2 antibodies[81]; and small molecule anti-cancer drugs[79,80]	Toxic degradation products[69,81]; Clinical application not well researched[78]
Inorganic - Silica-based NPs	Tunable pore size, high drug loading, controlled release, increased solubility of API[82–85]	Small molecule anti-cancer drugs[86–89]; antibiotics[90,91]; cancer cell inhibiting peptides[92,93]; nucleic acids for gene editing to treat genetic disorders and cancer[94–96]	Silanol groups on the surface are toxic[97]; causes an increase reactive oxygen species[97,98]; Clinical application not well researched[78]
Natural Polymer NPs	High degree of biocompatibility, non-immunogenic, low toxicity, solvent free, and tunable degradation rates[99–103]	Enzymes to treat ulcerative colitis[104,105]; antibodies[106]; anti-angiogenesis peptides for cancer treatment[107]; nucleic acids to inhibit Cox-2[108]	High degree of variability, structurally complex, costly extraction process[109,110]
Synthetic Polymer NPs	Highly modifiable, biodegradable, easily surface modified[100]; provide controlled release to the desired site and stabilize API[100,109]	Small molecule anti-cancer drugs[111,112]; nucleic acids for breast[113] and ovarian[114] cancer treatment; peptides to treat colorectal cancer[115] osteoarthritis[116–118];	Complicated synthesis method[119,120]; lack of research into clinical application[78]

Gold, iron oxide, and silicon-based are the most commonly researched inorganic NP due of their unique electrical, magnetic, and optical properties and their controllable size, structure, and geometry[61,70]. Gold and iron oxide NPs are primarily used for diagnostics and imaging[61], as well as used for the delivery of anti-cancer drugs[79,80]. Silica-based NPs (SNP) are used to load small molecule cancer drugs[86–89], antibiotic[90,91] and cancer cell inhibition peptides[84,92,93], and nucleic acids for gene editing to treat genetic disorders and cancers[94–96]. Inorganic NPs are a versatile approach for intracellular delivery of small and macromolecule therapeutics that are also tunable to the disease and tissue of interest. Current research aims to translate the use of inorganic NPs into clinical application which is currently overlooked in fundamental research[78].

Polymeric nanoparticles (PNPs) are able to be synthesized from natural or synthetic materials that allow for precise control over particle characteristics with tunable properties for hydrophobic or hydrophilic drug loading and offer easy platforms for surface modifications[61]. Natural PNPs are advantageous due to their high degree of biocompatibility, non-immunogenicity, and low toxicity, and have tunable degradation rates for the controlled release of APIs[99–103]. Natural PNPs are used to deliver enzymes to treat ulcerative colitis[104,105], antibodies for immunization[106], and anti-angiogenesis peptides into tumors[107]. Natural PNPs, however, have a high degree of variability and their extraction process is complicated and costly[109]. Synthetic PNPs are polymerized from monomers with distinct attributes to facilitate biocompatibility, drug loading, release, degradation, and retention time[100,109]. Current research into synthetic PNPs aims to reduce the use of organic solvents and complex synthesis, as well as generate particles with biocompatible degradation products[120].

Here, we specifically focus on nanoparticles for the treatment of OA, with an emphasis on studies utilizing intra-articular injections. Nanoparticles composed of lipids[121–124], metals[125–130], and polymers[116–118,131,132] are the most common nanotherapeutics used to treat OA[133–135]. Lipid-based NPs to treat OA are used to load small molecule drugs, such as

dexamethasone[123], methotrexate[136], and celecoxib[124], and increase retention time within the joint as well as inhibit inflammation to prevent the progression of OA[121,122]. While showing promising results, lipid-based NPs have low encapsulation efficiencies[137] and do not have sufficient mechanical resistance to the high pressures within joints[138]. Notably, there is one commercially available liposome-corticosteroid product to treat OA approved in Germany, Lipotalon®, which offers the sustained release of the corticosteroid dexamethasone[139]. Metallic NPs are used for OA diagnostics[127–129], imaging of the joint[128], and to counteract reactive oxidative species (ROS) produced within the joint[126,130]. Synthetic poly(lactic-co-glycolic acid) (PLGA) PNPs were used to encapsulate p66shc siRNA and p47phox siRNA, and were intra-articularly injected into the joint of OA-induced rats and inhibited inflammatory cytokine and ROS production[140,141]. Other studies used PLGA-poly(ethylene glycol) (PEG)-PLGA triblock copolymeric NPs to encapsulate etorixcoxib to inhibit the production of the inflammatory enzymes cyclooxygenase-2 (COX-2) and MMP-13 within OA-induced rat joint[142,143].

Zhou et al used a chitosan PNP to encapsulate a plasmid DNA-Cytokine response modifier A (CrmA) and inhibited IL-1β, which slowed cartilage destruction in surgically induced OA[108,133,144]. PNPs are able to load small molecule to macromolecule drugs and protect them from proteolytic degradation, and have tailorable degradation rates as well as increased joint retention time[145,146]. Intra-articular injection of therapeutics using PNPs allows for direct drug delivery into the joint, high therapeutic concentration with low drug dosage, minimized chances for off-target side effects, and increased bioavailability compared to systemic delivery[147,148]. This body of work focuses exclusively on the use of PNPs functionalized and/ or encapsulated with therapeutic peptides to prevent the progression of OA.

Thermoresponsive NPs (tNPs) are the most researched stimuli-responsive drug delivery systems[149]. tNPs are composed of either lipids or polymeric NPs. The thermoresponsive behavior of lipid-based NPs results from phase transitions between the lipid bilayers[150]. Lipid-based tNPs retained anti-cancer drugs at 37°C, were injected into a tumor where they were

heated to 39°C and subsequently released 90% of their payload[151]. However, lipid-based tNPs have low drug loading efficiency[152] and unpredictable drug release[153]. Some polymeric tNPs are composed of monomers that exhibit a lower critical solution temperature (LCST) or an upper critical solution temperature (UCST), while others melt at increased temperature[149]. The LCST allows the particles to miscible at all temperatures below the transition temperature, and the UCST allows the particles to be miscible above the transition temperature. tNPs with a LCST are primarily used in nanomedicine since most particles with an UCST that are biocompatible have transition temperatures outside of a physiologically relevant range[154]. The most common thermoresponsive polymers are poly(N-isopropyl acrylamide) (pNIPAm)[155,156], poly(N,N-diethylacrylamide)[157] (pDEAAm), poly(N-vinlycaprolactam)[158] (pVCL), poly(g-2-[2-(2-methoxyethoxy)ethoxy]ethoxy-3-caprolactone)[159] (pMOEEC), and poly[2-(dimethyl amino) ethyl methacrylate][160] (pDMAEMA). Of the thermoresponsive monomers, pNIPAm is the most researched due to its sharp LCST being closest to physiological temperatures at 32°C[149,161], pDEAAm has a LCST range of 25° to 32°C[157]; pVCL has a LCST between 25° to 35°C[158]; pMOEEC has a LCST of 47.5°C[159]; and pDMAEMA has a LCST around 50°C[160]. The LCST of pNIPAm allows the particles to load drugs in its swollen state, and release the drugs at physiological temperatures, and are the most used thermoresponsive polymeric NP used in biomedical applications[149]. Here we utilized pNIPAm-based nanoparticles in tandem with two therapeutic peptides to inhibit the progression of PTOA.

1.3.4 Therapeutic Peptides

Therapeutic peptides were discovered in the 1920s and since then over 60 peptide based drugs have been approved in the United States, Europe, and Japan[162]. Peptides are molecularly situated between small molecules and proteins, while being biochemically and therapeutically distinct[162]. Peptides are advantageous as therapeutics due to their high biological activity, specificity, and low toxicity[163]. However, using peptides as APIs has its challenges, as peptides are susceptible to enzymatic breakdown and low stability[163–165]. Conjugating

peptides to various moieties has shown to extend their half-life and improve solubility, and localized injection of peptide-based therapeutics has shown to reduce the frequency of treatment and improve stability[162,166]. Current research uses NPs to encapsulate peptides for their controlled release[116–118,167], and peptides conjugated to the surface of nanoparticles are used for imaging and detection[168,169], as well as cancer[170,171] and multiple sclerosis[172] treatment. Here, we used two therapeutic peptides: an anti-inflammatory MK2 inhibiting peptide and a hyaluronic acid binding peptide to inhibit the progression of OA.

1.3.5 Therapeutic Peptides to Treat Post Traumatic Osteoarthritis

Proteoglycan loss from articular cartilage happens early in OA and is considered reversible if caught early enough, whereas the breakdown of the collagen network is considered irreversible[173,174]. However, since cartilage is aneural, most patients do not feel the degradation within their joints until the damage has progressed too far and the collagen network has begun to breakdown[30]. PTOA presents a unique opportunity for early stage treatment as it is most common in younger, active, and military persons where the patient is acutely aware of the joint trauma[28,175]. Intra-articular injections are the preferred route of administration to locally treat PTOA. However, the currently used therapies have less than a 24 hour half-life within the joint[175]. Polymeric NPs are means to increase retention time within the joint and inhibit the progression of PTOA[175].

Within cells, MK2 (mitogen activated protein kinase activated protein kinase 2) is part of the p38 pathway, acts downstream of the p38 MAPK, and is responsible for stabilization of transcription factors for pro-inflammatory cytokines, i.e. IL-6, TNF-α[176–178]. The anti-inflammatory peptide KKKALNRQLGVAA (KKKAL) was originally identified by Hayess and Benndorf as a substrate inhibitor of MK2, and termed a MK2 inhibitor (MK2i) peptide[179]. The permeability of the MK2i peptide KALNRQLGVAA (KAL) into cells was improved by the addition of the cell-penetrating peptide (CPP) sequence WLRRIKAWLRRI (WLR) to its N-terminus domain, and reduced the phosphorylation of HSP27 *in vitro*[180].

Three other CPP domains were added to the N-terminus of the MK2 inhibiting KAL sequence: YARAAARQARA (YAR), KAFAKLAARLYR (KAF), and FAKLAARLYR (FAK). These were compared to the WLR-KAL (WLRRI) MK2i variant[181,182]. Of the four CPP-MK2i peptide sequences, YAR-KAL (YARA) was the most specific MK2 inhibitor, with KAK-KAL (KAFAK) and FAK-KAL (FAKLA) having similar MK2 inhibition, and WLRRI being the least specific to MK2[181]. YARA was the least toxic CPP-MK2i variant with a maximum non-lethal concentration of over 3000 μM, KAFAK and FAKLA had lower maximum non-lethal concentrations of 230 and 300 μM, respectively, and WLRRI the lowest at less than 40 μM[181,182]. However, the free-peptides are susceptible to proteolytic degradation and short residence times[183]. Encapsulating the MK2i peptide within polymeric nanoparticles and local delivery to the treatment area offers a solution to this problem.

Previously, our lab encapsulated the KAFAK CPP-MK2i variant within pNIPAM based nanoparticles and inhibited inflammation 48 hours after treatment[117,118], showing the promise of nanoparticles to increase the efficacy of peptides. Subsequent studies resulted in the development of hollow core-shell pNIAPm based nanoparticles after removal of a degradable, crosslinked core from a non-degradable crosslinked shell[116]. The hollow NPs (hNPs) allowed for increased KAFAK loading and release compared to their solid counterparts[116]. The non-degradable pNIPAm hNPs offered twice as much MK2i loading and 5 times greater KAFAK release than solid counter parts and significantly decreased IL-6 expression *ex vivo*[116]. The YARA, FAKLA, and WLRRI variants were not reported to be encapsulated by PNPs[116–118], presumably due to the YARA and FAKLA having a lower net charge at neutral pH making them more difficult to load, and WLRRI was likely not used since it's less specific to MK2 and more toxic than KAFAK[181,182]. Delivery of the more specific YARA using PNPs would be less toxic and has the potential to have fewer off-target side effects. Further building upon these studies, we aimed to synthesize a degradable hNP capable of loading and releasing YARA to inhibit inflammation locally within the joint to treat the progression of OA.

Inflammation is one facet to the progression of OA, another being the degradation of the ECM of articular cartilage. As stated above, aggrecan is a primary component of cartilage and protects it from degradation[11]. To address the loss of aggrecan associated with OA, our lab has previously developed an aggrecan mimetic comprised of the anionic glycosaminoglycan (GAG) chondroitin sulfate (CS) conjugated with the HA-binding peptide GAHWQFNALTVRGSG (GAH)[184]. The CS-GAH aggrecan mimetic was able to bind to HA, restore the compressive strength of aggrecan-depleted cartilage, and inhibit the further release of CS from *ex vivo* cartilage plugs — functionally mimicking aggrecan[184–187]. Other studies used GAH conjugated to heterobifunctional PEG chains with a collagen binding peptide and was able to slow the degradation of cartilage following joint trauma[188]. The anionic charge of the CS polymer within the CS-GAH therapeutic is believed to be responsible for the restoration of compressive strength[187]. Additionally, the binding to low molecular weight (LMW) HA using the HA-PEG therapeutic is believed to inhibit LMW HA binding to pro-inflammatory receptors and slow cartilage degradation[188]. Functionalizing GAH to the surface of negatively charged hNP may mimic the same protective effect of anionic GAGs in restoring the compressive strength of articular cartilage and slowing its degradation, while also having the added ability to load the MK2i peptide, which inhibits inflammation.

1.4 Thesis Outline & Contributions

In order to inhibit inflammation and restore functionality of osteoarthritic cartilage, this dissertation is divided into three aims: 1) developing and synthesizing degradable, thermoresponsive, hollow nanoparticles (hNP) to encapsulate and release YARA, the anti-inflammatory MK2i peptide; 2) conjugating the HA-binding peptide GAH to the surface of hNPs to prevent the degradation of the ECM of cartilage and restore its compressive strength; and 3) analyzing the efficacy of the nanoparticle-peptide therapeutic to prevent the progression of PTOA in a small animal pilot study.

Chapter 2 details the development and characterization of degradable, thermoresponsive

hNPs and the effect of crosslink density on ability of the particle to load and release YARA. Moreover, Chapter 2 illustrates the benefit of loading the thermoresponsive nanoparticle below the LCST of NIPAm, when the particle is swollen, compared to when the particle is in its constricted state, above the LCST of NIPAm. The chapter consists of a manuscript by Marcus Deloney, Kyra Smart, Prof. Blaine A. Christiansen, and Prof. Alyssa Panitch, published in the Journal of Controlled Release, Volume 323, Issue July 10th, 2020.

Chapter 3 describes the methodology and use of the HA-binding peptide GAH conjugated to the surface of the degradable hNP (GAH-hNP) to restore the compressive strength to aggrecan-depleted cartilage. Additionally, Chapter 3 details the chemistries used for peptide conjugation and effect of increased peptide concentration to the hNP with respect to polydispersity, size, and biological effect. The histology and immunohistochemistry staining were completed by UC Davis VMTH Anatomic Pathology Service - Histopathology Lab, *in vivo* images were completed by the UC Davis Center for Molecular and Genomic Imaging (CMGI), Parssa Garoosi aided in peptide synthesis and purification, Dr. Vanessa Dartora helped with some tissue sectioning, and Prof. Blaine A. Christiansen aided in the design of the retention study. All other experiments were designed, performed, and analyzed by myself with significant contribution from Prof. Alyssa Panitch.

Chapter 4 begins with combining the MK2i anti-inflammatory peptide within the GAH-conjugated hNPs and its drug release kinetics. Also, within Chapter 4 are the results of the *in vivo* small animal study of rats who underwent non-invasive ACL rupture to induce PTOA and injected with hNP or hNP loaded with MK2i. This study with the result of collaboration with Prof. Blaine A. Christiansen, Kristen Biris, and Dr. Hailey Cunningham with experimental design and controls planned by Prof. Alyssa Panitch, Prof. Blaine A. Christiansen, and myself.

Chapter 5 summarizes the collection of data as a whole and outlines potential future applications of these technologies.

References

1. Brown, T. D., Johnston, R. C., Saltzman, C. L., Marsh, J. L. & Buckwalter, J. A. Posttraumatic osteoarthritis: a first estimate of incidence, prevalence, and burden of disease. *Journal of orthopaedic trauma* **20,** 739–744 (2006).

2. Kotlarz, H., Gunnarsson, C. L., Fang, H. & Rizzo, J. A. Insurer and out-of-pocket costs of osteoarthritis in the US: Evidence from national survey data. *Arthritis & Rheumatism: Official Journal of the American College of Rheumatology* **60,** 3546–3553 (2009).

3. Desa, U. United Nations, Department of Economic and Social Affairs, Population Division. *World Population Prospects* (2019).

4. He, Y. *et al.* Pathogenesis of osteoarthritis: risk factors, regulatory pathways in chondrocytes, and experimental models. *Biology* **9,** 194 (2020).

5. Creamer, P. Osteoarthritis pain and its treatment. *Current opinion in rheumatology* **12,** 450–455 (2000).

6. Mow, V. C., Ratcliffe, A. & Poole, A. R. Cartilage and diarthrodial joints as paradigms for hierarchical materials and structures. *Biomaterials* **13,** 67–97 (1992).

7. Li, G. *et al.* Subchondral bone in osteoarthritis: insight into risk factors and microstructural changes. *Arthritis research & therapy* **15,** 1–12 (2013).

8. Pearle, A. D., Warren, R. F. & Rodeo, S. A. Basic science of articular cartilage and osteoarthritis. *Clinics in sports medicine* **24,** 1–12 (2005).

9. Knudson, C. B. & Knudson, W. *Cartilage proteoglycans* in *Seminars in cell & developmental biology* **12** (2001), 69–78.

10. Eyre, D. *The collagens of articular cartilage* in *Seminars in arthritis and rheumatism* **21** (1991), 2–11.

11. Roughley, P. J. & Mort, J. S. The role of aggrecan in normal and osteoarthritic cartilage. *Journal of experimental orthopaedics* **1,** 1–11 (2014).

12. Pratta, M. A. *et al.* Aggrecan protects cartilage collagen from proteolytic cleavage. *Journal of Biological Chemistry* **278,** 45539–45545 (2003).

13. Bidanset, D. J. *et al.* Binding of the proteoglycan decorin to collagen type VI. *Journal of Biological Chemistry* **267,** 5250–5256 (1992).

14. Zelenski, N. A. *et al.* Type VI collagen regulates pericellular matrix properties, chondrocyte swelling, and mechanotransduction in mouse articular cartilage. *Arthritis & Rheumatology* **67,** 1286–1294 (2015).

15. Aigner, T. *et al.* Type X collagen expression in osteoarthritic and rheumatoid articular cartilage. *Virchows Archiv B* **63,** 205–211 (1993).

16. Muir, H. The chondrocyte, architect of cartilage. Biomechanics, structure, function and molecular biology of cartilage matrix macromolecules. *Bioessays* **17,** 1039–1048 (1995).

17. Kiani, C., Liwen, C., Wu, Y. J., Albert, J. Y. & Burton, B. Y. Structure and function of aggrecan. *Cell research* **12,** 19–32 (2002).

18. Fosang, A. J. *et al.* The interglobular domain of cartilage aggrecan is cleaved by PUMP, gelatinases, and cathepsin B. *Journal of Biological Chemistry* **267,** 19470–19474 (1992).

19. Zheng, J., Luo, W. & Tanzer, M. L. Aggrecan synthesis and secretion: a paradigm for molecular and cellular coordination of multiglobular protein folding and intracellular trafficking. *Journal of Biological Chemistry* **273,** 12999–13006 (1998).

20. Watanabe, H., Cheung, S. C., Itano, N., Kimata, K. & Yamada, Y. Identification of hyaluronan-binding domains of aggrecan. *Journal of Biological Chemistry* **272,** 28057–28065 (1997).

21. Matsumoto, K. *et al.* Distinct interaction of versican/PG-M with hyaluronan and link protein. *Journal of Biological Chemistry* **278,** 41205–41212 (2003).

22. Luo, Y. *et al.* The minor collagens in articular cartilage. *Protein & cell* **8,** 560–572 (2017).

23. Tamer, T. M. Hyaluronan and synovial joint: function, distribution and healing. *Interdisciplinary toxicology* **6,** 111 (2013).

24. Hui, A. Y., McCarty, W. J., Masuda, K., Firestein, G. S. & Sah, R. L. A systems biology approach to synovial joint lubrication in health, injury, and disease. *Wiley Interdisciplinary Reviews: Systems Biology and Medicine* **4,** 15–37 (2012).

25. Dieppe, P. Developments in osteoarthritis. *Rheumatology* **50,** 245–247. ISSN: 1462-0324. eprint: `https://academic.oup.com/rheumatology/article-pdf/50/2/245/5055552/keq373.pdf`. `https://doi.org/10.1093/rheumatology/keq373` (Jan. 2011).

26. Abramson, S. B. & Attur, M. Developments in the scientific understanding of osteoarthritis. *Arthritis research & therapy* **11,** 1–9 (2009).

27. Little, C. B. & Hunter, D. J. Post-traumatic osteoarthritis: from mouse models to clinical trials. *Nature Reviews Rheumatology* **9,** 485–497 (2013).

28. Carbone, A. & Rodeo, S. Review of current understanding of post-traumatic osteoarthritis resulting from sports injuries. *Journal of orthopaedic research* **35,** 397–405 (2017).

29. Brown, S. B. *et al.* Characterization of post-traumatic osteoarthritis in rats following anterior cruciate ligament rupture by non-invasive knee injury (NIKI). *Journal of Orthopaedic Research®* **38,** 356–367 (2020).

30. Klatt, A. R. *et al.* A critical role for collagen II in cartilage matrix degradation: collagen II induces pro-inflammatory cytokines and MMPs in primary human chondrocytes. *Journal of orthopaedic research* **27,** 65–70 (2009).

31. Troeberg, L. & Nagase, H. Proteases involved in cartilage matrix degradation in osteoarthritis. *Biochimica et Biophysica Acta (BBA)-Proteins and Proteomics* **1824,** 133–145 (2012).

32. Tortorella, M. D. *et al.* Sites of aggrecan cleavage by recombinant human aggrecanase-1 (ADAMTS-4). *Journal of Biological Chemistry* **275,** 18566–18573 (2000).

33. Yamamoto, K., Wilkinson, D. & Bou-Gharios, G. Targeting dysregulation of metalloproteinase activity in osteoarthritis. *Calcified Tissue International,* 1–14 (2020).

34. Ohno, S., Im, H.-J., Knudson, C. B. & Knudson, W. Hyaluronan oligosaccharide–induced activation of transcription factors in bovine articular chondrocytes. *Arthritis & Rheumatism* **52,** 800–809 (2005).

35. Hu, Q. & Ecker, M. Overview of MMP-13 as a Promising Target for the Treatment of Osteoarthritis. *International Journal of Molecular Sciences* **22,** 1742 (2021).

36. Fosang, A. J., Last, K., Knäuper, V., Murphy, G. & Neame, P. J. Degradation of cartilage aggrecan by collagenase-3 (MMP-13). *FEBS letters* **380,** 17–20 (1996).

37. Mitchell, P. G. *et al.* Cloning, expression, and type II collagenolytic activity of matrix metalloproteinase-13 from human osteoarthritic cartilage. *The Journal of clinical investigation* **97,** 761–768 (1996).

38. Burrage, P. S., Mix, K. S., Brinckerhoff, C. E., *et al.* Matrix metalloproteinases: role in arthritis. *Front Biosci* **11,** 529–543 (2006).

39. Man, G. & Mologhianu, G. Osteoarthritis pathogenesis–a complex process that involves the entire joint. *Journal of medicine and life* **7,** 37 (2014).

40. Dare, D. & Rodeo, S. Mechanisms of post-traumatic osteoarthritis after ACL injury. *Current rheumatology reports* **16,** 1–5 (2014).

41. Kon, E. *et al.* Non-surgical management of early knee osteoarthritis. *Knee Surgery, Sports Traumatology, Arthroscopy* **20,** 436–449 (2012).

42. Rai, M. F. *et al.* Post-traumatic osteoarthritis in mice following mechanical injury to the synovial joint. *Scientific reports* **7,** 1–13 (2017).

43. Racine, J. & Aaron, R. K. Post-traumatic osteoarthritis after ACL injury. *RI Med J* **97,** 25–28 (2014).

44. Katz, J. N., Arant, K. R. & Loeser, R. F. Diagnosis and treatment of hip and knee osteoarthritis: a review. *Jama* **325,** 568–578 (2021).

45. Smelter, E. & Hochberg, M. C. New treatments for osteoarthritis. *Current opinion in rheumatology* **25,** 310–316 (2013).

46. Gislason, G. H. *et al.* Increased mortality and cardiovascular morbidity associated with use of nonsteroidal anti-inflammatory drugs in chronic heart failure. *Archives of internal medicine* **169,** 141–149 (2009).

47. Lee, A., Cooper, M. G., Craig, J. C., Knight, J. F. & Keneally, J. P. Effects of nonsteroidal anti-inflammatory drugs on postoperative renal function in adults with normal renal function. *Cochrane database of systematic reviews* (2007).

48. Rostom, A. *et al.* Prevention of NSAID-induced gastroduodenal ulcers. *Cochrane database of systematic reviews* (2002).

49. Bhala, N. *et al.* Vascular and upper gastrointestinal effects of non-steroidal anti-inflammatory drugs: meta-analyses of individual participant data from randomised trials. *Lancet (London, England)* **382,** 769–779 (2013).

50. Mora, J. C., Przkora, R. & Cruz-Almeida, Y. Knee osteoarthritis: pathophysiology and current treatment modalities. *Journal of pain research* **11,** 2189 (2018).

51. Webb, D. & Naidoo, P. Viscosupplementation for knee osteoarthritis: a focus on Hylan GF 20. *Orthopedic research and reviews* **10,** 73 (2018).

52. Gato-Calvo, L., Magalhaes, J., Ruiz-Romero, C., Blanco, F. J. & Burguera, E. F. Platelet-rich plasma in osteoarthritis treatment: review of current evidence. *Therapeutic advances in chronic disease* **10,** 2040622319825567 (2019).

53. De l'Escalopier, N., Anract, P. & Biau, D. Surgical treatments for osteoarthritis. *Annals of physical and rehabilitation medicine* **59,** 227–233 (2016).

54. Serwer, L., Hashizume, R., Ozawa, T. & James, C. D. Systemic and local drug delivery for treating diseases of the central nervous system in rodent models. *Journal of visualized experiments: JoVE* (2010).

55. Homayun, B., Lin, X. & Choi, H.-J. Challenges and recent progress in oral drug delivery systems for biopharmaceuticals. *Pharmaceutics* **11,** 129 (2019).

56. Rudmann, D. G. On-target and Off-target-based Toxicologic Effects. *Toxicologic Pathology* **41.** PMID: 23085982, 310–314. eprint: `https://doi.org/10.1177/0192623312464311`. `https://doi.org/10.1177/0192623312464311` (2013).

57. Rolfes, C., Howard, S., Goff, R. & A., P. Localized Drug Delivery for Cardiothoracic Surgery. *Current Concepts in General Thoracic Surgery* (2012).

58. Better safe than sorry: Understanding the toxicological properties of inorganic nanoparticles manufactured for biomedical applications. *Advanced Drug Delivery Reviews* **62,** 362–374. ISSN: 0169409X (2010).

59. Fenton, O. S., Olafson, K. N., Pillai, P. S., Mitchell, M. J. & Langer, R. Advances in Biomaterials for Drug Delivery. *Advanced Materials* **30,** 1–29. ISSN: 15214095 (2018).

60. Jahanshahi, M. & Babaei, Z. Protein nanoparticle: A unique system as drug delivery vehicles. *African Journal of Biotechnology* **7,** 4926–4934. ISSN: 16845315 (2008).

61. Mitchell, M. J. *et al.* Engineering precision nanoparticles for drug delivery. *Nature Reviews Drug Discovery* **20,** 101–124. ISSN: 14741784 (2021).

62. Anselmo, A. C. & Mitragotri, S. Nanoparticles in the clinic: An update. *Bioengineering & Translational Medicine* **4,** 1–16. ISSN: 2380-6761 (2019).

63. Schoenmaker, L. *et al.* mRNA-lipid nanoparticle COVID-19 vaccines: Structure and stability. *International Journal of Pharmaceutics* **601,** 120586. ISSN: 18733476 (2021).

64. Patel, S., Ryals, R. C., Weller, K. K., Pennesi, M. E. & Sahay, G. Lipid nanoparticles for delivery of messenger RNA to the back of the eye. *Journal of Controlled Release* **303,** 91–100. ISSN: 18734995. https://doi.org/10.1016/j.jconrel.2019.04.015 (2019).

65. Fonseca-Santos, B., Gremião, M. P. D. & Chorilli, M. Nanotechnology-based drug delivery systems for the treatment of Alzheimer's disease. *International Journal of Nanomedicine* **10,** 4981–5003. ISSN: 11782013 (2015).

66. Sercombe, L. *et al.* Advances and challenges of liposome assisted drug delivery. *Frontiers in Pharmacology* **6,** 1–13. ISSN: 16639812 (2015).

67. Vhora, I., Lalani, R., Bhatt, P., Patil, S. & Misra, A. Lipid-nucleic acid nanoparticles of novel ionizable lipids for systemic BMP-9 gene delivery to bone-marrow mesenchymal stem cells for osteoinduction. *International Journal of Pharmaceutics* **563,** 324–336. ISSN: 18733476 (2019).

68. Bobo, D., Robinson, K. J., Islam, J., Thurecht, K. J. & Corrie, S. R. Nanoparticle-Based Medicines: A Review of FDA-Approved Materials and Clinical Trials to Date. *Pharmaceutical Research* **33,** 2373–2387. ISSN: 1573904X. http://dx.doi.org/10.1007/s11095-016-1958-5 (2016).

69. Luther, D. C. *et al.* Delivery of drugs, proteins, and nucleic acids using inorganic nanoparticles. *Advanced Drug Delivery Reviews* **156,** 188–213. ISSN: 18728294. https://doi.org/10.1016/j.addr.2020.06.020 (2020).

70. Paul, W. & Sharma, C. P. *Inorganic nanoparticles for targeted drug delivery* 333–373. ISBN: 9780081026809 (Elsevier Ltd, 2019).

71. Ding, Y. *et al.* Gold nanoparticles for nucleic acid delivery. *Molecular Therapy* **22,** 1075–1083. ISSN: 15250024 (2014).

72. El-Sayed, I. H., Huang, X. & El-Sayed, M. A. Selective laser photo-thermal therapy of epithelial carcinoma using anti-EGFR antibody conjugated gold nanoparticles. *Cancer Letters* **239,** 129–135. ISSN: 03043835 (2006).

73. Patel, P. C., Giljohann, D. A., Seferos, D. S. & Mirkin, C. A. Peptide antisense nanoparticles. *Proceedings of the National Academy of Sciences of the United States of America* **105,** 17222–17226. ISSN: 00278424 (2008).

74. Kaur, A., Shimoni, O. & Wallach, M. Novel screening test for celiac disease using peptide functionalised gold nanoparticles. *World Journal of Gastroenterology* **24,** 5379–5390. ISSN: 22192840 (2018).

75. Agasti, S. S. *et al.* Photoregulated release of caged anticancer drugs from gold nanoparticles. *Journal of the American Chemical Society* **131,** 5728–5729. ISSN: 00027863 (2009).

76. Kim, C. K. *et al.* Entrapment of Hydrophobic Drugs in Nanoparticle Monolayers with Efficient Release into Cancer Cells. *J. Am. Chem. Soc* **4,** 1360–1361 (2009).

77. Ghosh, P., Han, G., De, M., Kim, C. K. & Rotello, V. M. Gold nanoparticles in delivery applications. *Advanced Drug Delivery Reviews* **60,** 1307–1315. ISSN: 0169409X (2008).

78. Dai, Z. *et al.* Translational Research: Bridging the Gap between Fundamental Research and the Clinic. *Bioconjugate Chemistry* **30,** 2989–2990. ISSN: 15204812 (2019).

79. Unterweger, H. *et al.* Development and characterization of magnetic iron oxide nanoparticles with a cisplatin-bearing polymer coating for targeted drug delivery. *International Journal of Nanomedicine* **9,** 3659–3676. ISSN: 11782013 (2014).

80. Jeon, H. *et al.* Poly-paclitaxel/cyclodextrin-SPION nano-assembly for magnetically guided drug delivery system. *Journal of Controlled Release* **231,** 68–76. ISSN: 18734995. `http://dx.doi.org/10.1016/j.jconrel.2016.01.006` (2016).

81. Yu, M. K. *et al.* Drug-loaded superparamagnetic iron oxide nanoparticles for combined cancer imaging and therapy in vivo. *Angewandte Chemie - International Edition* **47,** 5362–5365. ISSN: 14337851 (2008).

82. Xu, C., Lei, C. & Yu, C. Mesoporous silica nanoparticles for protein protection and delivery. *Frontiers in Chemistry* **7,** 1–12. ISSN: 22962646 (2019).

83. Tang, S., Huang, X., Chen, X. & Zheng, N. Hollow mesoporous zirconia nanocapsules for drug delivery. *Advanced Functional Materials* **20,** 2442–2447. ISSN: 1616301X (2010).

84. Niu, Y. *et al.* Understanding the contribution of surface roughness and hydrophobic modification of silica nanoparticles to enhanced therapeutic protein delivery. *Journal of Materials Chemistry B* **4,** 212–219. ISSN: 2050750X (2015).

85. Niu, Y. *et al.* Synthesis of silica nanoparticles with controllable surface roughness for therapeutic protein delivery. *Journal of Materials Chemistry B* **3,** 8477–8485. ISSN: 2050750X (2015).

86. Thomas, H. & Coley, H. M. Overcoming multidrug resistance in cancer: An update on the clinical strategy of inhibiting P-glycoprotein. *Cancer Control* **10,** 159–165. ISSN: 10732748 (2003).

87. Bertucci, A. *et al.* Combined Delivery of Temozolomide and Anti-miR221 PNA Using Mesoporous Silica Nanoparticles Induces Apoptosis in Resistant Glioma Cells. *Small* **11,** 5687–5695. ISSN: 16136829 (2015).

88. Vivero-Escoto, J. L. & Elnagheeb, M. Mesoporous silica nanoparticles loaded with cisplatin and phthalocyanine for combination chemotherapy and photodynamic therapy in vitro. *Nanomaterials* **5,** 2302–2316. ISSN: 20794991 (2015).

89. Xiong, L., Du, X., Kleitz, F. & Qiao, S. Z. Cancer-Cell-Specific Nuclear-Targeted Drug Delivery by Dual-Ligand-Modified Mesoporous Silica Nanoparticles. *Small* **11,** 5919–5926. ISSN: 16136829 (2015).

90. Li Li, L. & Wang, H. Enzyme-coated mesoporous silica nanoparticles as efficient antibacterial agents in vivo. *Advanced Healthcare Materials* **2,** 1351–1360. ISSN: 21922659 (2013).

91. Doadrio, J. C. *et al.* Functionalization of mesoporous materials with long alkyl chains as a strategy for controlling drug delivery pattern. *Journal of Materials Chemistry* **15,** 462–466. ISSN: 13645501 (2006).

92. Slowing, I. I., Trewyn, B. G. & Lin, V. S. Mesoporous silica nanoparticles for intracellular delivery of membrane-impermeable proteins. *Journal of the American Chemical Society* **129,** 8845–8849. ISSN: 00027863 (2007).

93. Yang, Y. *et al.* Structure-Dependent and Glutathione-Responsive Biodegradable Dendritic Mesoporous Organosilica Nanoparticles for Safe Protein Delivery. *Chemistry of Materials* **28,** 9008–9016. ISSN: 15205002 (2016).

94. Him, C. *et al.* Mesoporous Silica Nanoparticles Facilitate Delivery of siRNA to Shutdown Signaling Pathways in Mammalian Cells. *Small2* **6,** 1185–1190. ISSN: 15378276 (2010).

95. Li, X., Xie, Q. R., Zhang, J., Xia, W. & Gu, H. The packaging of siRNA within the mesoporous structure of silica nanoparticles. *Biomaterials* **32,** 9546–9556. ISSN: 01429612 (2011).

96. Kim, M. H. *et al.* Facile synthesis of monodispersed mesoporous silica nanoparticles with ultralarge pores and their application in gene delivery. *ACS Nano* **5,** 3568–3576. ISSN: 19360851 (2011).

97. Affonso De Oliveira, J. F. *et al.* Dual Functionalization of Nanoparticles for Generating Corona-Free and Noncytotoxic Silica Nanoparticles. *ACS Applied Materials and Interfaces* **10,** 41917–41923. ISSN: 19448252 (2018).

98. Palanikumar, L., Choi, E. S., Cheon, J. Y., Joo, S. H. & Ryu, J. H. Noncovalent polymer-gatekeeper in mesoporous silica nanoparticles as a targeted drug delivery platform. *Advanced Functional Materials* **25,** 957–965. ISSN: 16163028 (2015).

99. Amhare, A. F. *et al.* Biomedical application of chondroitin sulfate with nanoparticles in drug delivery systems: systematic review. *Journal of Drug Targeting* **29,** 259–268. ISSN: 10292330. https://doi.org/10.1080/1061186X.2020.1833018 (2021).

100. Jarai, B. M., Kolewe, E. L., Stillman, Z. S., Raman, N. & Fromen, C. A. *Polymeric nanoparticles* 303–324. ISBN: 9780128166628. http://dx.doi.org/10.1016/B978-0-12-816662-8.00018-7 (Elsevier Inc., 2019).

101. Valo, H. *et al.* Drug release from nanoparticles embedded in four different nanofibrillar cellulose aerogels. *European Journal of Pharmaceutical Sciences* **50,** 69–77. ISSN: 18790720. http://dx.doi.org/10.1016/j.ejps.2013.02.023 (2013).

102. Fedel, M. *et al.* Blood compatibility of polymers derived from natural materials. *Journal of Bioactive and Compatible Polymers* **27,** 295–312. ISSN: 08839115 (2012).

103. Zargar, V., Asghari, M. & Dashti, A. A Review on Chitin and Chitosan Polymers: Structure, Chemistry, Solubility, Derivatives, and Applications. *ChemBioEng Reviews* **2,** 204–226. ISSN: 21969744 (2015).

104. Sinha, V. R. & Kumria, R. Polysaccharides in colon-specific drug delivery. *International Journal of Pharmaceutics* **224,** 19–38. ISSN: 03785173 (2001).

105. Rubinstein, A. Natural polysaccharides as targeting tools of drugs to the human colon. *Drug Development Research* **50,** 435–439. ISSN: 02724391 (2000).

106. Vila, A. *et al.* Low molecular weight chitosan nanoparticles as new carriers for nasal vaccine delivery in mice. *European Journal of Pharmaceutics and Biopharmaceutics* **57,** 123–131. ISSN: 09396411 (2004).

107. Chen, Y., Mohanraj, V. J. & Parkin, J. E. Chitosan-dextran sulfate nanoparticles for delivery of an anti-angiogenesis peptide. *Letters in Peptide Science* **10,** 621–629. ISSN: 09295666 (2003).

108. Zhou, P. H. *et al.* Chondroprotective effects of hyaluronic acid-chitosan nanoparticles containing plasmid DNA encoding cytokine response modifier A in a rat knee osteoarthritis model. *Cellular Physiology and Biochemistry* **47,** 1207–1216. ISSN: 14219778 (2018).

109. Bhatia, S. *Natural Polymer Drug Delivery Systems* ISBN: 9783319411286 (2016).

110. Tiwari, G. *et al.* Drug delivery systems: An updated review. *International Journal of Pharmaceutical Investigation* **2,** 2. ISSN: 2230-973X (2012).

111. Shi, H. *et al.* Programmed co-delivery of platinum nanodrugs and gemcitabine by a clustered nanocarrier for precision chemotherapy for NSCLC tumors. *Journal of Materials Chemistry B* **8,** 332–342. ISSN: 20507518 (2020).

112. Guo, F. *et al.* Matrix metalloprotein-triggered, cell penetrating peptide-modified star-shaped nanoparticles for tumor targeting and cancer therapy. *Journal of Nanobiotechnology* **18,** 1–16. ISSN: 14773155. https://doi.org/10.1186/s12951-020-00595-5 (2020).

113. Lim, W. Q., Phua, S. Z. F. & Zhao, Y. Redox-Responsive Polymeric Nanocomplex for Delivery of Cytotoxic Protein and Chemotherapeutics. *ACS Applied Materials and Interfaces* **11,** 31638–31648. ISSN: 19448252 (2019).

114. Zhang, F. *et al.* Genetic programming of macrophages to perform anti-tumor functions using targeted mRNA nanocarriers. *Nature Communications* **10.** ISSN: 20411723. http://dx.doi.org/10.1038/s41467-019-11911-5 (2019).

115. Clegg, J. R. *et al.* Synthetic networks with tunable responsiveness, biodegradation, and molecular recognition for precision medicine applications. *Science Advances* **5,** 1–16. ISSN: 23752548 (2019).

116. McMasters, J., Poh, S., Lin, J. B. & Panitch, A. Delivery of anti-inflammatory peptides from hollow PEGylated poly(NIPAM) nanoparticles reduces inflammation in an ex vivo osteoarthritis model. *Journal of Controlled Release* **258,** 161–170. ISSN: 18734995. http://dx.doi.org/10.1016/j.jconrel.2017.05.008 (2017).

117. Poh, S., Lin, J. B. & Panitch, A. Release of Anti-inflammatory Peptides from Thermosensitive Nanoparticles with Degradable Cross-Links Suppresses Pro-inflammatory Cytokine Production. *Biomacromolecules* **16,** 1191–1200. ISSN: 15264602 (2015).

118. Lin, J. B., Poh, S. & Panitch, A. Controlled release of anti-inflammatory peptides from reducible thermosensitive nanoparticles suppresses cartilage inflammation. *Nanomedicine: Nanotechnology, Biology and Medicine* **12,** 2095–2100. ISSN: 15499634. http://linkinghub.elsevier.com/retrieve/pii/S1549963416300570 (2016).

119. Lu, Y., Aimetti, A. A., Langer, R. & Gu, Z. Bioresponsive materials. *Nature Reviews Materials* **2.** ISSN: 20588437 (2016).

120. Lu, Z.-R. & Sakuma, S. *Nanomaterials in Pharmacology* ISBN: 9781493931200 (2016).

121. Cipollaro, L. *et al.* Liposomes for intra-articular analgesic drug delivery in orthopedics: State-of-art and future perspectives. insights from a systematic mini-review of the literature. *Medicina (Lithuania)* **56,** 1–17. ISSN: 16489144 (2020).

122. Corciulo, C. *et al.* Intraarticular injection of liposomal adenosine reduces cartilage damage in established murine and rat models of osteoarthritis. *Scientific Reports* **10,** 1–16. ISSN: 20452322. https://doi.org/10.1038/s41598-020-68302-w (2020).

123. Koning, G. A. *et al.* Targeting of angiogenic endothelial cells at sites of inflammation by dexamethasone phosphate-containing RGD peptide liposomes inhibits experimental arthritis. *Arthritis and Rheumatism* **54,** 1198–1208. ISSN: 00043591 (2006).

124. Dong, J. *et al.* Intra-articular delivery of liposomal celecoxib-hyaluronate combination for the treatment of osteoarthritis in rabbit model. *International Journal of Pharma-*

ceutics **441,** 285–290. ISSN: 03785173. http://dx.doi.org/10.1016/j.ijpharm.2012.11.031 (2013).

125. Wang, J. X., Fan, Y. B., Gao, Y., Hu, Q. H. & Wang, T. C. TiO2 nanoparticles translocation and potential toxicological effect in rats after intraarticular injection. *Biomaterials* **30,** 4590–4600. ISSN: 01429612. http://dx.doi.org/10.1016/j.biomaterials.2009.05.008 (2009).

126. Kumar, S., Adjei, I. M., Brown, S. B., Liseth, O. & Sharma, B. Manganese dioxide nanoparticles protect cartilage from inflammation-induced oxidative stress. *Biomaterials* **224,** 119467. ISSN: 18785905. https://doi.org/10.1016/j.biomaterials.2019.119467 (2019).

127. Eichaker, L. R., Cho, H., Duvall, C. L., Werfel, T. A. & Hasty, K. A. Future nanomedicine for the diagnosis and treatment of osteoarthritis. *Nanomedicine* **9,** 2203–2215. ISSN: 17486963 (2014).

128. Xie, M. *et al.* Intra-articular tracking of adipose-derived stem cells by chitosan-conjugated iron oxide nanoparticles in a rat osteoarthritis model. *RSC Advances* **9,** 12010–12019. ISSN: 20462069 (2019).

129. Peng, S. *et al.* Detection of ADAMTS-4 activity using a fluorogenic peptide-conjugated Au nanoparticle probe in human knee synovial fluid. *ACS Applied Materials and Interfaces* **5,** 6089–6096. ISSN: 19448244 (2013).

130. Leonavičiene, L. *et al.* Effect of gold nanoparticles in the treatment of established collagen arthritis in rats. *Medicina (Lithuania)* **48,** 91–101. ISSN: 1010660X (2012).

131. She, P. *et al.* Dextran sulfate-triamcinolone acetonide conjugate nanoparticles for targeted treatment of osteoarthritis. *International Journal of Biological Macromolecules* **158,** 1082–1089. ISSN: 18790003. https://doi.org/10.1016/j.ijbiomac.2020.05.013 (2020).

132. Morgen, M. *et al.* Nanoparticles for improved local retention after intra-articular injection into the knee joint. *Pharmaceutical Research* **30,** 257–268. ISSN: 07248741 (2013).

133. Jin, G. Z. Current nanoparticle-based technologies for osteoarthritis therapy. *Nanomaterials* **10,** 1–20. ISSN: 20794991 (2020).

134. Ji, X. & Zhang, H. Current Strategies for the Treatment of Early Stage Osteoarthritis. *Frontiers in Mechanical Engineering* **5,** 1–8. ISSN: 22973079 (2019).

135. Chinnagounder Periyasamy, P., Leijten, J. C., Dijkstra, P. J., Karperien, M. & Post, J. N. Nanomaterials for the local and targeted delivery of osteoarthritis drugs. *Journal of Nanomaterials* **2012.** ISSN: 16874110 (2012).

136. Vanniasinghe, A. S., Bender, V. & Manolios, N. The Potential of Liposomal Drug Delivery for the Treatment of Inflammatory Arthritis. *Seminars in Arthritis and Rheumatism* **39,** 182–196. ISSN: 00490172. `http://dx.doi.org/10.1016/j.semarthrit.2008.08.004` (2009).

137. Charcosset, C., Juban, A., Valour, J. P., Urbaniak, S. & Fessi, H. Preparation of liposomes at large scale using the ethanol injection method: Effect of scale-up and injection devices. *Chemical Engineering Research and Design* **94,** 508–515. ISSN: 02638762. `http://dx.doi.org/10.1016/j.cherd.2014.09.008` (2015).

138. Maudens, P., Jordan, O. & Allémann, E. Recent advances in intra-articular drug delivery systems for osteoarthritis therapy. *Drug Discovery Today* **23,** 1761–1775. ISSN: 18785832. `https://doi.org/10.1016/j.drudis.2018.05.023` (2018).

139. Maudens, P., Jordan, O. & Allémann, E. Recent advances in intra-articular drug delivery systems for osteoarthritis therapy. *Drug Discovery Today* **23,** 1761–1775. ISSN: 18785832. `https://doi.org/10.1016/j.drudis.2018.05.023` (2018).

140. Shin, H. J. *et al.* p66shc siRNA nanoparticles ameliorate chondrocytic mitochondrial dysfunction in osteoarthritis. *International Journal of Nanomedicine* **15,** 2379–2390. ISSN: 11782013 (2020).

141. Shin, H. J. *et al.* p47phox siRNA-loaded PLGA nanoparticles suppress ROS/oxidative stress-induced chondrocyte damage in osteoarthritis. *Polymers* **12,** 1–14. ISSN: 20734360 (2020).

142. Martín Arias, L. H., Martín González, A., Sanz Fadrique, R. & Vazquez, E. S. Cardiovascular Risk of Nonsteroidal Anti-inflammatory Drugs and Classical and Selective Cyclooxygenase-2 Inhibitors: A Meta-analysis of Observational Studies. *Journal of Clinical Pharmacology* **59,** 55–73. ISSN: 15524604 (2019).

143. Liu, P. *et al.* Intra-articular injection of etoricoxib-loaded PLGA-PEG-PLGA triblock copolymeric nanoparticles attenuates osteoarthritis progression. *American journal of translational research* **11,** 6775–6789. ISSN: 1943-8141. http://www.ncbi.nlm.nih.gov/pubmed/31814887%0Ahttp://www.pubmedcentral.nih.gov/articlerender.fcgi?artid=PMC6895527 (2019).

144. Viral inhibition of inflammation: Cowpox virus encodes an inhibitor of the interleukin-1β converting enzyme. *Cell* **69,** 597–604. ISSN: 00928674 (1992).

145. Singh, A. *et al.* Nano-engineered particles for enhanced intra-articular retention and delivery of proteins. *Adv Healthc Mater* **3,** 1562–7 (2014).

146. Kavanaugh, T. E., Werfei, T. A., Cho, H., Hasty, K. A. & Duvall, C. L. Particle Based Technologies for Osteoarthritis Detection and Therapy. *Drug Deliv Transl Res* **6,** 132–147 (2016).

147. Wolinsky, J. B., Colson, Y. L. & Grinstaff, M. W. Local drug delivery strategies for cancer treatment: Gels, nanoparticles, polymeric films, rods, and wafers. *Journal of Controlled Release* **159,** 14–26. ISSN: 01683659. http://dx.doi.org/10.1016/j.jconrel.2011.11.031 (2012).

148. Kang, M. L. & Im, G. I. Drug delivery systems for intra-articular treatment of osteoarthritis. *Expert Opinion on Drug Delivery* **11,** 269–282. ISSN: 17425247 (2014).

149. Mura, S., Nicolas, J. & Couvreur, P. Stimuli-responsive nanocarriers for drug delivery. *Nature materials* **12,** 991–1003 (2013).

150. Tagami, T. *et al.* MRI monitoring of intratumoral drug delivery and prediction of the therapeutic effect with a multifunctional thermosensitive liposome. *Biomaterials* **32,** 6570–6578 (2011).

151. Rehman, M. *et al.* Solid lipid nanoparticles for thermoresponsive targeting: evidence from spectrophotometry, electrochemical, and cytotoxicity studies. *International journal of nanomedicine* **12,** 8325 (2017).

152. Brezaniova, I. *et al.* Temoporfin-loaded 1-tetradecanol-based thermoresponsive solid lipid nanoparticles for photodynamic therapy. *Journal of Controlled Release* **241,** 34–44 (2016).

153. Christensen, K. Y. *et al.* Risk of selected cancers due to occupational exposure to chlorinated solvents in a case–control study in Montreal. *Journal of occupational and environmental medicine* **55,** 198–208 (2013).

154. Seuring, J. & Agarwal, S. Polymers with upper critical solution temperature in aqueous solution. *Macromolecular rapid communications* **33,** 1898–1920 (2012).

155. Pourjavadi, A., Kohestanian, M. & Streb, C. pH and thermal dual-responsive poly (NIPAM-co-GMA)-coated magnetic nanoparticles via surface-initiated RAFT polymerization for controlled drug delivery. *Materials Science and Engineering: C* **108,** 110418 (2020).

156. Adibfar, A. *et al.* VEGF delivery by smart polymeric PNIPAM nanoparticles affects both osteogenic and angiogenic capacities of human bone marrow stem cells. *Materials Science and Engineering: C* **93,** 790–799 (2018).

157. Ngadaonye, J. I., Geever, L. M., Cloonan, M. O. & Higginbotham, C. L. Photopolymerised thermo-responsive poly (N, N-diethylacrylamide)-based copolymer hydrogels for potential drug delivery applications. *Journal of Polymer Research* **19,** 1–15 (2012).

158. Cortez-Lemus, N. A. & Licea-Claverie, A. Poly (N-vinylcaprolactam), a comprehensive review on a thermoresponsive polymer becoming popular. *Progress in Polymer Science* **53,** 1–51 (2016).

159. Hao, J., Servello, J., Sista, P., Biewer, M. C. & Stefan, M. C. Temperature-sensitive aliphatic polyesters: synthesis and characterization of γ-substituted caprolactone monomers and polymers. *Journal of Materials Chemistry* **21,** 10623–10628 (2011).

160. San Miguel, V., Limer, A., Haddleton, D. M., Catalina, F. & Peinado, C. Biodegradable and thermoresponsive micelles of triblock copolymers based on 2-(N, N-dimethylamino) ethyl methacrylate and ε-caprolactone for controlled drug delivery. *European Polymer Journal* **44,** 3853–3863 (2008).

161. Wang, H. Dispersing carbon nanotubes using surfactants. *Current Opinion in Colloid & Interface Science* **14,** 364–371 (2009).

162. Lau, J. L. & Dunn, M. K. Therapeutic peptides: Historical perspectives, current development trends, and future directions. *Bioorganic and Medicinal Chemistry* **26,** 2700–2707. ISSN: 14643391. `https://doi.org/10.1016/j.bmc.2017.06.052` (2018).

163. Zompra, A. A., Galanis, A. S., Werbitzky, O. & Albericio, F. Manufacturing peptides as active pharmaceutical ingredients. *Future Medicinal Chemistry* **1,** 361–377. ISSN: 17568919 (2009).

164. Bruckdorfer, T., Marder, O. & Albericio, F. From Production of Peptides in Milligram Amounts for Research to Multi-Tons Quantities for Drugs of the Future. *Current Pharmaceutical Biotechnology* **5,** 29–43. ISSN: 13892010 (2005).

165. Albericio, F. & Kruger, H. G. Therapeutic peptides. *Future Medicinal Chemistry* **4,** 1527–1531. ISSN: 17568919 (2012).

166. Lalatsa, A., Schatzlein, A. G. & Uchegbu, I. F. Strategies to deliver peptide drugs to the brain. *Molecular Pharmaceutics* **11,** 1081–1093. ISSN: 15438392 (2014).

167. McMasters, J. & Panitch, A. Prevention of Collagen-Induced Platelet Binding and Activation by Thermosensitive Nanoparticles. *The AAPS Journal* **17,** 1117–1125. ISSN: 1550-7416. http://link.springer.com/10.1208/s12248-015-9794-9 (2015).

168. Xia, B. *et al.* Activatable Cell-Penetrating Peptide Conjugated Polymeric Nanoparticles with Gd-Chelation and Aggregation-Induced Emission for Bimodal MR and Fluorescence Imaging of Tumors. *ACS Applied Bio Materials* **3,** 1394–1405. ISSN: 25766422 (2020).

169. Choi, K. M. *et al.* A monitoring method for Atg4 activation in living cells using peptide-conjugated polymeric nanoparticles. *Autophagy* **7,** 1052–1062. ISSN: 15548635 (2011).

170. Kulhari, H., Pooja, D., Shrivastava, S., V.G.M, N. & Sistla, R. *Peptide conjugated polymeric nanoparticles as a carrier for targeted delivery of docetaxel* 2014.

171. Wang, R. T., Zhi, X. Y., Yao, S. Y. & Zhang, Y. LFC131 peptide-conjugated polymeric nanoparticles for the effective delivery of docetaxel in CXCR4 overexpressed lung cancer cells. *Colloids and Surfaces B: Biointerfaces* **133,** 43–50. ISSN: 18734367 (2015).

172. Kuo, R., Saito, E., Miller, S. D. & Shea, L. D. Peptide-Conjugated Nanoparticles Reduce Positive Co-stimulatory Expression and T Cell Activity to Induce Tolerance. *Molecular Therapy* **25,** 1676–1685. ISSN: 15250024. http://dx.doi.org/10.1016/j.ymthe.2017.03.032 (2017).

173. Mort, J. S. & Billington, C. J. Articular cartilage and changes in arthritis matrix degradation. *Arthritis Research* **3,** 337–341. ISSN: 14659905 (2001).

174. Bondeson, J., Wainwright, S., Hughes, C. & Caterson, B. The regulation of the ADAMTS4 and ADAMTS5 aggrecanases in osteoarthritis: A review. *Clinical and Experimental Rheumatology* **26,** 139–145. ISSN: 0392856X (2008).

175. Brown, S., Kumar, S. & Sharma, B. Intra-articular targeting of nanomaterials for the treatment of osteoarthritis. *Acta Biomaterialia* **93,** 239–257. ISSN: 18787568. https://doi.org/10.1016/j.actbio.2019.03.010 (2019).

176. MK2 targets AU-rich elements and regulates biosynthesis of tumor necrosis factor and interleukin-6 independently at different post-transcriptional levels. *Journal of Biological Chemistry* **277,** 3065–3068. ISSN: 00219258. http://dx.doi.org/10.1074/jbc.C100685200 (2002).

177. Soni, S., Anand, P. & Padwad, Y. S. MAPKAPK2: The master regulator of RNA-binding proteins modulates transcript stability and tumor progression. *Journal of Experimental and Clinical Cancer Research* **38,** 1–18. ISSN: 17569966 (2019).

178. Wang, C. *et al.* Selective inhibition of the p38α MAPK-MK2 axis inhibits inflammatory cues including inflammasome priming signals. *Journal of Experimental Medicine* **215,** 1315–1325. ISSN: 15409538 (2018).

179. Hayess, K. & Benndorf, R. Effect of protein kinase inhibitors on activity of mammalian small heat- shock protein (HSP25) Kinase. *Biochemical Pharmacology* **53,** 1239–1247. ISSN: 00062952 (1997).

180. Lopes, L. B. *et al.* Cell permeant peptide analogues of the small heat shock protein, HSP20, reduce TGF-β1-induced CTGF expression in keloid fibroblasts. *Journal of Investigative Dermatology* **129,** 590–598. ISSN: 0022202X. http://dx.doi.org/10.1038/jid.2008.264 (2009).

181. Ward, B., Seal, B. L., Brophy, C. M. & Panitch, A. Design of a bioactive cell-penetrating peptide: When a transduction domain does more than transduce. *Journal of Peptide Science* **15,** 668–674. ISSN: 10752617. arXiv: NIHMS150003 (2009).

182. Brugnano, J. L., Chan, B. K., Seal, B. L. & Panitch, A. Cell-penetrating peptides can confer biological function: Regulation of inflammatory cytokines in human mono-

cytes by MK2 inhibitor peptides. *Journal of Controlled Release* **155,** 128–133. ISSN: 01683659. http://dx.doi.org/10.1016/j.jconrel.2011.05.007 (2011).

183. Kumar Malik, D., Baboota, S., Ahuja, A., Hasan, S. & Ali, J. Recent Advances in Protein and Peptide Drug Delivery Systems. *Current Drug Delivery* **4,** 141–151. ISSN: 15672018 (2007).

184. Bernhard, J. C. & Panitch, A. Synthesis and characterization of an aggrecan mimic. *Acta Biomaterialia* **8,** 1543–1550. ISSN: 17427061. http://dx.doi.org/10.1016/j.actbio.2011.12.029 (2012).

185. Stuart, K., Sharma, S. & Panitch, A. Development of an aggrecan mimic to halt osteoarthritis progression. *Osteoarthritis and Cartilage* **22,** S473–S474 (2014).

186. Sharma, S., Panitch, A. & Neu, C. P. Incorporation of an aggrecan mimic prevents proteolytic degradation of anisotropic cartilage analogs. *Acta Biomaterialia* **9,** 4618–4625. ISSN: 17427061. http://dx.doi.org/10.1016/j.actbio.2012.08.041 (2013).

187. Sharma, S., Vazquez-Portalatin, N., Calve, S. & Panitch, A. Biomimetic Molecules Lower Catabolic Expression and Prevent Chondroitin Sulfate Degradation in an Osteoarthritic ex Vivo Model. *ACS Biomaterials Science & Engineering* **2,** 241–250. ISSN: 2373-9878. http://pubs.acs.org/doi/abs/10.1021/acsbiomaterials.5b00458 (2016).

188. Faust, H. J. *et al.* A hyaluronic acid binding peptide-polymer system for treating osteoarthritis. *Biomaterials* **183,** 93–101. ISSN: 18785905 (2018).

CHAPTER II

Thermoresponsive, Hollow, Degradable Core-Shell Nanoparticles for Intra-Articular Delivery of Anti-Inflammatory Peptides

2.1 Abstract

Inflammation following joint trauma contributes to cartilage degradation and progression of post traumatic osteoarthritis (PTOA). Therefore, drug delivery vehicles that deliver effective anti-inflammatory treatments have the potential to prevent PTOA. We have developed solid and hollow, thermoresponsive nanoparticles for the controlled release of our anti-inflammatory MK2-inhibiting (MK2i) peptide for intra-articular injection to halt inflammation that contributes to the advancement of PTOA. This system exploits the thermosensitive characteristic of N-isopropyl acrylamide (NIPAm) to transition phases when passing through its lower critical solution temperature (LCST). The nanoparticles (NPs) swell below the LCST and constrict above it. Non-crosslinked poly(NIPAm) (pNIPAm), held above its LCST, formed hydrophobic cores around which shells composed of NIPAm, degradable crosslinker N, N'-bis (acryloyl) cystamine (BAC), sulfated 2-acrylamido-2-methyl-1-propanesulfonic acid (AMPS), and acrylic acid (AAc) were polymerized. Removal of the non-crosslinked pNIPAm cores via diffusion produced, thermosensitive, degradable nanoparticles with low density, or hollow, cores. The data presented here revealed low-density, termed hollow, nanoparticles (hNPs) load and release significantly more MK2i than solid nanoparticles (sNPs). Furthermore, drug loading below the LCST of NIPAm results in roughly 2.5 times more therapeutic encapsulation compared to loading particles in their constricted state. Hollow nanoparticles increase drug loading compared to solid nanoparticles, are taken

up into chondrocytes within 24 h, cleared from the cells within 6 days, significantly decrease the secretion of the proinflammatory cytokine IL-6, and, via intra-articular injection, are successfully delivered into the joint space of rats. The peptide loaded nanoparticles provide a reproducible platform for intra-articular delivery of therapeutics.

2.2 Introduction

Osteoarthritis (OA) is the most prevalent joint disease worldwide and causes significant pain, disability, and economic loss. OA affects more than 50 million people accounting for $185.5 billion in healthcare costs annually in the U.S. alone[1,2]. OA is characterized by inflammation of the synovial joint, including the synovial tissue, and degradation of extracellular matrix (ECM) molecules of articular cartilage resulting in the breakdown of the cartilage itself. Injury to articular cartilage triggers the release of inflammatory cytokines (e.g. IL-6, TNF-α) that increase the secretion of catabolic enzymes by chondrocytes[2]. The enzymatic fragments of degraded articular cartilage further stimulate inflammation resulting in the upregulation of cytokines and matrix metalloproteases (MMPs), thus generating a damaging cyclic process perpetuating OA[2]. Suppressing inflammation within the synovial joint may halt the vicious cascade that perpetuates cartilage matrix breakdown and the progression of OA following joint trauma.

Current non-surgical OA treatments, including non-steroidal anti-inflammatory drugs (NSAIDs), opioids, and intra-articular (IA) injections of viscosupplements and corticosteroids, are primarily palliative, and are meant to control pain rather than prevent further joint degeneration. However, overuse of NSAIDs can lead to increased gastrointestinal[3,4], cardiovascular[5], and kidney complications[6], and opioids can have severe adverse side effects, primarily addiction[7]. Corticosteroids are the most prominent IA injection used for treating OA, but may promote chondrocyte destruction and increase the necessity for joint replacement and the likelihood for surgical intervention[7]. Therefore, there is a need for a safe, targeted therapeutic that can slow or stop the progression of PTOA.

Within the inflammatory pathway, mitogen-activated protein kinase-activated protein (MAPKAP) kinase 2 (MK2) is activated by p38 MAPK during OA and stabilizes the mRNA encoding pro-inflammatory cytokines (i.e. IL-1β, IL-6, and TNF-α)[8,9]. Our lab has developed a series of MK2 inhibiting (MK2i) cell-penetrating peptides (CPPs) that suppress MK2 phosphorylation, thus suppressing pro-inflammatory cytokine production; two variants of MK2i peptides, YARAAARQARAKALARQLGVAA (YARA) and KAFAKLAARLYRKALARQLGVAA (KAFAK), differ in sequence only in their CPP region, however differ tremendously in their kinase inhibition selectivity profiles[10,11]. Despite their therapeutic value, both MK2i peptides are highly susceptible to enzymatic degradation within the extracellular space. To overcome enzymatic degradation of the MK2i peptide and prolong sustained delivery time, thermoresponsive, anionic NPs were synthesized and investigated for MK2i peptide loading, release, and subsequent *in vitro* bioactivity[12,13].

Our previous two generations of thermoresponsive NPs were either termed "solid" nanoparticles (sNPs) or "hollow" nanoparticles (hNPs) with the latter synthesized as core-shell particles followed by core removal that required disulfide bond reduction leaving a nondegradable shell. Limitations in peptide loading and release from the previous nanoparticle generations led us to modify synthesis protocols and to alter the crosslinking strategy to improve core removal, peptide loading and release, and to support particle degradation *in vitro* and *in vivo*[14–16]. Here, the cores are synthesized with a high initiator to monomer ratio to limit polymer molecular weight and potentially enhance removal of the core from the fully formed core-shell nanoparticle. In addition, shells, formed directly around the cores, contained a labile disulfide crosslink, N,N′-bis(acryloyl) cystamine (BAC), to facilitate particle degradation and controlled release of the loaded peptide. Below the LCST, the nanoparticles swelled to aid peptide diffusion into the particle as well as support the formation of ionic bonds between the peptide and particle. The particle shell contained degradable crosslinker BAC as well as negative acrylamido-2-methyl-1-propanesulfonic acid (AMPS) to interact ionically with the cationic MK2i peptide, and acrylic acid (AAc) for future particle modification. These

nanoparticles presented here will be used to encapsulate and deliver MK2i anti-inflammatory peptide into the joint space.

In previous generations of nanoparticles, YARA retention within the particle was unsuccessful, limiting the usefulness of the delivery system, while KAFAK was retained and used as the MK2i[14–16]. However, YARA has been found to be more specific to MK2 inhibition[10,11,17], making it desirable to deliver this version of the MK2 inhibitor peptide. The nanoparticles presented here allows for YARA retention within monodispersed, thermoresponsive, degradable NPs allowing for its sustained release into inflamed chondrocytes. In this work, we seek to understand how crosslink density effected particle degradation and YARA loading and release. Fluorophore labeling of the core polymer, via co-polymerization with vinyl-fluorophore monomers, allowed quantification of core removal using flow cytometry as well as nanoparticle visualization. Fluorescent labeling also allowed the use of intravital imaging to track particle retention within the synovial joint of rats. The body of results presented here support the hypothesis that lowering the crosslink density within the hollow poly(NIPAm-co-AMPS-AAc-BAC) nanoparticles will increase YARA uptake into the particles. Further, the incorporation of the degradable crosslinker, BAC, will allow therapeutic release and NP clearance from the cell, thus supporting suppression of the production of the inflammatory cytokine interleukin 6 (IL-6) in chondrocytes treated with YARA-loaded, lower crosslink density hollow nanoparticles as compared to YARA-loaded crosslink density matched solid nanoparticles, see Figure 2.1.

2.3 Materials & Methods

2.3.1 Cell Culture

Fetal bovine knees were purchased from Animal Technologies (Tyler, TX) and primary chondrocytes were harvested 24 h after slaughter as previously described[18]. Briefly, cartilage slices, 150–200 μm thick, were shaved from the load-bearing femoral condyle and washed

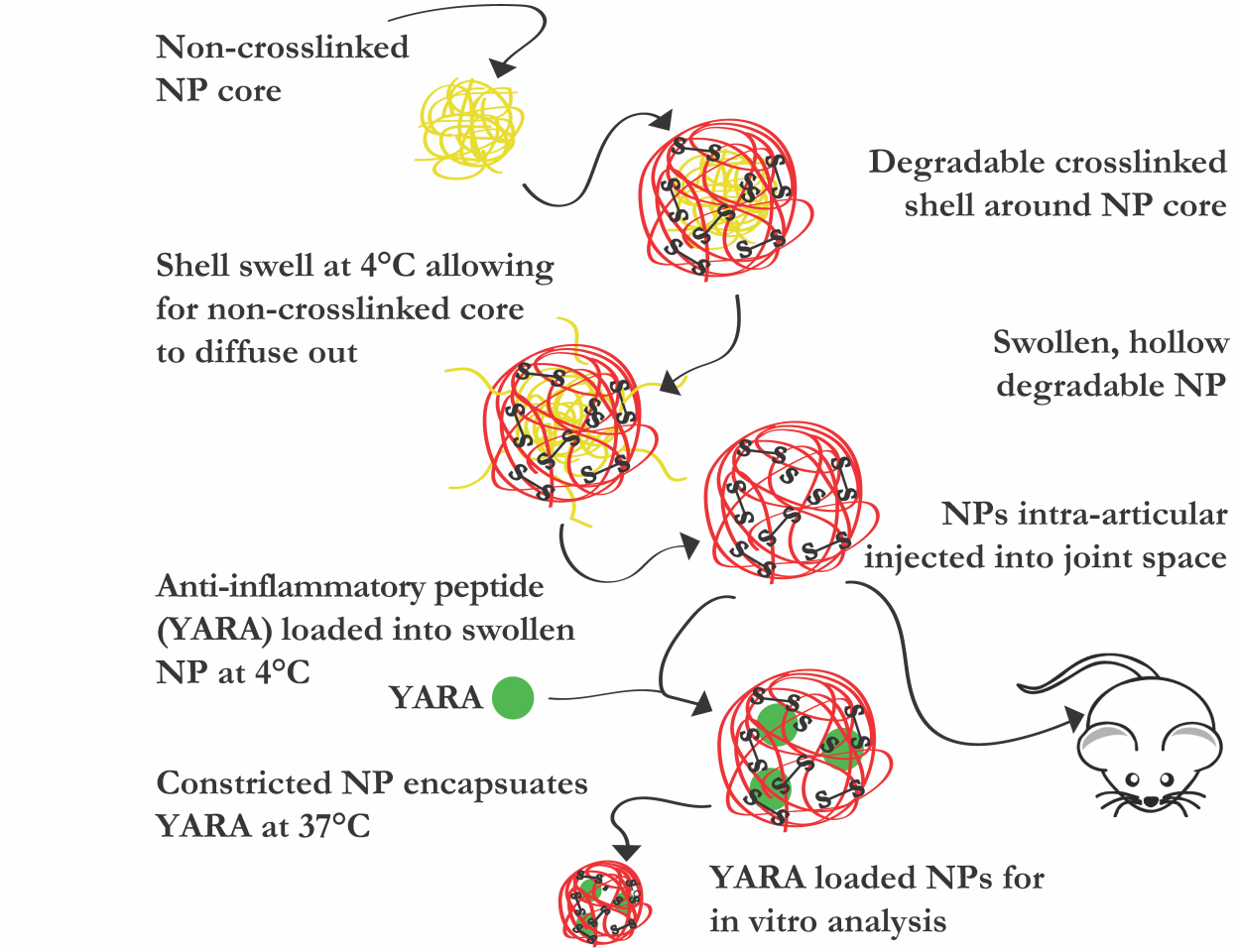

Figure 2.1: Graphical representation of reported studies. Diffusion of pNIPAm chains diffuse out of poly(NIPAm-co-AMPS-AAc-BAC) shell to generate hollow, thermoresponsive, degradable nanoparticle to load anti-inflammatory YARA for *in vitro* studies and *in vivo* delivery.

three times with 1x PBS. In 2.5 ml increments, shaved cartilage was added to 25 ml of Dulbecco's Modified Eagle Media (FBS DMEM)/F12 containing 0.1% bovine serum albumin, 0.2% w/v collagenase P, 100 units/ml penicillin, 100 μg streptomycin, and 3% FBS), then incubated at 37°C for 2 h. Released chondrocytes were filtered through sterile 70 μm cell strainer and centrifuged at 1,000 RPM for 5 min. The supernatant was removed and the pellet re-suspended in 10 ml of 10% FBS DMEM/F12. The centrifugation and resuspension were repeated three times. Chondrocytes were counted and plated at 20,000 cells/cm^2 at 37°C and 5% CO_2 in a humidified incubator. Initial media was changed after 24 h. All

chondrocytes were used between passage 2 and 6.

2.3.2 Materials

N-isopropyl acrylamide (NIPAm, $\geq$ 98%), N,N′-Bis(acryloyl) cystamine (99%, BAC), N, N′-methylene-bis-diacrylaminde (MBA), sodium dodecyl sulfate (SDS; 20% w/v in water), 2-acrylamido- 2-methyl-1-propanesulfonic acid (99%, AMPS), dithiothreitol (98%, DTT), fluorescein o-acrylate (98%, FL), rhodamine B isothiocyanate (98%, RBITC), ethanol (99.5%, EtOH), N-diisopropylethylamine (99%, DIPEA), potassium persulfate (99%, KPS), trifluoroacetic acid (TFA), and dimethyl sulfoxide (DMSO) were acquired from Sigma Aldrich (St. Louis, MO). Dimethylformamide (DMF), dichloromethane (DCM), acetonitrile (ACN), trifluoroacetic acid (TFA), triisopropylsilane (TIPS), and phenol were purchased from Thermo Fisher (Waltham, MA). Dialysis membrane tubing was purchased from Spectrum Laboratories (Dominguez, CA). NIPAm and BAC were stored under nitrogen at 4°C and -20°C, respectively. AMPS was stored at room temperature in a desiccator. All water used in synthesis, dialysis, and testing was treated by a Millipore milliQ system (Billerica, MA; 18.2 MΩ·cm resistivity).

2.3.3 Nanoparticle Synthesis

Solid Particles: Solid NPs (sNPs) were synthesized via precipitation reaction by dissolving 794.7 mg NIPAm, 78.0 mg AMPS, 48.2 mg BAC, 4.81 μl AAc, and 164 μl of a 20% SDS solution in 5 ml milliQ water into the reaction flask. After 15 min, 33.7 mg KPS dissolved in 2 ml milliQ water was injected into the reaction flask, still under nitrogen blanket, and refluxed at 70°C for 4 hours. sNPs were allowed to equilibrate to room temperature before purification.

Hollow Particles: The nanoparticle (NP) core-shell complex was polymerized via precipitation reaction. The NP cores were synthesized by dissolving 394.5 mg NIPAm in 3 ml milliQ water in a scintillation vial and injecting it into a 100 ml three-neck flask under reflux

and a nitrogen blanket with 35 ml milliQ water and 164 μl of a 20% SDS solution at 70°C. Following a 15 min equilibration time, 67.4 mg KPS dissolved in 2 ml milliQ water was injected into the reaction flask to initiate the core polymerization, which continued for 2 h. NP cores were exposed to atmospheric oxygen for 45 min to terminate free-radical polymerization followed by a 15 min nitrogen purge. The NP shells were polymerized around the cores by injection of 794.7 mg NIPAm, 78.0 mg AMPS, 48.2 mg BAC, 4.81 μl AAc, and 164 μl 20% SDS dissolved in 5 ml milliQ water into the reaction flask. After 15 min, 33.7 mg KPS dissolved in 2 ml milliQ water was injected into the reaction flask, still under nitrogen blanket, and the mixture was refluxed at 70°C for 4 hours. Following polymerization, pre-dialysis NP (pd-NP) core-shell solution was allowed to equilibrate to room temperature before purification via transverse flow filtration (TFF). To remove core polymer by diffusion, half of each lyophilized, TFF-purified pd-NP batch was dissolved in 50 ml of milliQ water and dialyzed in 10 kDa dialysis tubing (Spectrum Laboratories, Dominguez, CA) at 4°C for 14 days; milliQ water was changed daily. Following dialysis, the now hollow NPs (hNPs) were frozen and lyophilized. Each batch was placed in opaque coverings during dialysis and lyophilization to prevent photobleaching.

Varying Crosslink Density: sNP and hNP batches with differing crosslink density were used for drug loading and release studies. Varying amounts of BAC were added to the NP reaction mixture [24.1 mg BAC (0.5x NPs), 48.2 mg BAC (1x NPs), and 96.4 mg BAC (2x NPs)] for polymerization into the shells and solid particles (nomenclature in Table 2.1) via respective methods for sNP and hNP listed above to investigate the role of crosslink density on therapeutic loading and release.

Fluorophore Incorporation: For FL-core NP batches, 0.1 mol% FL dissolved in 1 ml DMSO was injected after initial NIPAm and SDS injection, then core polymerization was initiated, creating the fluorescently-labeled co-poly(NIPAm-FL) core. For RBITC-shell NP batches, 0.1 mol% RBITC dissolved in 1 ml DMSO was injected following NIPAm, AMPS, BAC, AAc, and SDS addition and before shell polymerization initiation, resulting

in fluorescently-labeled co-poly(NIPAm-AMPS-AAc-BAC-RBITC) shells formed around the core. Each NP batch was synthesized three times for experimental replicated, and tested three times for technical replicates. All nomenclature for the various batches is shown in Table 2.1.

Non-degradable Fluorescent Particles: Non-degradable particles were synthesized via the same fluorophore incorporation protocol as described above, except using non-degradable crosslinker N, N′-methylenediacrylaminde (MBA) instead of BAC to generate non-degradable co-poly(NIPAm-AMPS-AAc-MBA-RBITC) (sNPsRBITC-MBA) particles.

Table 2.1: Nanoparticle Fluorophore Nomenclature

	Pre-Core Removal	**Post Core Removal**
Unlabeled Core, Unlabeled Shell	NP	hNP
FITC Core, Unlabeled Shell	NPcFITC	hNPcFITC
Unlabeled Core, RHB Shell	NPsRHB	hNPsRHB
FITC Core, RHB Shell	NPcFITCsRHB	hNPcFITCsRHB
	Solid	**Hollow**
24.1 mg BAC	0.5x sNP	0.5x hNP
48.2 mg BAC	1x sNP	1x hNP
96.4 mg BAC	2x sNP	2x hNP
	RBITC Labeled Shell	
Degradable Fluorescent	hNPsRBITC-BAC	
Non-Degradable Fluorescent	sNPsRBITC-MBA	

2.3.4 Nanoparticle Purification

All sNP batches were purified using tangential flow filtration (TFF), KR2i from Spectrum Laboratories (Dominguez, CA), equipped with 10 kDa filter. sNPs and pd-NPs were filtered against 18.2 MΩ·cm resistivity until 100 ml of permeate was collected. Following purification, respective particle batches were frozen, lyophilized, and stored at room temperature. During all times, NPs were covered to prevent photo-bleaching.

2.3.5 Nanoparticle Characterization

During the 45 min oxygen purge following core polymerization, 1 ml of reaction solution was analyzed using dynamic light scattering (DLS) on Nano-ZS90 Zetasizer (Malvern, Westborough, MA) at 70°C to size the cores.

Following purification and lyophilization, sNP and pd-NP batches were respectively dissolved at 1 mg/ml in milliQ water, and subjected to temperature sweeps from 18.0°C – 42.0°C, in 1.5°C increments, equilibrating for 3 min between each step, and measuring three times per step using DLS. The same procedure was followed for hNPs after dialysis to obtain their physical characteristics. Zeta (ζ)-potential was obtained on a Nano-ZS90 Zetasizer at 1 mg/ml sample concentration in milliQ water at 18.0°C and 24.0°C using folded capillary cells. All temperature trends and ζ-potential measurements were run in experimental and technical triplicate.

2.3.6 Flow Cytometry

Confirmation of core removal was performed using pd-NPs with cores labeled with 0.1 mol% FL. Pd-NPs and hNPs were analyzed using Attune NxT Flow Cytometry (Thermofisher Scientific, Rockford, IL) to quantify the absorbance of the NPs before and after dialysis across all batches. The Attune flow cytometer with YL2 and BL1 lasers set to 225 mV assessed pd-NP and hNP fluorescence. Samples of each pd-NP and hNP batch were prepared at 1 mg/ml. The Attune flow cytometer pulled 150 μl of each solution at 150 μl/min and record the fluorescence; two rinses between samples and 1 ml of focusing fluid were flushed through to prevent potential contamination. Flow cytometry data was analyzed using FlowJo software.

2.3.7 Drug Loading & Release

One mg of each sNP and hNP batch were dissolved with 2 mg YARA in 1 ml ethanol (EtOH), incubated for 24 h at 4°C or 42.0°C for drug loading. Following incubation, loaded

sNPs/hNPs were centrifuged at 17,000 g for 90 min and 500 μl of the supernatant was collected, centrifuged again for 90 min at 17,000 g, then 300 μl of that supernatant was collected for post-load analysis to quantify remaining unloaded peptide using a C18 reverse phase column on a high-performance liquid chromatography (HPLC). Respectively, 1 ml of milliQ water was added to loaded sNP and hNP to resuspend them prior to freezing and lyophilizing.

Drug release was measured by dissolving loaded sNPs and hNPs, respectively, at 1 mg/ml in 1x PBS and incubating in a shaker at 37°C and 200 RPM. For all time points, the solution was centrifuged for 10 min at 17,000 g, 500 μl of solution was removed and replaced with 500 μl of fresh 1x PBS, and frozen. Drug release was quantified using reverse phase HPLC. Briefly, 300 μl/ml supernatant from respective time-points was thawed and analyzed for peptide content.

2.3.8 Nanoparticle Degradation

In vitro degradation using glutathione: 1x hNPs were dissolved at 500 μl/ml in solutions of: 10 mM glutathione (GSH) pH 5.2, 0.01 mM GSH, pH 7.2, and ultrapure water pH 7.2 to mimic intracellular (intra) and extracellular (extra) GSH concentrations, respectively, with water serving as the control. Dynamic light scattering measurements were taken using a Nano-ZS90 Zetasizer (Malvern, Westborough, MA) at 37°C from samples collected at Day 0, 1, 3, 5, 7, and 9 to obtain the respective diameter, PDI, and particle size distribution.

TEM: One mg of 0.5x, 1x, or 2x hNPs was dissolved in 1x PBS or 1 mM DTT, and mixed at 37°C at 200 RPM. Daily, the solutions were centrifuged at 17,000 g for 10 min, 0.5 ml of the supernatant was removed, and then 0.5 ml of fresh solution was added. Ten μl of each suspended NP treatment was adsorbed onto 400 mesh copper grids for 10 min, then excess solvent was removed. Mesh grids were stained with 2% urinal acylate for 10 sec and immediately blotted to remove excess solution. Samples were then analyzed using transmission electron microscopy (TEM) (F.E.I. Company, Hillsboro, OR) at the UC Davis

core facility.

2.3.9 Peptide Synthesis & Purification

YARAAARQARAKALARQLGVAA (YARA) was synthesized using a CEM Liberty Blue Peptide Synthesizer (Matthews, NC). Briefly, FMOC protected L-amino acids were individually dissolved in synthesis grade DMF to yield 0.2 M solutions. Rink-Amide (Sigma Aldrich, St. Louis, MO) resin was added to the reaction vessel of the CEM Liberty Blue peptide synthesizer. Synthesis occurred at 90°C for 4 – 30 min per amino acid, time varying for each amino acid. YARA was cleaved from the Rink-Amide resin using 2 ml of a cleavage cocktail (4.4 ml TFA, 0.25 ml phenol, 0.25 ml milliQ water, and 0.10 ml TIPS) for 3 h, precipitated with 0°C diethyl ether, centrifuged at 1,000 g for 5 min four times, and dried overnight at room temperature. YARA was purified using reverse phase fast-protein liquid chromatography (FPLC). Quantification of molecular weight was assessed using Matrix Assisted Laser Desorption/Ionization – Time of Flight (MALDI-TOF) mass spectroscopy.

2.3.10 *In Vitro* Nanoparticle Update, Clearance, & Imaging

Chondrocytes were seeded at 30,000 cells/cm^2 into 24-well IBIDI cell culture plate and incubated for 24 h at 37°C. Media was removed and frozen for later analysis, then cells were washed three times with Hank's Balanced Salt Solution (HBSS) followed by addition of 400 μl of: media (n = 6), 400 μl of media containing 2 mg/ml of degradable hNPsRBITC-BAC (n = 6), or 2 mg/ml of non-degradable sNPsRBITC-MBA (n = 6) to the respective wells and cells were incubated for 24 h at 37°C. Following incubation, media was aliquoted and frozen, then all wells were washed three times with HBSS then 400 μl of 75 nM Lysotracker Blue DND-22 in media (ThermoFisher Waltham, MA) was added to each well and incubated for 45 min at 37°C under low light conditions. Each well was washed with HBSS and imaged. Following imaging, 400 μl of fresh FBS DMEM media replaced HBSS. Brightfield and fluorescent images were collected daily for 8 days; Lysotracker Blue DND-22 was only

imaged after day 1. For all images, wells were washed three times and imaged in HBSS, then HBSS was replaced with fresh FBS DMEM media. All confocal images, brightfield, Lysotracker Blue DND-22 (excitation: 373 nm, emission: 422 nm), and RBITC (excitation: 570 nm, emission: 623 nm), were taken using FV3000 Confocal Laser Scanning Microscope (Olympus, Tokyo, Japan) at 60x magnification. The fluorescence of the aliquoted media was analyzed using Spectramax M5 to quantify of RBITC in media (excitation: 570 nm, emission: 623 nm).

2.3.11 Nanoparticle Cytotoxicity

CellTiter Aqueous One assay was used to assess the cytotoxicity of all YARA loaded nanoparticles. Briefly, the respective batches of sNPs and hNPs were loaded as described previously. Chondrocytes seeded at 20,000 cells/cm^2 into a 96-well plate were incubated for 24 h at 37°C at 5% CO_2. Nanoparticles were added at a concentration of 2, 4. 6, 8, 10, and 12 mg/ml for a total volume of 150 μl to each well, n = 4 per treatment; cells treated only with FBS DMEM media served as the control and were incubated for 24 h. Each well was washed three times with PBS, and 100 μl of fresh FBS DMEM media plus 20 μl of CellTiter Aqueous One (Promega, Madison, WI) added to each well and incubated for 3 h at 37°C. Absorbance of each well was measured using a Spectramax M5 plate reader according to manufacturer's protocol.

2.3.12 *In Vitro* Inflammatory Stimulation & Cytokine Analysis

CellTiter Aqueous One assay was used to assess the cytotoxicity of all YARA loaded nanoparticles. Briefly, the respective batches of sNPs and hNPs were loaded as described previously. Chondrocytes seeded at 20,000 cells/cm^2 into a 96-well plate were incubated for 24 h at 37°C at 5% CO_2. Nanoparticles were added at a concentration of 2, 4. 6, 8, 10, and 12 mg/ml for a total volume of 150 μl to each well, n = 4 per treatment; cells treated only with FBS DMEM media served as the control and were incubated for 24 h. Each well was

washed three times with PBS, and 100 μl of fresh FBS DMEM media plus 20 μl of CellTiter Aqueous One (Promega, Madison, WI) added to each well and incubated for 3 h at 37°C. Absorbance of each well was measured using a Spectramax M5 plate reader according to manufacturer's protocol.

2.3.13 *In Vivo* Nanoparticle Retention

Following acclimation, 10-week old Fisher 344 rats purchased from Envigo (Huntingdon, UK) were anesthetized with isoflurane and hair was removed from both rat knees. Next, 150 μl of 2.0 mg/ml hNPsRBITC in PBS (n =5) or 150 μl PBS alone for negative control (n = 3) was injected into their left joint space, with the right joint serving as the untreated control. Rats were imaged and fluorescence intensity measured using an In Vivo Image System (IVIS) at the UC Davis Center for Molecular and Genomic Imaging (CMGI) at 557 nm excitation and 623 nm emission. IVIS was used to examine the fluorescence of hNPsRBITC and to quantify the presence of the fluorescent hNPsRBITC within rat joints with timepoints taken: immediately prior to injection, immediately after injection, daily for seven days, and immediately following dissection. Rats were imaged daily for 7 days then sacrificed using CO_2 euthanasia. The hind limbs were dissected and imaged again to verify successful injection into the joint space. Total radiance emission (TRE) fluorescence was collected and analyzed.

2.3.14 Statistical Analysis

Paired student's t-test was used to analyze significant difference between particle diameter for the various batches listed in Table 2.1 in Table S2.2 and Table S2.3 see Figure S2.10. Paired student's t-test was also used to assess the statistical difference between daily TRE measured in PBS and hNPsRBITC treated knees *in vivo*; $p < 0.05$. Two-way multi-comparison ANOVA was used to access differences in treatments for *in vitro* IL-6 knockdown, $p < 0.05$, as well as the TRE *in vivo* significant difference pre- and post-injection. Data is

expressed as mean values ± standard deviation unless otherwise noted. Each batch of NPs was synthesized in experimental triplicate and each experimental run in technical triplicate, unless otherwise stated.

2.4 Results & Discussion

2.4.1 Nanoparticle Synthesis & Characterization

Poly(NIPAm) (pNIPAm) has an LCST of approximately 32°C, where it transitions between a hydrophilic (swollen) phase below its LCST, and a hydrophobic (collapsed) phase above its LCST. Wide-spread investigation of pNIPAm and its derivatives in biomedical applications include: drug delivery triggered by reactive oxygen species[19], tumor-cell imaging[20], gram positive bacteria detection[21], controlled release of biomolecules[22], and delivery of macromolecular therapeutics[23,24], and are due in large part to the tunability of the LCST near physiological temperature. Numerous micro- and nanoparticles exploit the thermoresponsive behavior of pNIPAm to form core-shell particles with metallic[25–31], inorganic[32–36], or polymer cores[14,37–41] and polymeric shells. Of the mentioned thermoresponsive particles, only those synthesized around inorganic cores (IC) or polymer cores (PC) form hollow particles, with a majority of the hollow particles being derived from those with inorganic (e.g. silica) cores. However, current core removal processes require the use of solvents; ICs were degraded using 0.05 M NaOH[32,35] or hydrofluoric acid[33,34], and PCs were degraded with either: 1 mM DTT[14], chloroform[38], tetrahydrofuran (THF)[40], or etched out using sodium carbonate[39]. These core degradation methods introduce additional solvents necessitating further purification and have the potential to modify the particle. Rather than use additional solvents, here we exploited the LCST of pNIPAm to generated non-crosslinked, removable pNIPAm cores, around which a crosslinked poly(NIPAm-co-AMPS-AAc-BAC) shell was polymerized to create particles with low-polymer density centers, termed hollow NP (hNP), for loading and release of cationic CPPs.

Polymerized non-crosslinked pNIPAm readily forms 50 – 60 nm particle cores and poly(NIPAm-FL) chains form 80 – 100 nm cores above their LCST (70°C) and dissociate when temperature is dropped to below the LCST, Table S2.2. Polymerizing poly(NIPAm-co-AMPS-AAc-BAC) or fluorescently-labeled poly(NIPAM-co-AMPS-AAc-BAC-RBITC) shells around these cores at 70°C allowed for formation of stable particles from which the non-crosslinked core can be removed via diffusion.

All pre-dialyzed and hollow nanoparticle batches (nomenclature is listed in Table 2.1) were sized using DLS and ζ-potential was evaluated to investigate the effect of fluorophore incorporation into the polymer backbone on size and the charge at the surface of the nanoparticles, Table S2.2. Previously, fluorescein O-acrylate (FL) was polymerized into crosslinked poly(NIPAm-co-BAC-FL) cores to track core removal, and was also polymerized into the shell of primarily pNIPAm particles to track endocytosis into macrophages or bovine chondrocytes, but this study did not show the effect of FL on particle size[14–16,37]. Here, FL was polymerized into the core to verify core-shell formation and core removal. DLS measurements show that FL incorporation caused a 63.26% increase in core diameter, Table S2.2. After shell polymerization around the FL core, pd-NPcFL were 49.22% and 55.77% larger than pd-NP at 18.0°C and 42.0°C respectively, while hNPcFL exhibited a 49.60% at 18.0°C and 47.56% at 42.0°C increase compared to hNP, Figure 2.2 and Table S2.2. This suggests that FL either affects particle size sterically or through altered hydrophobic interactions of the pNIPAm chains. RBITC was polymerized into the shells to validate shell formation around FL-labeled cores, rather than simply new NP formation, and caused the size of both pd-NPsRBITCs and hNPsRBITCs to increase as shown in Figure 2.10 and Table S2.2; when compared to unlabeled pd-NPs, the pd-NPsRBITCs had a 32.21% at 18.0°C and 31.02% at 42.0°C increase in size and the hNPsRBITC increased 30.62% at 18.0°C and 28.48% at 42.0°C compared to hNP. The dual labeled pd-NPcFLsRBITC/hNPcFLsRBITC batch followed the same trend, increasing both core size and shell size, but not altering the pd-NPcFLsRBITC nor hNPcFLsRBITC thermosensitive behavior, Figure 2.2 and Table

S2.2. While the fluorophores did increase the relative size of the core, shell, and core-shell complex, these data serve as excellent indicators of both core removal and core-shell particle formation.

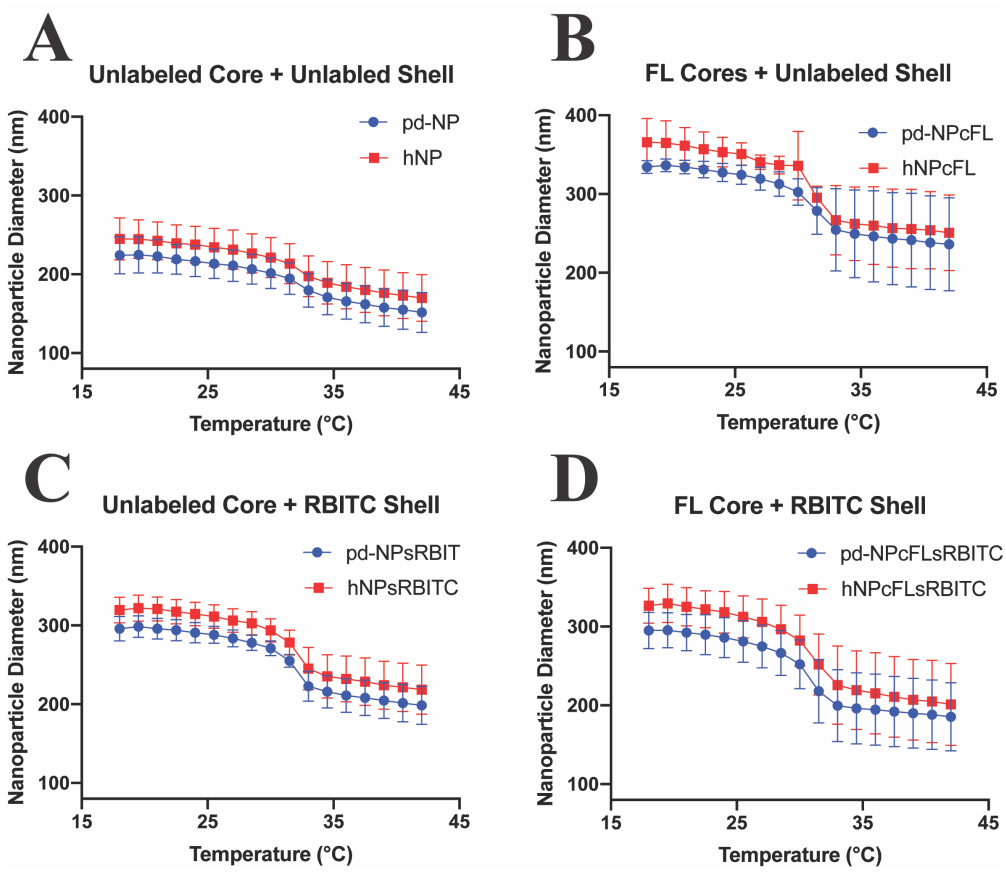

Figure 2.2: DLS hydrodynamic diameter temperature sweep from 18.0°C – 42.0°C of pre-dialyzed (blue) and hollow (red) nanoparticle batches. Each batch was synthesized three times, and each synthesis tested three times. A) Unlabeled Core + Unlabeled Shell; B) FL-labeled Core + Unlabeled Shell; C) Unlabeled Core + RBITC-labeled Shell; D) FL-labeled Core + RBITC Labeled Shell. Statistical size difference between the various nanoparticle batches is displayed in Figure S2.10

Interestingly, all hNP batches were slightly larger than their pd-NP and sNP counterparts. This is believed to be due to the non-crosslinked chains from the core diffusing out of the particles and leaving increased space for shell polymer chain rearrangement, which perhaps increases chain mobility and supports particle swelling. The characteristics match previously published work where the hNPs were shown to be larger than sNP counterparts[14,32,35,39,42].

A majority of the hNPs reported had a diameter greater than 300 nm[14,32,34,35,37,38,42], and particles larger than 200 nm have been shown to initiate an inflammatory response[43], thus our goal was to develop a method to repeatedly produce particles that maintained a size below 200 nm when delivered at 37°C.

Particles with ζ-potential values between -20 to -30 mV are considered moderately stable and -30 mV or lower are highly stable[44]. All pd-NPs, hNPs, and sNPs presented here were colloidally stable with ζ-potential -25 to -35 mV, except for pd-NPcFLsRBITC. pd-NPcFLsRBITC exhibited a ζ-potential of -4.51 ± 0.63 mV and was considered unstable[44]. Surprisingly, hNPcFLsRBITC was colloidally stable with a ζ-potential of -24.54 ± 9.42 mV, suggesting the interaction between FL and RBITC fluorophores partially masked the negative charge from the sulfate groups at the particle surface and the removal of the pNIPAm-FL core restored the surface presentation of sulfate groups. All hNPs had a more negative ζ-potential than their pre-dialyzed counterparts, further substantiating the claim that the shell polymer chains are better able to rearrange, resulting in increased surface charge following core removal. The size, polydispersity, and ζ-potential of the various NPs are listed in Table S2.2 and Table S 2.3 above and below their LCST at 18.0°C and 42.0°C. Importantly, the increased negative ζ-potential of the particles presented here, as compared to previous versions reported by our laboratory, has improved colloidal stability and facilitated improved loading of CPP, particularly the highly specific MK2 inhibitor peptide YARA. Statistical size difference between the various nanoparticle batches is displayed in Figure S2.10A.

Further attesting to the robust synthesis method, the polydispersity (PDI) of the particles was found to be low. The PDI recorded by DLS is a measure of size uniformity, and a PDI < 0.1 is considered to indicate that a particle population is monodisperse[44]. All particle batches presented here were shown to be monodisperse, Table S2.2. Overall, the synthesis methods was shown to produce particles of repeatable and uniform size[14,38].

2.4.2 Dialysis of Nanoparticles & Core Removal Quantification using Flow Cytometry

Following particle synthesis, suspending the pre-dialyzed core-shell particles in an aqueous environment at 4°C supported particle swelling, which in turn allowed the non-crosslinked pNIPAm chains within the core to diffuse from the particle to generate hNPs. Removal of the non-crosslinked core was quantified using: DLS, TEM, and, for the first time to our knowledge, flow cytometry.

For analysis by flow cytometry, particles were maintained below the LCST, in their swollen state, to ensure that they were larger than 200 nm (the minimum size detectable by the flow cytometer). The data presented in Figure S2.11 shows the emergence of a secondary, FL-negative population in hNPcFL compared to the FL-positive pd-NPcFL batch as a result of the core polymer chains diffusing through the crosslinked shell, albeit not completely. At moderate to low monomer to initiator ratio, NIPAm is known to self-crosslink, however here a significantly higher monomer to initiator ratio was used limiting self-crosslinking of NIPAm[45]. The reason full core removal is not observed is likely due to a combination of: some NIPAm self-crosslinking occurring, physical entanglement between the non-crosslinked poly(NIPAm-co-FL) chains and crosslinked poly(NIPAm-co-AMPS-AAc-BAC) shell, and steric hinderance. However, there is a clear emergence of a secondary FL-negative population demonstrating that the majority of poly(NIPAm-co-FL) diffuses from the core-shell particle complex, Figure S2.11. Additional analysis via flow cytometry, Figure S2.11, showed pd-NPsRBITC and hNPsRBITC were unaffected by the dialysis, indicating dialysis does not affect the particle shell. Flow cytometry results confirmed the majority of core removal was achieved after 14 days of dialysis.

2.4.3 Core-Shell Nanoparticle Formation - Confirmed with Flow Cytometry

To verify the intended shell formed around the existing cores rather than forming new particles separate from the cores, RBITC-labeled shells were polymerized around FL-labeled

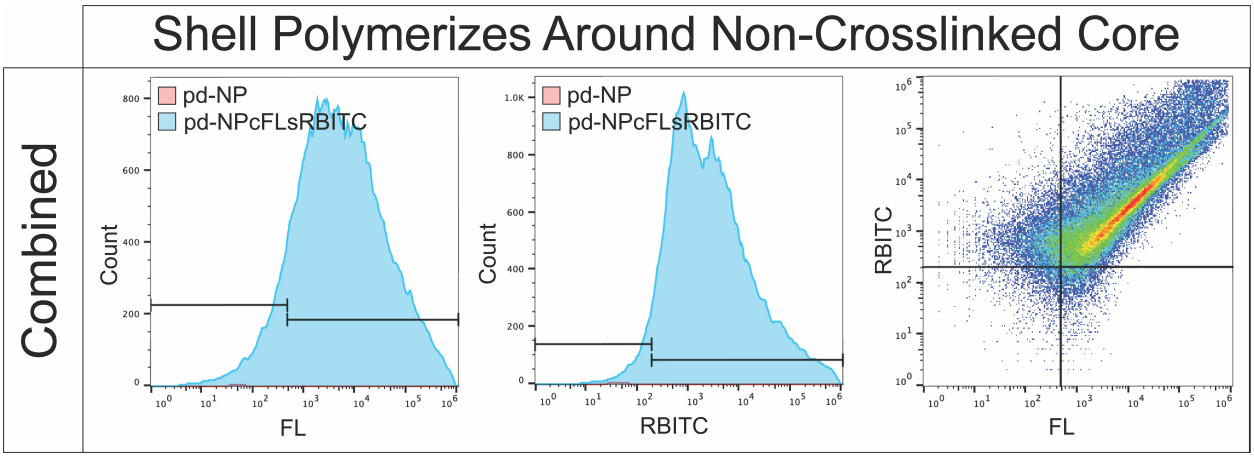

Figure 2.3: Flow cytometry confirms RBITC labeled crosslinked shells primarily polymerize around FL-labeled non-crosslinked cores forming a single nanoparticle core-shell complex, rather than two distinct particles.

cores (pd-NPcFLsRBITC). The data in Figure 2.3 shows the existence of minor particle populations that only contain FL (core) or RBITC (new particles), but a major core-shell complex population existed within pd-NPcFLsRBITC batch (count 44,387) compared to unlabeled particle batch (count 1,292) confirming a relatively pure population of core-shell particles for further study. Further, confirmation that the core polymer was removed during the 14 days of dialysis support the use of unlabeled particles for evaluating drug release and *in vivo* function as ultimately, unlabeled particles would be used for *in vivo* drug delivery.

2.4.4 Drug Loading & Release from Nanoparticles of Varying Crosslink Density

Unlabeled hNPs and sNPs were synthesized with various amounts of BAC (0.5x NPs, 1x NPs, and 2x NPs) to assess the benefits of hollow vs. solid nanoparticles as well as the effects of crosslink density on particle swelling and drug loading and release, nomenclature shown in Table 2.1. The size of each sNP, pd-NP, and hNP batch of varying crosslink density and physical characteristics (ζ-potential, and PDI data) are shown in Figure 2.4, Figure S2.12, and Table S2.3, respectively, with the statistical size differences between sNPs and hNPs displayed in Figure S2.10B.

As expected, at lower crosslink density hNPs show increased overall diameter compared to their pd-NP counterparts and as compared to corresponding sNPs for all batches. The 0.5x particles exhibited the greatest increase in diameter with hNPs being 18.73% at 18.0°C and 19.91% at 42.0°C larger than 0.5x pd-NPs. There was an evident, but lesser, size difference in the 1x particles, with 1x hNPs being 9.32% at 18.0°C and 12.16% at 42°C larger than 1x pd-NPs. Noticeably, the 2x pd-NP and hNP exhibited similar sizes across the temperature profile, with only 0.32% difference at 18.0°C, and 2.36% difference at 42.0°C respectively; showing that increasing the crosslink density affects NP swelling, Figure S2.12 and Table S2.3. Comparing sNPs and hNPs, the 0.5x hNPs were 40.09% at 18.0°C and 20.41% at 42.0°C larger than 0.5x sNPs; 1x hNPs were 20.47% at 18.0°C larger than sNPs, but were statistically identical at 42.0°C; 2x hNPs were 36.67% at 18.0°C and 11.26% at 42.0°C larger than 2x sNP counter parts, Figure 2.4 and Table S2.3, and statistics displayed in Figure S2.10B.

While the authors are unaware of studies investigating drug loading and crosslink density on hollow, thermosensitive nanoparticles, Bartlett et al. found increasing crosslink density for poly(NIPAm)-based particles decreased the size of the particle uniformly both above and below the LCST of pNIPAm, agreeing with the findings presented here. However, their lower crosslink density poly(NIPAm)-based particles had a more positive ζ-potential and thus a lower charge to volume ratio, which Bartlett et al. believed caused lower drug loading. However, here the 2x hNPs have a more positive ζ-potential and load more peptide than the 2x sNPs, showing drug loading isn't solely dependent on particle charge, Table S2.3.

These data support the theory presented by Bartlett et al that increased drug loading is a result of increased crosslink density at lower crosslink densities, as shown in Figure 2.4 and Table S2.2, with the 0.5x loading the least amount of peptide. However, these data contradict that same theory as 1x NPs load more than their respective 2x NP counterparts suggesting that crosslink density, which is inversely related to polymer mesh size, can retard peptide loading by decreasing mesh size to a point where it interferes with peptide diffusion

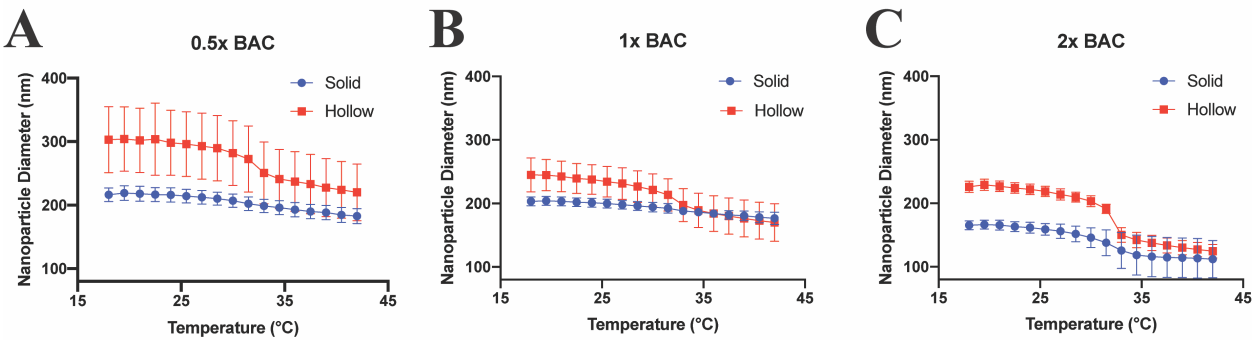

Figure 2.4: Lowering crosslink density increases swelling difference between solid (blue) and hollow (red) nanoparticles. DLS hydrodynamic diameter temperature sweep from 18.0 – 42.0°C of solid (blue) and hollow (red) nanoparticle with varying crosslink density. A) 24.1 mg BAC (0.5x NPs); B) 48.2 mg BAC (1x NPs); C) 96.4 mg BAC (2x NPs). Statistical size difference between the various nanoparticle batches is displayed in Figure S2.10B

into the particles.

Hypothetically, the sNPs and hNPs should load more YARA when swollen at 4°C, than when collapsed at 42°C, with hNPs loading more YARA than sNPs due to removal of the unsulfated core and decreased polymer density of the hNPs. To test this, 1,000 μg NPs and 2,000 μg YARA were dissolved in 1 ml EtOH at either 4°C or 42°C. Below the LCST of pNIPAm at 4°C, 0.5x sNPs and hNPs loaded 14.3% and 19.2% of YARA respectively, while only loading 0.0% and 5.2% above its LCST at 42°C, respectively, Figure 2.5, Figure S2.13, and Table S2.3. Interestingly, the 1x hNPs loaded the most YARA above and below the LCST when compared to 0.5 and 2x hNP and sNP; loading 57.4% at 4°C and 24.6% at 42°C. The 1x sNPs also loaded more YARA below the LCST, 25.3% at 4°C and 8.7% at 42°C as compared to 0.5x and 2x sNP. Consistent with 1x hNPs, the 2x hNPs, both above and below the LCST, loaded more YARA than the 2x sNPs. The 2x hNPs loaded 42.1% below the LCST and 18.1% above their LCST, while 2x sNPs loaded 11.1% below the LCST and 8.7% above the LCST, Figure 2.5, Figure S2.13, and Table S2.3. The results also suggest that while mesh size is important, temperature, which will affect the strength of the ionic bonds between particle and peptide, also plays a role in peptide loading; at low temperatures

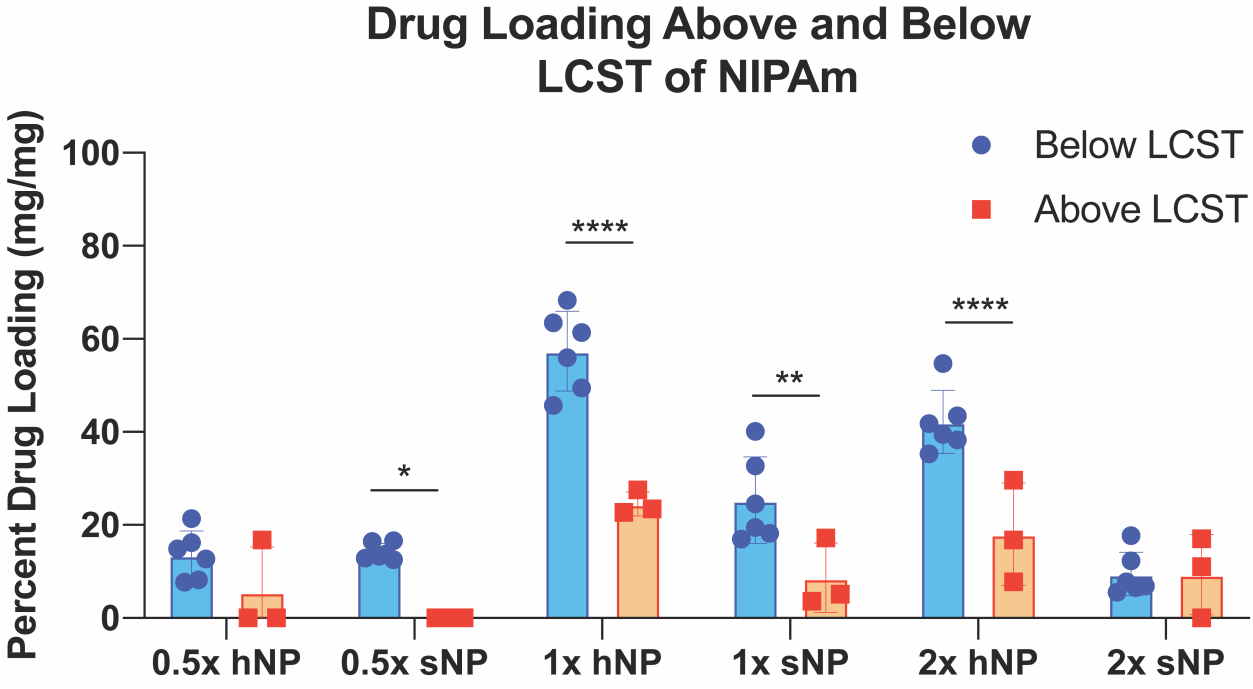

Figure 2.5: YARA loading into the primarily pNIPAm nanoparticles is dependent on temperature and crosslink density with 1x hNPs loading the most YARA above and below the LCST of NIPAm. Stats: * = $p < 0.05$, ** = $p < 0.01$, *** = $p < 0.0001$. Statistical differences between YARA loading between batches loaded at the same temperature shown in Figure S2.13

the expanded particles that support rapid peptide diffusion into the particle also support stronger polymer-peptide interactions and high loading. Previous studies only examined drug loading into the reported particles[14,39] or pNIPAm gels[46] below the LCST of pNIPAM, when the particles were swollen. Here we confirmed the hypothesis that more peptide is loaded into the nanoparticle when loaded below the LCST of NIPAm. However, these results also suggest the void space created by the removal of the core influences the amount of drug that is loaded into the particle, as confirmed by 0.5x and 1x hNPs loading more than their sNP counterparts. Of the six batches analyzed for drug loading, 1x hNPs loaded the most YARA below the LCST, Figure 2.5, Figure S2.13A, and Table S2.3. In summary, crosslink density, the thermoresponsive property of NIPAm, and loading temperature all play a role in drug loading.

Previous studies suggested that a portion of the loaded peptide became permanently entrapped in collapsed particles[14–16], and it was theorized that the peptide was stuck within the non-degradable high polymer density core. For this research, we hypothesized that lower density hNPs would support greater peptide release than sNPs. These data presented here support this hypothesis where all hNP batches release more YARA than the respective sNP counterparts, Figure 2.6. Notably, increasing crosslink density decreases the difference between hNP and sNP release, shown in Figure 2.6. The 0.5x hNPs release a higher percent of loaded peptide at any point compared to 0.5x sNPs; releasing 77.6% at the end of 5 days whereas sNPs release 43.5%. The 1x hNPs also continuously released more YARA than 1x sNPs, releasing 49.9% and 30.8%, respectively. The 2x particles showed the smallest difference in release when comparing hNPs to sNPs, releasing 48.2% and 40.5%, respectively.

All of the described sNPs and hNPs show continual sustained release at the conclusion of 5 days, but begin to plateau around day 3. However, as also seen previously, not all of the peptide is released at this timepoint. A limitation of this *in vitro* study is that the particles do not degrade in PBS, Figure S2.14, and therefore it is likely that total YARA release will occur within the cells as the NPs degrade completely via reduction of the disulfide bonds. In comparison to previous studies showing CPP release from thermosensitive particles, KAFAK-hNPs loaded 470 ± 18 mg of peptide and released 53% over 4 days, with 89% release happening within the first 12 hours,14 while here the 1x hNPs loaded 1147 ± 172 mg of YARA, and released roughly 24% within the first 12 hours, and 49.9% after 5 days. While previous hNPs were unable to encapsulate YARA, the comparisons between 1x hNP+YARA and previous 1x hNP+KAFAK[14], demonstrates an improved sustained release of a more specific MK2i CPP. Thus, the particles presented here appear to be preferable in situations where sustained, rather than a more burst-type release is necessary.

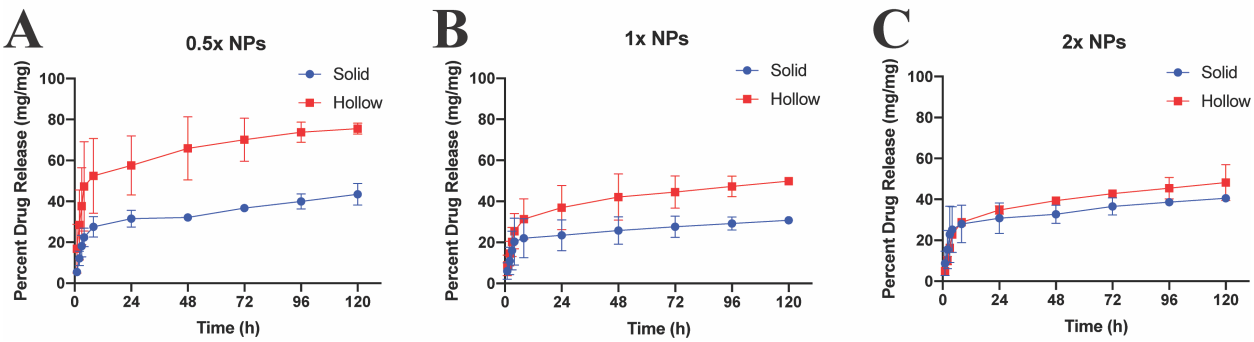

Figure 2.6: Sustained release of YARA from solid (blue) and hollow (red) nanoparticles of varying crosslink density at 37°C at 200 RPM for 120 hours. While controlled release of YARA is observed at all crosslink densities studied, the amount released at any timepoint is affected by crosslink density.

2.4.5 Degradation, Cytotoxicity, Uptake, and Clearance of Nanoparticles

Dithiothreitol (DTT) is a synthetic analog of glutathione (GSH) found naturally within the cytoplasm of cells.48,49 Glutathione reduces disulfide bonds and these nanoparticles exploit this ability for their breakdown and clearance from the cell. DTT was used *in vitro* to assess NP degradation. Each of the 0.5x hNP, 1x hNP, and 2x hNP batches show degradation in the presence of DTT as compared to PBS, Figure S2.14. The 0.5x hNPs degraded fully after 2 days, while the 1x and 2x hNPs had not fully degraded after 4 days, and exhibited different morphology and were present at a lower concentration, suggesting that some particles degraded more quickly than others, as compared to particles incubated in PBS alone.

Next, GSH was used to mimic the intracellular and extracellular environment to which nanoparticle are expected to be exposed, and degradation of the particles was assessed. The endosomal/lysosomal concentration of glutathione (GSH) is 10 mM and the pH 5, while the extracellular concentration of GSH is 0.01 mM at pH 7.2. The hNPs dissolved in 10 mM GSH show a significant increase in particle diameter (300% at Day 9) and particle distribution, Figure S2.15A/C, due to the disulfide bond being cleaved within the particle shell. Conversely, the diameter, distribution, and PDI of hNPs dissolved in extracellular

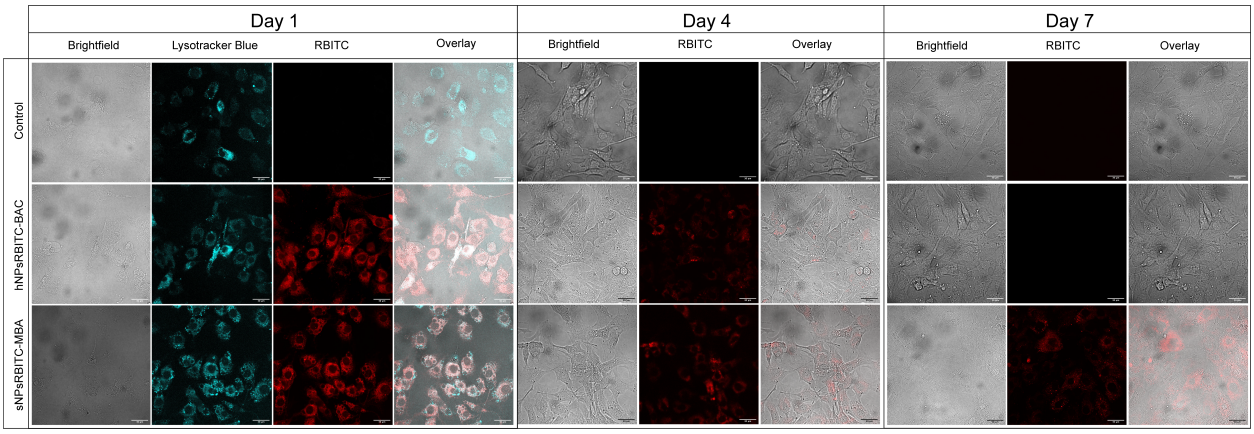

Figure 2.7: Chondrocytes endocytose hNPsRBITC-BAC and sNPsRBITC-MBA into the cytoplasm of the cells and BAC crosslinked particles were degraded/cleared from cells within 7 days. Daily images from day 1 through 8 shown in Figure S2.17. Scale bar: 30 μm.

concentrations of GSH and water remain relatively unchanged, Figure 2.15A/D/E, show the intracellular environment supports degradation via the cleavage of the disulfide bond within the BAC crosslinker. To the authors' knowledge, these fully degradable particles are unique among hollow pNIPAm particles. However, two studies using solid particles examined degradation[16,39], both of which exploited reducible disulfide crosslinkers. Complete degradation of pNIPAM-based particles is expected to be critical for complete drug release and possibly also for *in vivo* clearance of the particles or degraded polymer chains.

The *in vitro* cytotoxicity of 0.5x, 1x, and 2x sNPs and hNPs was accessed utilizing bovine chondrocytes. Shown in Figure S2.16, all sNPs and hNPs treatments were nontoxic compared to untreated control chondrocytes. This mirrors previous work were pNIPAm-incorporated particles were non-cytotoxic to chondrocytes,[16] macrophages[14,15], human hepatocellular carcinoma (HepG2) cells[30], and alveolar basal epithelial cells[47].

In order to knockdown the inflammatory response, YARA must be taken up into chondrocytes prior to its degradation. To evaluate uptake via endocytosis, RBITC-labeled nanoparticles were synthesized using degradable hNPsRBITC crosslinked with BAC (hNPsRBITC-BAC) and compared to non-degradable N, N'-methylenediacryl aminde (MBA) crosslinker

(sNPsRBITC-MBA). The hNPsRBITC-BAC and sNPsRBITC-MBA were respectively incubated with chondrocytes and compared to media control, Figure 2.7. As the endosome becomes more acidic, the environment is conducive to disulfide bonds cleavage51 and, in conjunction with glutathione, is believed to be responsible for the degradation of the nanoparticles. The majority of the hNPsRBITC-BAC particles were cleared from chondrocytes by Day 5, while the non-degradable sNPsRBITC-MBA particles were observable within the cell for the duration of the 8 day experiment suggesting that loss of fluorescence in cells treated with degradable particles is not due entirely to fluorescence quenching, or loss from oxidation, but from polymer removal from the cells. All images from Day 1 to 8 are shown in Figure S2.17. Additionally, the media was analyzed for RBITC; fluorescence was detected in the media from cells treated with hNPsRBITC-BAC only through day 5, while the media obtained from cells incubated with sNPsRBITC-MBA had no detectable RBITC following initial incubation, Figure S2.18. The data here agrees with previous work demonstrating that pNIPAm particles were endocytosed into chondrocytes,14–16 but shows the degradation/clearance of the BAC crosslinked particles from the cells. The chondrocyte data in conjunction with TEM data shows nanoparticle degradation as well as clearance from chondrocytes.

2.4.6 Inflammation Inhibition in Bovine Chondrocytes

IL-6 is an inflammatory cytokine that leads to the progression of OA. There are currently therapies for the prevention of IL-6 secretion, but they lack of specificity – knocking down other essential biological pathways[48]. Previously, a series of MK2i peptides were developed that are capable of knocking down proinflammatory cytokine production, including IL-6. While studies have examined the non-specific MK2i variant KAFAK encapsulation within particles, only two of the studies investigated the KAFAK-loaded particles with bovine chondrocytes[12,16]. Other studies either did not examine loaded-particle effect in cells[32,37,40], or investigated the effects on monocytes and macrophage cell lines[12,14,15]. Here we examine the specific peptide MK2i variant YARA, which leaves a multitude of crucial pathways un-

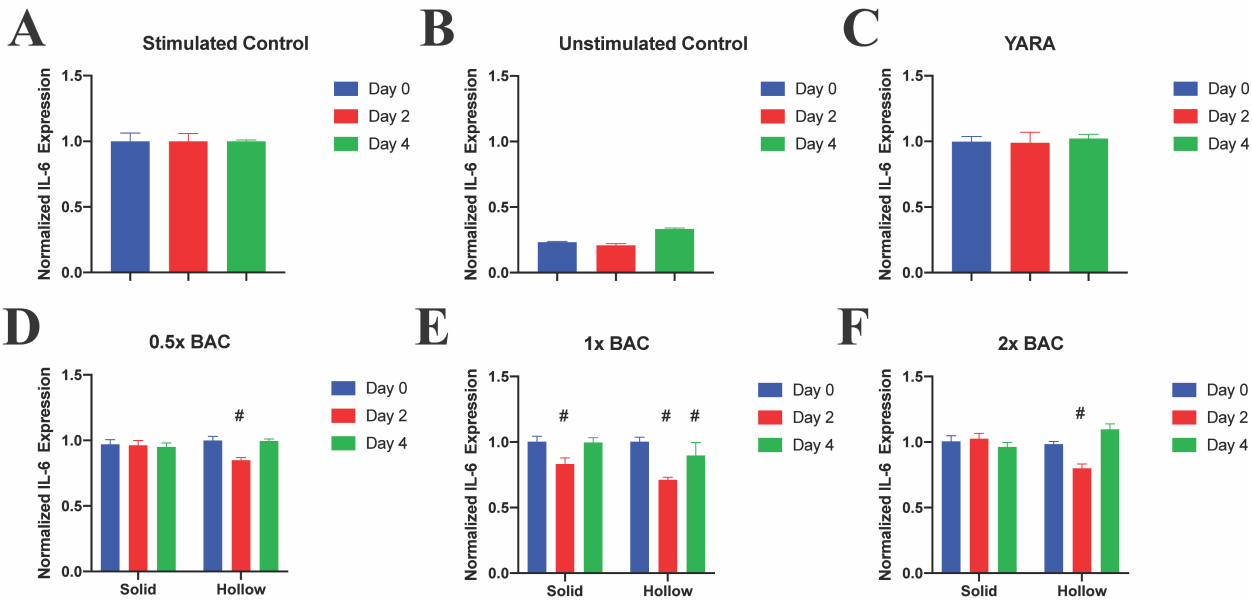

Figure 2.8: IL-1β-stimulated chondrocytes treated with sNP+YARA, hNP+YARA, or free YARA once on Day 2. All treatments significantly reduce IL-6 expression, with 1x hNPs reducing expression until Day 4, while free YARA did not alter IL-6 expression. Stats: # represents statistical significance compared to Day 0.

altered[10]. Chondrocytes were stimulated with IL-1β to induce inflammation as measured by IL-6 production, Figure 2.8A, or left unstimulated to serve as a baseline, Figure 2.8B. Following stimulation, chondrocytes were further stimulated with IL-1β (untreated control), Figure 2.8A, or treated with additional IL-1β plus 250 μM free-YARA, Figure 2.8C, or IL-1β plus NPs containing 250 μM YARA to analyze the suppression of IL-6 secretion induced by delivery of the YARA peptide Figure 2.8D - F. IL-6 production was detected in all control and treatment groups, Figure S2.19, and analyzed by normalizing, by day, to the unstimulated control of the same day and using a 2-way multi-comparison ANOVA. Notably, free YARA did not have a significant effect in reducing IL-6 expression (Fig. 7C), likely due in part to proteolytic degradation and in part due to impaired caveolae-induced endocytosis of YARA when cells are cultured on stiff polystyrene culture plates, demonstrating the advantage of using nanoparticle carriers. Of the six different nanoparticle treatments, only 1x hNP significantly reduced IL-6 production 2 and 4 days after a single treatment on Day

0, Figure 2.8E. The continual IL-6 knockdown is believed to be attributed to the sustained release of YARA from 1x hNPs shown in Figure 2.6 and degradation of the particle, Figure 2.7 and Figure S2.14, potentially allowing for full drug release. Combining increased drug release and slow particle degradation allows for prolonged peptide activity.

A single treatment of YARA-loaded NPs was used to fully assess the release of YARA into the cell. While these data presented does not show clinical relevance for IL-6 knockdown, it provides a basis for further studies. These data show 1x hNPs allow for the most YARA loading compared to the five other presented NP batches, in addition to being the only treatment to show significant IL-6 knockdown 4 days after the initial, single treatment. Future studies will build upon these data to optimize the dose and frequency of treatments to match unstimulated chondrocyte IL-6 secretion levels.

2.4.7 Intra-Articular (IA) Delivery of Nanoparticles into Rats Joint Space

IA injections support effective delivery with limited potential for systemic side-effects[49,50]. Numerous studies are underway involving IA injection, with a few focusing on micro- and nanoparticle treatments specifically for OA[49,50]. To assess the IA retention time of our particles, rats were injected with hNPsRBITC (n = 5) or 1x PBS (n = 3) as control. The rats injected with hNPsRBITC had 1004.72% increase in total radiant efficiency (TRE) following injection compared to the TRE prior to injection, where the PBS injected rats only saw a 9.04% TRE increase, Figure 2.9A, showing that increased TRE is due to RBITC within hNPsRBITC and there for a successful injection. The region of interest (ROI) was analyzed for all rats and all time points, Figure 2.9B, to quantify hNPsRBITC retention time. Analysis of the ROI over time demonstrated that the particles remain in the joint space for up to 7 days. The rat's hind limbs were dissected following sacrifice and imaged again to further confirmed the successful injection of hNPsRBITCs into the joint space, Figure 2.9C. Previous studies examined IA delivery of unbound therapeutics into the synovial space and showed retention time was less than 72 h[51,52]. However, in 2014 Morgen et al found that the use of

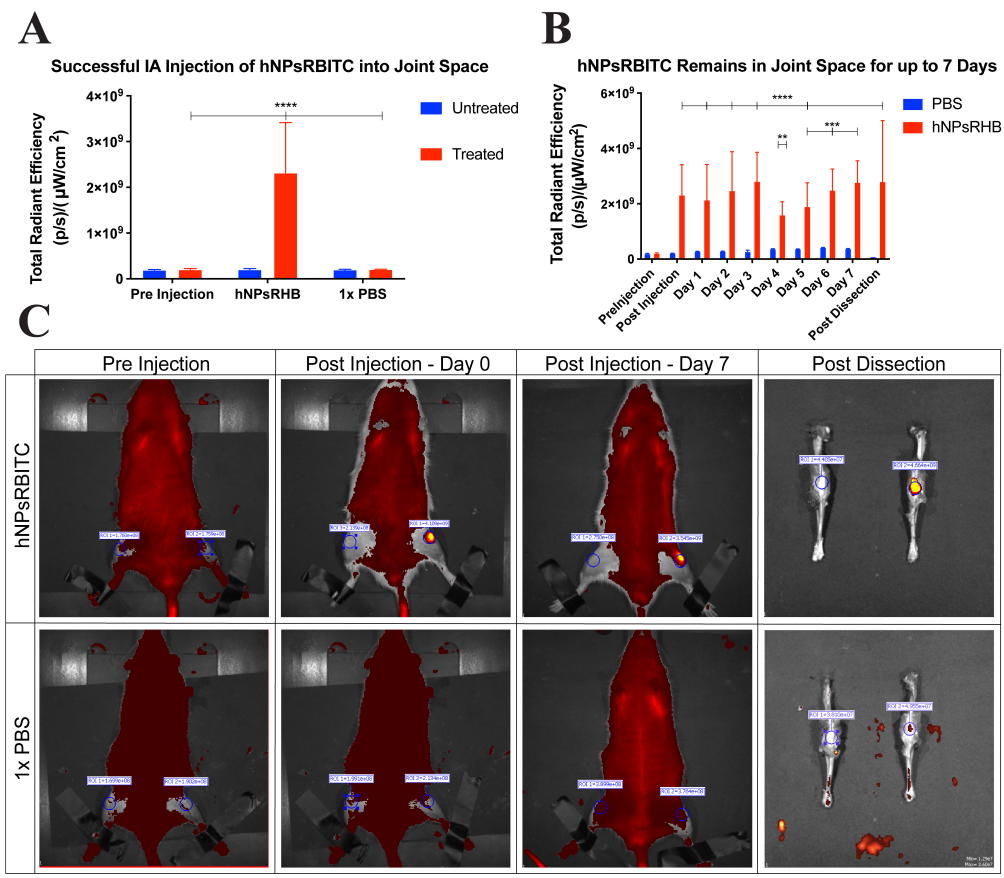

Figure 2.9: hNPsRBITC was successfully injected into the intra-articular joint space of rats and remained within the joint for 7 days. n=5 for hNPsRBITC injected rats, n = 3 for PBS injected rats. A) TRE comparison pre and post intra-articular injection of hNPsRBITC and PBS into rats; B) Daily TRE of rat joints; C) IVIS images of rats pre- and post-injection as well as post dissection.tats: * = $p < 0.05$, ** = $p < 0.01$, *** = $p < 0.001$, *** = $p < 0.0001$.

cationic solid dextran-based nanoparticles allowed for 70% retention of particles within the joint after 7 days[53], showing the benefit of nanocarriers and the potential correlation between particle charge and retention time within the joint space as both their cationic particles and these anionic particles remain in the joint for up to 7 days.

2.5 Conclusion

This work demonstrates the uptake and release of MK2 inhibiting peptide YARA from various nanoparticle systems to knock down the inflammatory cytokine IL-6 in stimulated bovine chondrocytes. The 1x hNPs presented here significantly improve upon previous work to produce monodisperse solid and hollow nanoparticles with repeatable ζ-potential, drug loading, and release. The benefit of loading low crosslink density poly(NIPAm-co-AMPS-AAc-BAC) nanoparticles below their LCST to increase drug loading is noted here as well. In addition, cationic CPP showed continual released up to 5 days. Importantly, the *in vitro* experiments here suggest that hNPsRBITC were cleared from chondrocytes approximately 5 days after treatment, and can suppress IL-6 production for 4 days. Finally, the hNPsRBITC particles were successfully delivered *in vivo* into the joint space, via intra-articular injection, and remain within the joint space for up to 7 days in agreement with previously IA delivery of charge particles[53]. Together, this body of data shows the promise of hollow, thermoresponsive poly(NIPAm-co-AMPS-AAc-BAC) nanoparticles loaded with cationic MK2i peptide YARA.

2.6 Acknowledgements

We wish to thank Dr. Vasilios Morikis for his training and assistance in our flow cytometry work and Vanessa Dartora for her training with our HPLC drug release. Additionally, we would like to thank the National Center for Advancing Translational Sciences for their funding and training.

2.7 Supplemental

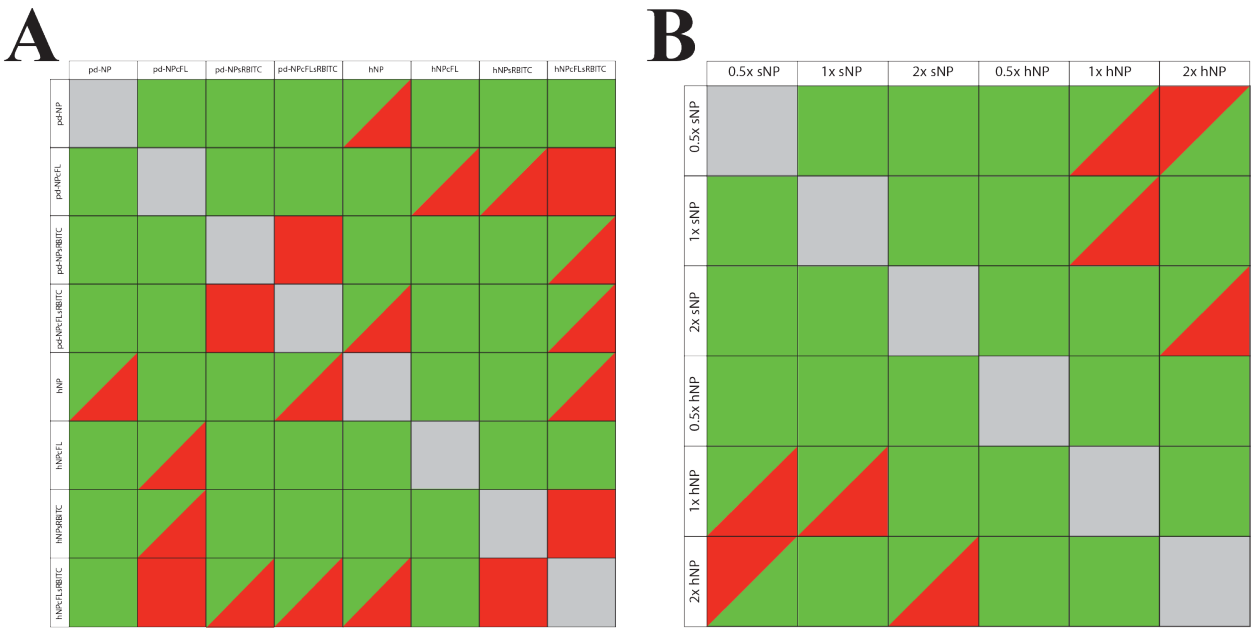

Figure S 2.10: Statistical differences between various nanoparticle diameters. Green represents statistical significance, $p < 0.05$; red is not statistically significant. For split squares, the top represents temperatures below 33°C, and the bottom represents temperatures above 33°C. A) Fluorophore incorporated nanoparticles pre-dialysis (pd) and post dialysis when hollow (hNP); B) Hollow nanoparticles (hNPs) compared to solid nanoparticles (sNPs).

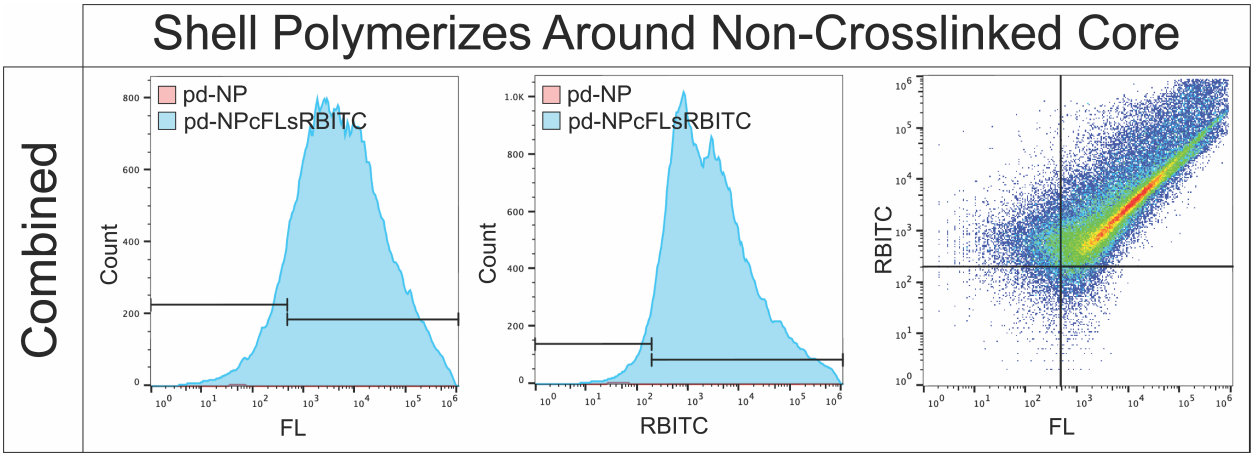

Figure S 2.11: FL Labeled cores diffuse from the RBITC labeled shells. Secondary population of unlabeled arises in the hNPcFL batch showing diffusion of the non-crosslinked core from the shell. Additionally, the RBITC labeled shell is unaltered by core removal.

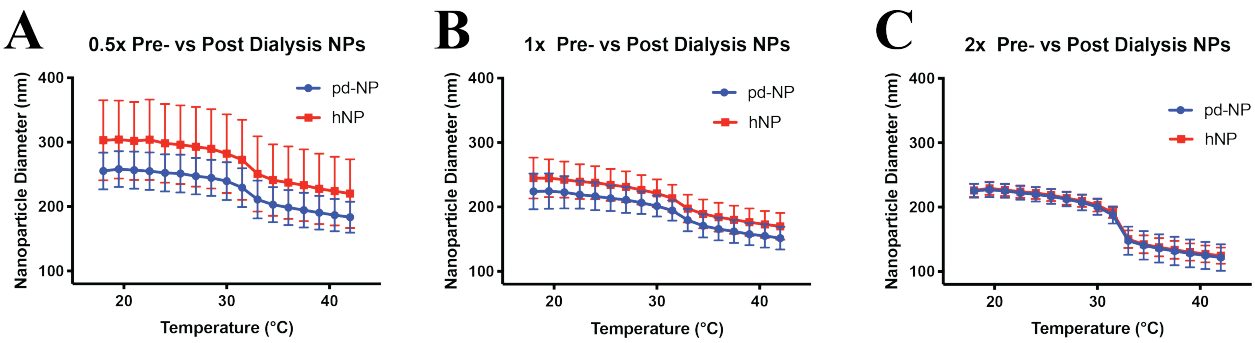

Figure S 2.12: Comparison between pre-dialysis and hollow nanoparticles show the effects of increasing crosslink density on the degree of swelling following core removal.

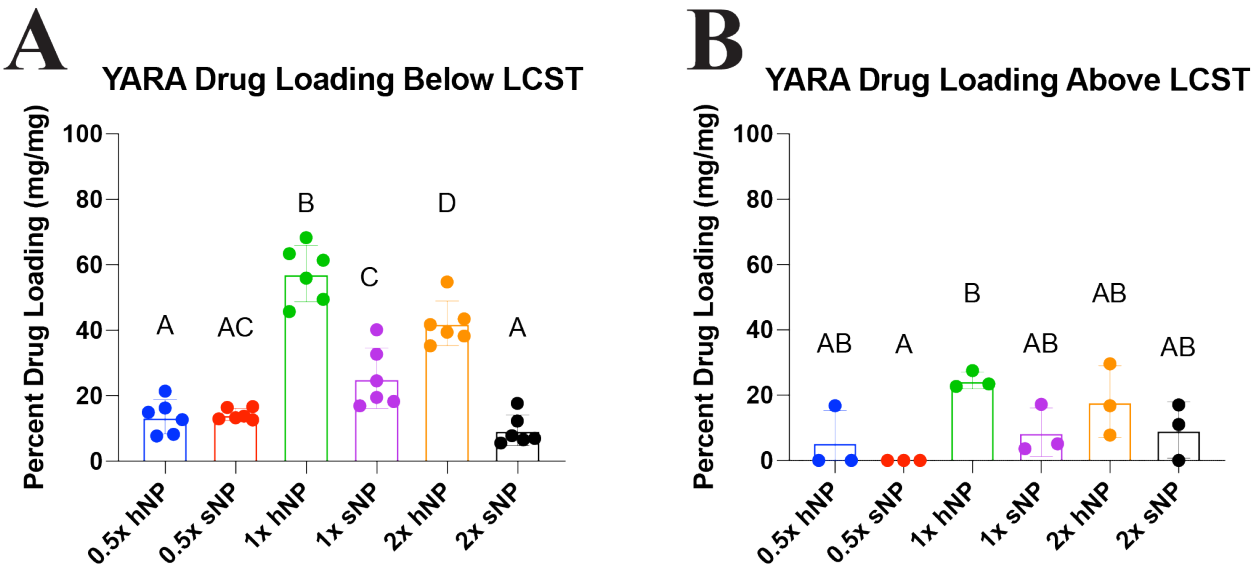

Figure S 2.13: Statistics on drug loading of various crosslinked nanoparticle batches above and below the LCST of NIPAm.

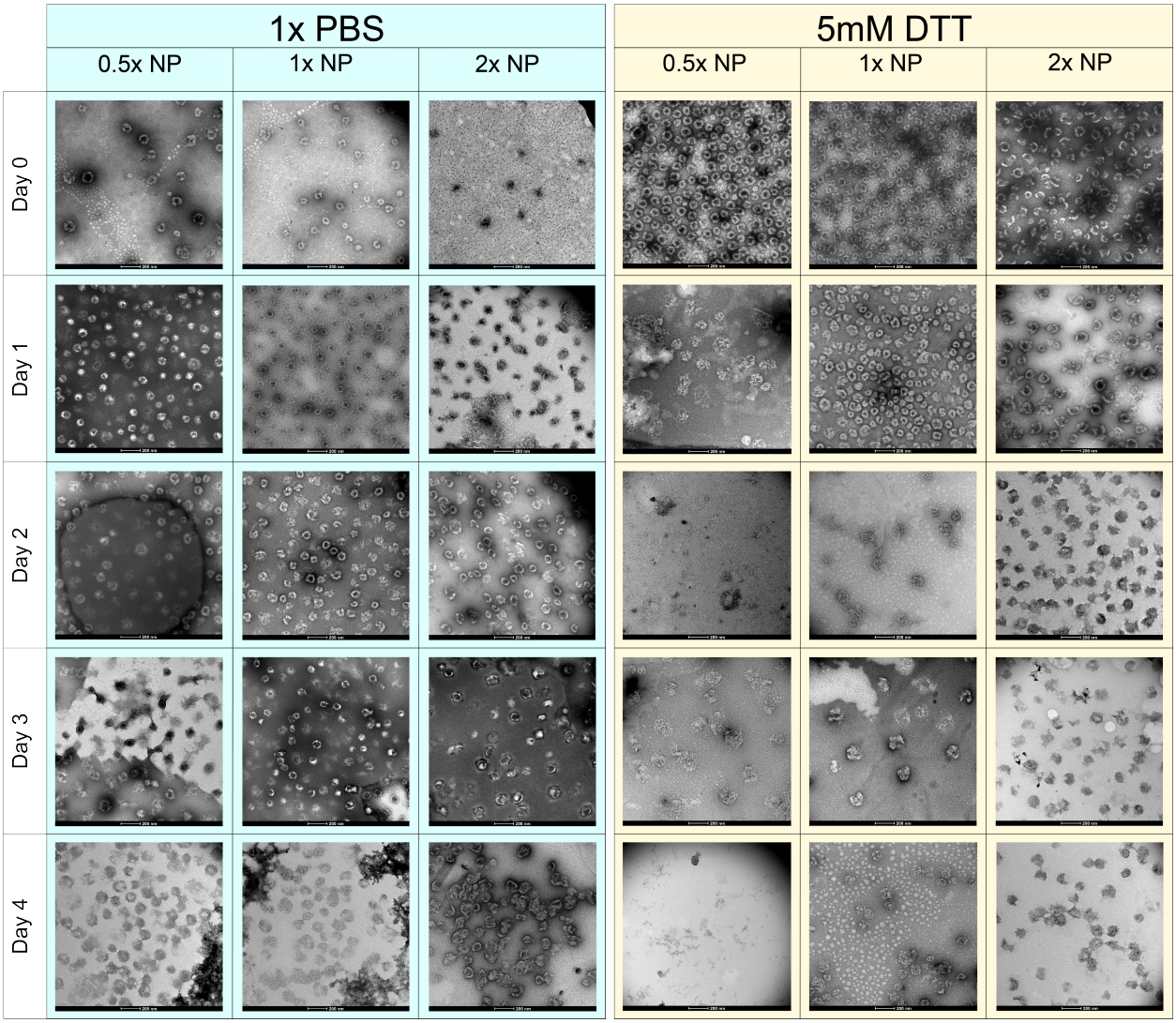

Figure S 2.14: 0.5x hNPs degrade fastest, followed by 1x hNP, then 2x hNP in 1mM DTT while NPs dissolved in PBS unaltered. Particle breakdown begins showing significance around day 2. Scale bar 200 nm.

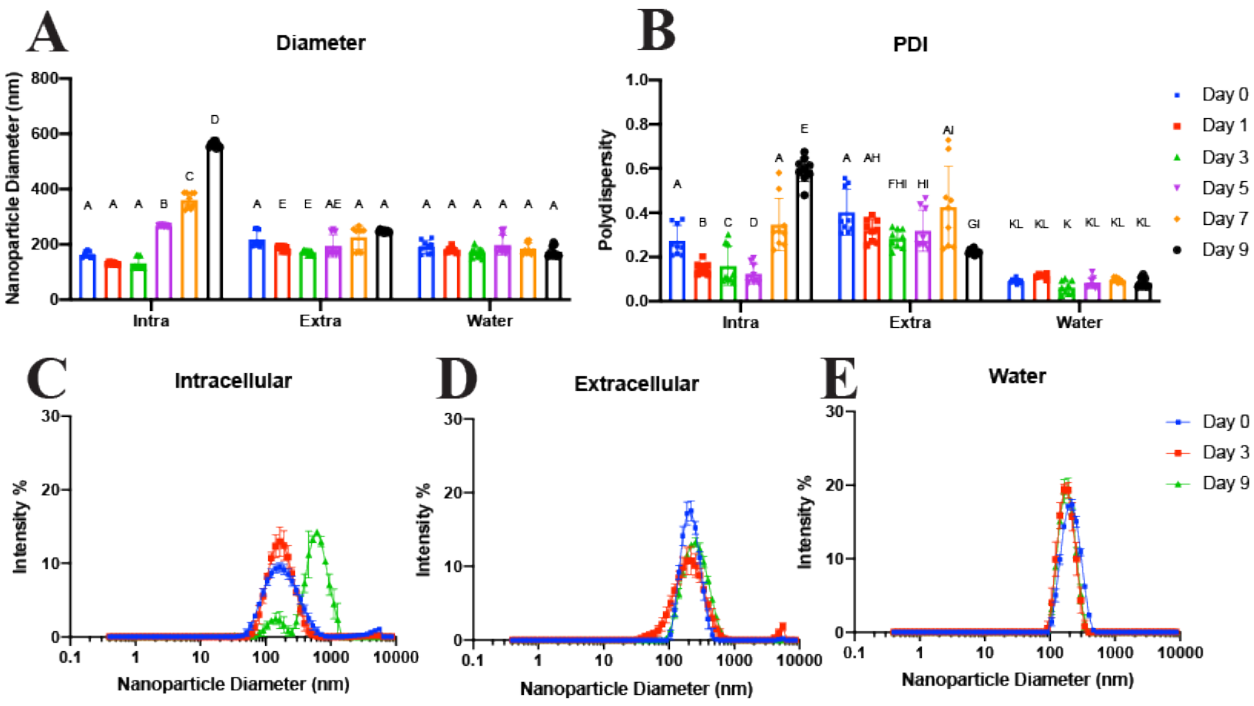

Figure S 2.15: Dynamic Light Scattering Data of hNPs dissolved in 10 mM GSH pH 5.0 (intra), 10 μM GSH pH 7.2 (extra), or ultrapure water pH 7.2. A) Diameter of hNPs; B) PDI of hNPs. Distribution for nanoparticles dissolved in: C) Intracellular GSH concentration; D) Extracellular GSH concentration; E) Ultrapure water. Statistics: $p < 0.05$

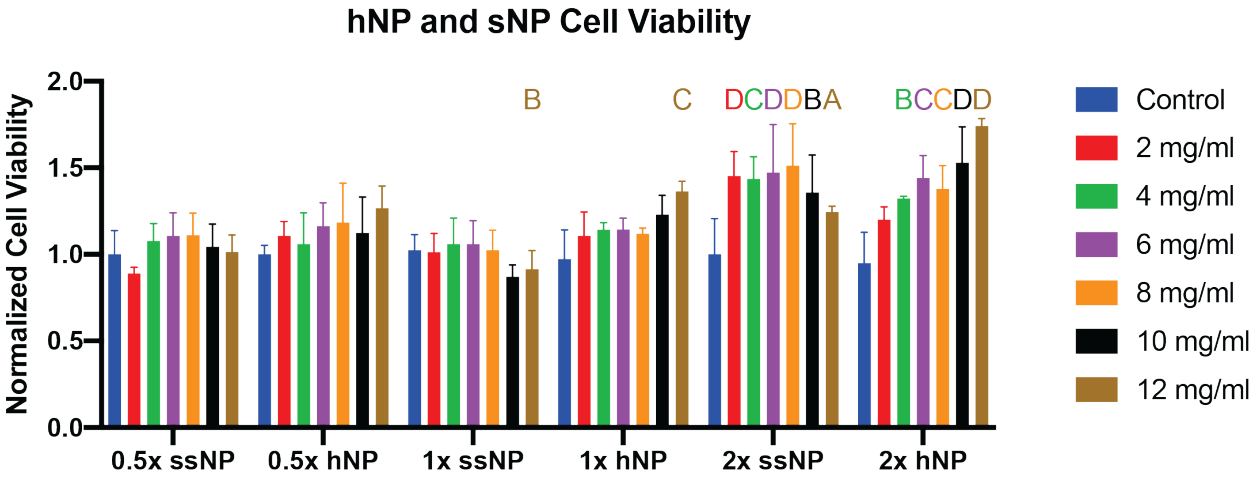

Figure S 2.16: Nanoparticles are not cytotoxic as shown by normalized cell viability of bovine chondrocytes treated with 0.5x, 1x, and 2x sNP and hNPs.

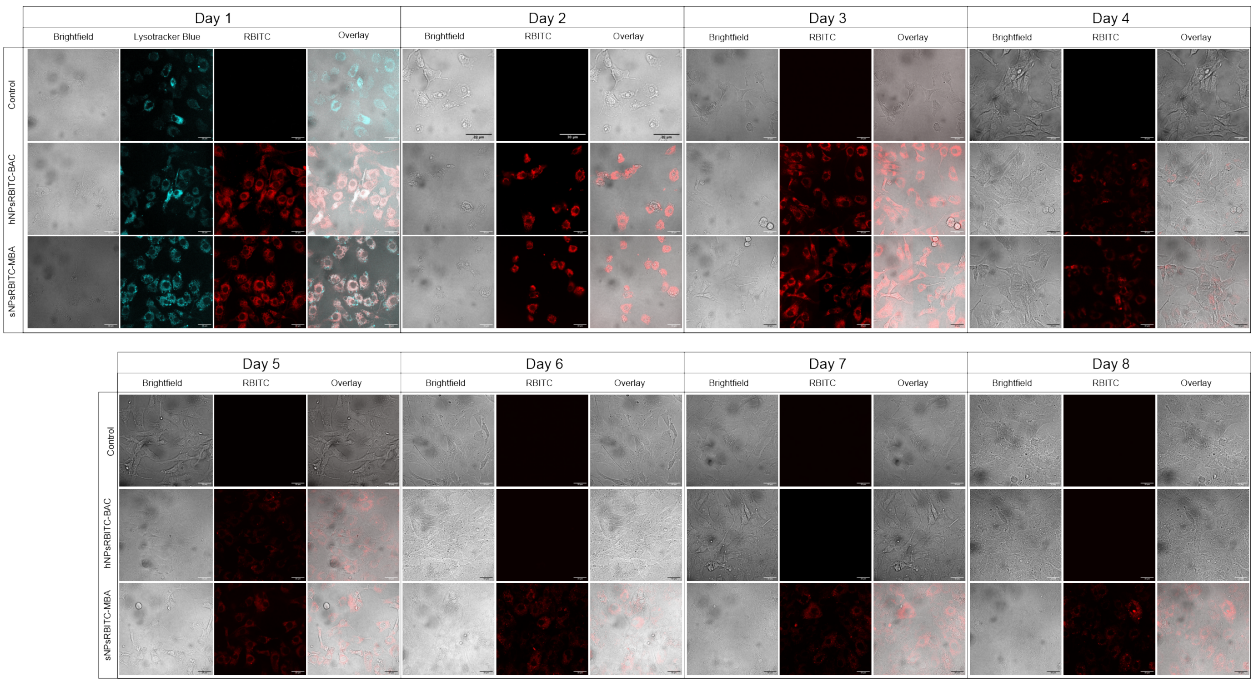

Figure S 2.17: Chondrocytes endocytose hNPsRBITC-BAC and sNPsRBITC-MBA particles into the cytoplasm of the cells and only the BAC crosslinked hNPsRBITC-BAC particles degrade within 7 days.

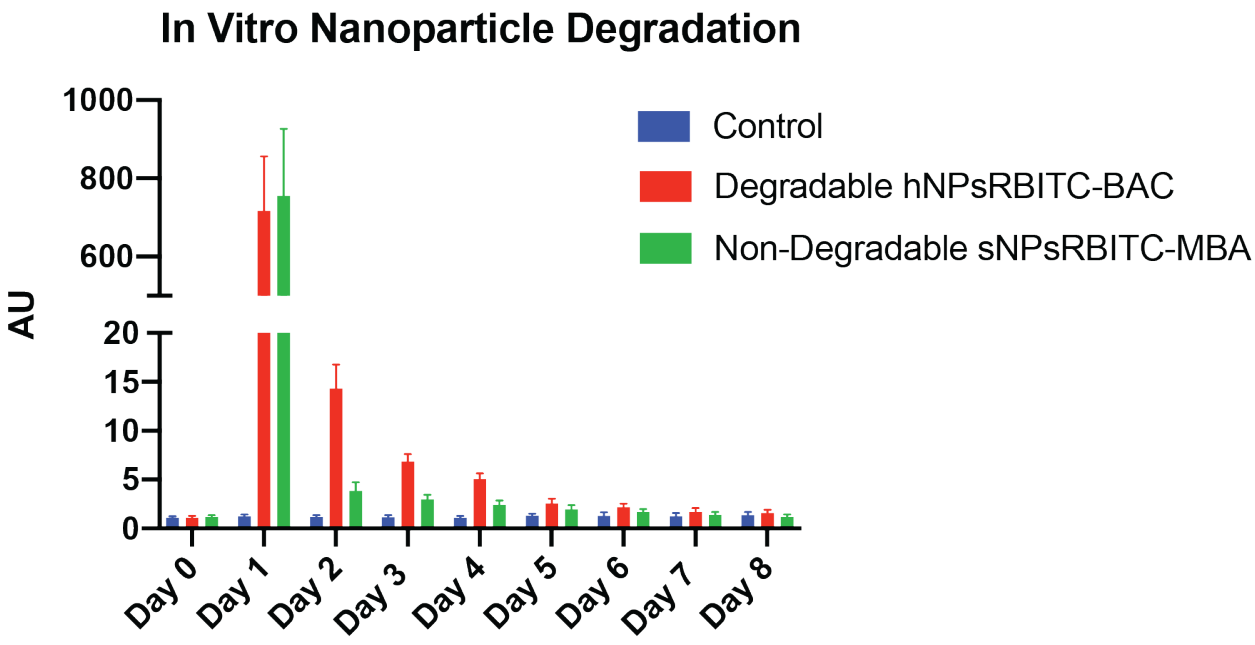

Figure S 2.18: Fluorescence analysis of media following incubation of chondrocytes with degradable hNPsRBITC-BAC and non-degradable sNPsRBITC-MBA particles reveal degradation/clearance of hNPsRBITC-BAC from chondrocytes around day 5. sNPsRBITC-MBA incubated chondrocytes do not release/degrade the non-degradable particles.

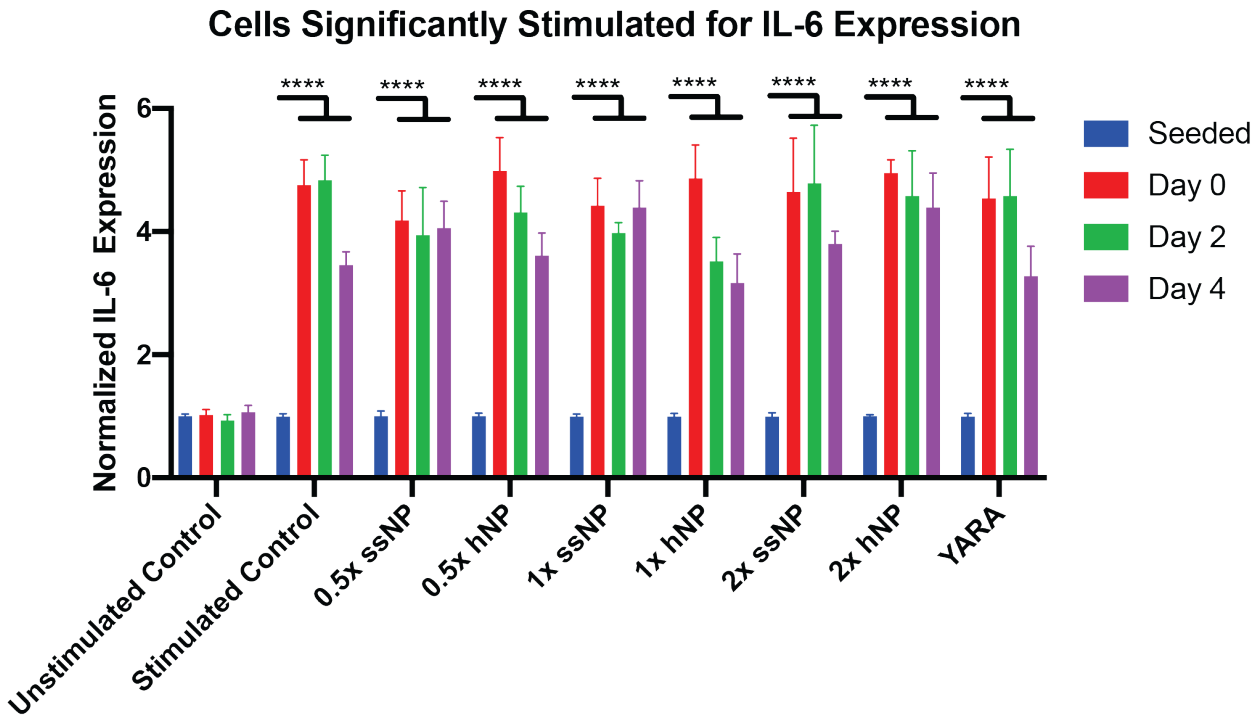

Figure S 2.19: Normalized expression of IL-6 of each respective treatment compared to unstimulated chondrocytes. All treatments significantly expressed IL-6 and are considered appropriately stimulated.

Table S 2.2: Physical Characteristics (size, PDI, and zeta potential) of the various nanoparticle batches below and above the LCST of pNIPAm

Nanoparticle	**Core Diameter (nm) ± STDEV 70.0°C**	**Core PDI ± STDEV 70.0°C**	**NP Diameter (nm) ± STDEV 18.0°C**	**PDI ± STDEV 18.0°C**	**NP Diameter (nm) ± STDEV 42.0°C**	**PDI ± STDEV 42.0°C**	**ζ Potential ± STDEV (mV) 25.0°C**
pd-NP	51.51 ± 5.84	0.01 ± 0.01	224.08 ± 23.56	0.05 ± 0.03	151.61 ± 25.22	0.07 ± 0.01	-25.07 ± 6.54
hNP	-	-	244.96 ± 26.76	0.09 ± 0.03	170.10 ± 29.66	0.09 ± 0.02	-27.69 ± 6.11
pd-NPcFITC	99.54 ± 17.01	0.04 ± 0.04	334.38 ± 8.17	0.09 ± 0.06	236.16 ± 58.91	0.04 ± 0.02	-34.98 ± 2.23
hNPcFITC	-	-	365.67 ± 30.12	0.12 ± 0.12	250.91 ± 48.19	0.08 ± 0.03	-35.34 ± 3.62
pd-NPsRHB	68.73 ± 2.07	0.01 ± 0.01	295.97 ± 15.69	0.08 ± 0.03	198.65 ± 24.15	0.06 ± 0.02	-30.81 ± 0.96
hNPsRHB	-	-	319.54 ± 16.21	0.08 ± 0.03	218.48 ± 31.26	0.09 ± 0.02	-34.67 ± 0.62
pd-NPcFITCsRHB	96.75 ± 6.80	0.01 ± 0.01	295.10 ± 22.93	0.06 ± 0.03	185.44 ± 43.15	0.05 ± 0.03	-4.50 ± 0.63
hNPcFITCsRHB	-	-	326.56 ± 22.05	0.08 ± 0.03	201.31 ± 52.19	0.07 ± 0.02	-24.57 ± 9.42

Table S 2.3: Physical Characteristics (size, PDI, and zeta potential) of the various nanoparticle batches below and above the LCST of pNIPAm

Nanoparticle	Pre-Dialysis Core Diameter (nm) ± STDEV 70.0°C	Core PDI ± STDEV 70.0°C	NP Diameter (nm) ± STDEV 18.0°C	PDI ± STDEV 18.0°C	NP Diameter (nm) ± STDEV 42.0°C	PDI ± STDEV 42.0°C	ζ Potential ± STDEV (mV) 25.0°C	Percent Drug Loading 4°C (mg/mg)	ζ Potential ± STDEV (mV) 42.0°C	Percent Drug Loading 42°C (mg/mg)
0.5x sNP	-	-	216.37 ± 10.71	0.13 ± 0.06	182. 81 ± 11.67	0.13 ± 0.06	-31.13 ± 2.02	14.3 ± 1.8	-33.13 ± 1.62	0.0 ± 0.0
0.5x pd-NP	51.84 ± 1.27	0.03 ± 0.01	255.32 ± 24.01	0.08 ± 0.05	183.57 ± 20.09	0.09 ± 0.04	-26.37 ± 2.15	-	-31.91 ± 1.30	-
0.5x hNP	-	-	303.13 ± 52.11	0.16 ± 0.08	220.12 ± 44.48	0.13 ± 0.07	-28.37 ± 4.01	19.2 ± 5.4	-29.01 ± 4.55	5.2 ± 10.1
1x sNP	-	-	203.33 ± 6.97	0.06 ± 0.02	176.59 ± 09.57	0.06 ± 0.02	-30.03 ± 4.98	25.3 ± 9.3	-30.86 ± 5.31	8.7 ± 7.5
1x pd-NP	50.51 ± 5.84	0.02 ± 0.01	224.08 ± 23.56	0.06 ± 0.03	151.61 ± 25.22	0.07 ± 0.01	-25.06 ± 5.71	-	-29.84 ± 4.49	-
1x hNP	-	-	244.96 ± 26.76	0.09 ± 0.03	170.05 ± 29.66	0.09 ± 0.02	-27.69 ± 5.46	57.4 ± 8.6	-31.25 ± 2.61	24.6 ± 2.6
2x sNP	-	-	165.41 ± 7.05	0.08 ± 0.03	112.11 ± 29.28	0.11 ± 0.04	-27.11 ± 5.86	11.1 ± 8.5	-34.72 ± 2.13	8.7 ± 9.6
2x pd-NP	52.16 ± 1.65	0.02 ± 0.01	225.33 ± 10.97	0.15 ± 0.05	121.83 ± 17.62	0.10 ± 0.07	11.02 ± 7.03	-	-31.61 ± 3.25	-
2x hNP	-	-	226.06 ± 8.96	0.14 ± 0.03	124.71 ± 10.68	0.10 ± 0.03	-12.91 ± 3.19	42.1 ± 6.8	-31.43 ± 2.11	18.1 ± 10.9

References

1. Hootman, J. M., Helmick, C. G., Barbour, K. E., Theis, K. A. & Boring, M. A. Updated projected prevalence of self-reported doctor-diagnosed arthritis and arthritis-attributable activity limitation among US adults, 2015–2040. *Arthritis & rheumatology* **68,** 1582–1587 (2016).

2. Klatt, A. R. *et al.* A critical role for collagen II in cartilage matrix degradation: collagen II induces pro-inflammatory cytokines and MMPs in primary human chondrocytes. *Journal of orthopaedic research* **27,** 65–70 (2009).

3. Rostom, A. *et al.* Prevention of NSAID-induced gastroduodenal ulcers. *Cochrane database of systematic reviews* (2002).

4. Bhala, N. *et al.* Vascular and upper gastrointestinal effects of non-steroidal anti-inflammatory drugs: meta-analyses of individual participant data from randomised trials. *Lancet (London, England)* **382,** 769–779 (2013).

5. Gislason, G. H. *et al.* Increased mortality and cardiovascular morbidity associated with use of nonsteroidal anti-inflammatory drugs in chronic heart failure. *Archives of internal medicine* **169,** 141–149 (2009).

6. Lee, A., Cooper, M. G., Craig, J. C., Knight, J. F. & Keneally, J. P. Effects of nonsteroidal anti-inflammatory drugs on postoperative renal function in adults with normal renal function. *Cochrane database of systematic reviews* (2007).

7. Mora, J. C., Przkora, R. & Cruz-Almeida, Y. Knee osteoarthritis: pathophysiology and current treatment modalities. *Journal of pain research* **11,** 2189 (2018).

8. Jones, S. *et al.* Mitogen-activated protein kinase-activated protein kinase 2 (MK2) modulates key biological pathways associated with OA disease pathology. *Osteoarthritis and cartilage* **17,** 124–131 (2009).

9. Philp, A. M., Davis, E. T. & Jones, S. W. Developing anti-inflammatory therapeutics for patients with osteoarthritis. *Rheumatology* **56,** 869–881 (2017).

10. Ward, B., Seal, B. L., Brophy, C. M. & Panitch, A. Design of a bioactive cell-penetrating peptide: when a transduction domain does more than transduce. *Journal of peptide science: an official publication of the European Peptide Society* **15,** 668–674 (2009).

11. Brugnano, J. L., Chan, B. K., Seal, B. L. & Panitch, A. Cell-penetrating peptides can confer biological function: regulation of inflammatory cytokines in human monocytes by MK2 inhibitor peptides. *Journal of controlled release* **155,** 128–133 (2011).

12. Bartlett, R. L. & Panitch, A. Thermosensitive nanoparticles with pH-triggered degradation and release of anti-inflammatory cell-penetrating peptides. *Biomacromolecules* **13,** 2578–2584 (2012).

13. Bartlett II, R. L., Sharma, S. & Panitch, A. Cell-penetrating peptides released from thermosensitive nanoparticles suppress pro-inflammatory cytokine response by specifically targeting inflamed cartilage explants. *Nanomedicine: Nanotechnology, Biology and Medicine* **9,** 419–427 (2013).

14. McMasters, J., Poh, S., Lin, J. B. & Panitch, A. Delivery of anti-inflammatory peptides from hollow PEGylated poly (NIPAM) nanoparticles reduces inflammation in an ex vivo osteoarthritis model. *Journal of Controlled Release* **258,** 161–170 (2017).

15. Poh, S., Lin, J. B. & Panitch, A. Release of anti-inflammatory peptides from thermosensitive nanoparticles with degradable cross-links suppresses pro-inflammatory cytokine production. *Biomacromolecules* **16,** 1191–1200 (2015).

16. Lin, J. B., Poh, S. & Panitch, A. Controlled release of anti-inflammatory peptides from reducible thermosensitive nanoparticles suppresses cartilage inflammation. *Nanomedicine: Nanotechnology, Biology and Medicine* **12,** 2095–2100 (2016).

17. Ward, B. C., Kavalukas, S., Brugnano, J., Barbul, A. & Panitch, A. Peptide inhibitors of MK2 show promise for inhibition of abdominal adhesions. *Journal of Surgical Research* **169,** e27–e36 (2011).

18. Bartlett, R. L., Sharma, S. & Panitch, A. Cell-penetrating peptides released from thermosensitive nanoparticles suppress pro-inflammatory cytokine response by specifically targeting inflamed cartilage explants. *Nanomedicine: Nanotechnology, Biology, and Medicine* **9,** 419–427. ISSN: 15499634 (2013).

19. Gupta, M. K. *et al.* Cell protective, ABC triblock polymer-based thermoresponsive hydrogels with ROS-triggered degradation and drug release. *Journal of the American Chemical Society* **136,** 14896–14902 (2014).

20. Wang, H. *et al.* Responsive polymer–fluorescent carbon nanoparticle hybrid nanogels for optical temperature sensing, near-infrared light-responsive drug release, and tumor cell imaging. *Nanoscale* **6,** 7443–7452 (2014).

21. Swift, T. *et al.* Highly-branched poly (N-isopropyl acrylamide) functionalised with pendant Nile red and chain end vancomycin for the detection of Gram-positive bacteria. *Acta biomaterialia* **87,** 197–206 (2019).

22. Lin, C.-C. & Anseth, K. S. PEG hydrogels for the controlled release of biomolecules in regenerative medicine. *Pharmaceutical research* **26,** 631–643 (2009).

23. Karg, M. *et al.* Nanogels and microgels: From model colloids to applications, recent developments, and future trends. *Langmuir* **35,** 6231–6255 (2019).

24. Zhang, S., Langer, R. & Traverso, G. Nanoparticulate drug delivery systems targeting inflammation for treatment of inflammatory bowel disease. *Nano Today* **16,** 82–96 (2017).

25. Liu, G., Wang, D., Zhou, F. & Liu, W. Electrostatic self-assembly of Au nanoparticles onto thermosensitive magnetic core-shell microgels for thermally tunable and magnetically recyclable catalysis. *Small* **11,** 2807–2816 (2015).

26. Reimhult, E., Schroffenegger, M. & Lassenberger, A. Design Principles for Thermoresponsive Core–Shell Nanoparticles: Controlling Thermal Transitions by Brush Morphology. *Langmuir* **35,** 7092–7104 (2019).

27. Kakwere, H. *et al.* Functionalization of strongly interacting magnetic nanocubes with (thermo) responsive coating and their application in hyperthermia and heat-triggered drug delivery. *ACS applied materials & interfaces* **7,** 10132–10145 (2015).

28. Hannecart, A. *et al.* Nano-thermometers with thermo-sensitive polymer grafted USPIOs behaving as positive contrast agents in low-field MRI. *Nanoscale* **7,** 3754–3767 (2015).

29. Shen, S. *et al.* Near-infrared light-responsive nanoparticles with thermosensitive yolk-shell structure for multimodal imaging and chemo-photothermal therapy of tumor. *Nanomedicine: Nanotechnology, Biology and Medicine* **13,** 1607–1616 (2017).

30. Xiao, Q. *et al.* Rational design of a thermalresponsive-polymer-switchable FRET system for enhancing the temperature sensitivity of upconversion nanophosphors. *Nanoscale* **6,** 10179–10186 (2014).

31. Schroffenegger, M. & Reimhult, E. Thermoresponsive Core-Shell Nanoparticles: Does Core Size Matter? *Materials* **11,** 1654 (2018).

32. Dubbert, J., Nothdurft, K., Karg, M. & Richtering, W. Core–Shell–Shell and Hollow Double-Shell Microgels with Advanced Temperature Responsiveness. *Macromolecular rapid communications* **36,** 159–164 (2015).

33. Liu, T., Zhang, W., Song, T., Yang, X. & Li, C. Hollow double-layered polymer microspheres with pH and thermo-responsive properties as nitric oxide-releasing reservoirs. *Polymer Chemistry* **6,** 3305–3314 (2015).

34. Li, C., Ma, Y., Niu, H. & Zhang, H. Hydrophilic hollow molecularly imprinted polymer microparticles with photo-and thermoresponsive template binding and release properties in aqueous media. *ACS applied materials & interfaces* **7,** 27340–27350 (2015).

35. Schmid, A. J. *et al.* Multi-shell hollow nanogels with responsive shell permeability. *Scientific reports* **6,** 22736 (2016).

36. Su, Y. *et al.* Thermoresponsive Coatings on Hollow Particles with Mesoporous Shells Serve as Stimuli-Responsive Gates to Species Encapsulation and Release. *Langmuir* **34,** 14608–14616 (2018).

37. Kitayama, Y., Yoshikawa, K. & Takeuchi, T. Efficient pathway for preparing hollow particles: Site-specific crosslinking of spherical polymer particles with photoresponsive groups that play a dual role in shell crosslinking and core shielding. *Langmuir* **32,** 9245–9253 (2016).

38. Naseem, K., Begum, R., Wu, W., Irfan, A. & Farooqi, Z. H. Advancement in multifunctional poly (styrene)-poly (N-isopropylacrylamide) based core–shell microgels and their applications. *Polymer Reviews* **58,** 288–325 (2018).

39. Moghaddam, S. P. H., Yazdimamaghani, M. & Ghandehari, H. Glutathione-sensitive hollow mesoporous silica nanoparticles for controlled drug delivery. *Journal of Controlled Release* **282,** 62–75 (2018).

40. Chu, F. *et al.* Thermosensitive hollow Janus dumbbells. *Colloid and Polymer Science* **292,** 1785–1793 (2014).

41. Brändel, T., Dirksen, M. & Hellweg, T. Tuning the Swelling Properties of Smart Multiresponsive Core-Shell Microgels by Copolymerization. *Polymers* **11,** 1269 (2019).

42. Herman, E. S. *Exploring complex interactions within microgels and microgel assemblies* PhD thesis (Georgia Institute of Technology, 2014).

43. García-Couce, J. *et al.* Targeting Polymeric Nanobiomaterials as a Platform for Cartilage Tissue Engineering. *Current pharmaceutical design* **25,** 1915–1932 (2019).

44. Bhattacharjee, S. DLS and zeta potential–what they are and what they are not? *Journal of Controlled Release* **235,** 337–351 (2016).

45. Gao, J. & Frisken, B. J. Influence of reaction conditions on the synthesis of self-cross-linked N-isopropylacrylamide microgels. *Langmuir* **19,** 5217–5222 (2003).

46. Cao, M. *et al.* Reversible Thermoresponsive Peptide–PNIPAM Hydrogels for Controlled Drug Delivery. *Biomacromolecules* **20,** 3601–3610 (2019).

47. Chen, J. *et al.* Poly (N-isopropylacrylamide) derived nanogels demonstrated thermosensitive self-assembly and GSH-triggered drug release for efficient tumor Therapy. *Polymer Chemistry* **10,** 4031–4041 (2019).

48. Jones, S. A., Scheller, J. & Rose-John, S. Therapeutic strategies for the clinical blockade of IL-6/gp130 signaling. *The Journal of clinical investigation* **121,** 3375–3383 (2011).

49. Brown, S., Kumar, S. & Sharma, B. Intra-articular targeting of nanomaterials for the treatment of osteoarthritis. *Acta Biomaterialia* **93,** 239–257 (2019).

50. Maudens, P., Jordan, O. & Allémann, E. Recent advances in intra-articular drug delivery systems for osteoarthritis therapy. *Drug discovery today* **23,** 1761–1775 (2018).

51. Owen, S., Francis, H. & Roberts, M. Disappearance kinetics of solutes from synovial fluid after intra-articular injection. *British journal of clinical pharmacology* **38,** 349–355 (1994).

52. Gerwin, N., Hops, C. & Lucke, A. Intraarticular drug delivery in osteoarthritis. *Advanced drug delivery reviews* **58,** 226–242 (2006).

53. Morgen, M. *et al.* Nanoparticles for improved local retention after intra-articular injection into the knee joint. *Pharmaceutical research* **30,** 257–268 (2013).

CHAPTER III

Hyaluronic acid-binding, anionic, hollow nanoparticles inhibit ECM degradation and restore compressive strength in aggrecan-depleted articular cartilage explants

3.1 Abstract

Joint trauma results in the production of inflammatory cytokines that stimulate the secretion of catabolic enzymes which degrade articular cartilage. Molecular fragments of the degraded articular cartilage further stimulate inflammatory cytokine production with this process eventually resulting in post-traumatic osteoarthritis (PTOA). The loss of aggrecan is considered an early step in the progression of PTOA. Aggrecan, composed of a core protein linked to sulfated glycosaminoglycans (GAGs), associates with hyaluronic acid (HA) via a link protein. The fragmentation of aggrecan allows diffusion of its anionic GAGs out of the cartilage and results in the loss of compressive strength in articular cartilage. Binding to HA within aggrecan-depleted cartilage and restoring the tissue anionic charge has the potential to restore the osmotic pressure responsible for the compressive strength of articular cartilage. Presented here, we conjugated the HA-binding peptide GAHWQFNALTVRGSG functionalized with a hydrazide (GAH-Hyd) to anionic hollow nanoparticles (hNPs). The hNPs are composed of: N-isopropyl acrylamide (NIPAm), N, N′-bis (acryloyl) cystamine (BAC), 2-acrylamido-2-methyl-1-propanesulfonic acid (AMPS), and acrylic acid (AAc). Reaction of AAc with GAH-Hyd resulted in GAH functionalized hNPs (GAH-hNPs). Increasing the molar ratio of GAH to AAc resulted in increased peptide conjugation to the hNPs. Nanoparticles conjugated with roughly 19 GAH peptides, termed 19 GAH-hNP, bound to HA in

solution and increased the dynamic viscosity by 94.0% compared to free HA solution treated with unconjugated hNPs. Moreover, 3 mm diameter, full thickness, aggrecan-depleted (AD) cartilage explants treated with 0.10 mg of 19 GAH-hNP restored the compressive strength to healthy cartilage levels, 95.9 ± 16.2 kPa compared to 123.7 ± 26.5 kPa, respectively, six days after a single dose of the therapeutic. AD explants treated with 0.10 mg of 19 GAH-hNP inhibited the degradation of articular cartilage shown by a 180.09% decrease in chondroitin sulfate (CS) release from cartilage explants into media compared to untreated-AD control, and had 409.03% more collagen type II and 597.58% more GAG content than untreated-AD explants. Finally, fluorescent hNP conjugated with GAH were retained within the joint space of rats for up to 7 days. The 19 GAH-hNP therapeutic presented here was able to slow ECM degradation in AD cartilage explants and restored the compressive strength of damaged cartilage. This therapeutic shows promise as a localized treatment for PTOA.

3.2 Introduction

Post traumatic osteoarthritis (PTOA) accounts for 12.5% of the over 21 million cases of osteoarthritis (OA) within the United States annually[1]. PTOA is characterized by inflammation of the joint and degradation of articular cartilage[2]. The extracellular matrix (ECM) of cartilage is primarily composed of proteoglycans (4-7% wet weight) and collagen type II (15-22% wet weight), and their interactions significantly control the biology of cartilage[3]. The most abundant proteoglycan in articular cartilage is aggrecan and is composed of a core protein with covalently bonded sulfated glycosaminoglycan (GAG) chains. The sulfated GAG chains within aggrecan provide a high density of anionic charge, generating an osmotic gradient and enabling cartilage to retain water. This gives articular cartilage its compressive strength[4]. Link protein stabilizes the aggrecan-hyaluronic acid (HA) interaction to anchor aggrecan within the ECM of articular cartilage[3–5]. Further, aggrecan protects the cartilage ECM by interfering with the ability of collagenases to permeate the cartilage and cleave collagen type II[5]. However, following joint trauma, early loss of aggrecan as a result

of digestion by upregulated aggrecanase causes the anionic GAGs to diffuse from the cartilage[5,6]. The loss of the GAGs leads to a reduced osmotic gradient within cartilage and the associated compressive strength within cartilage[5,7]. Binding anionic polymers may restore the mechanical function and protect damaged osteoarthritic cartilage.

Currently there is no FDA approved therapeutic to treat OA. The present gold-standards to treat OA and PTOA focus on suppressing the pain associated with OA and include intra-articular injections of non-steroidal anti-inflammatory drugs (NSAIDs), corticosteroids, glucosteroids, and viscosupplements. However, NSAIDs, corticosteroids, and glucosteroids are non-specific and only address joint inflammation and pain, not the damaged cartilage itself[8,9]. Viscosupplements, commonly used once the patient complains of pain, aim to increase mobility and reduce discomfort. However, viscosupplements only delay surgical intervention and have conflicting evidence of efficacy[10,11]. The discovery and subsequent use of peptides able to bind to components within the ECM of articular cartilage present a solution to treat early-stage joint trauma and potentially prevent the progression of PTOA. Peptide-conjugated therapeutics are able to bind to aggrecan-depleted HA and can restore the compressive strength of osteoarthritic cartilage[7,12–14]. Previous studies utilized the HA-binding peptide GAH conjugated to polymers to inhibit the progression of OA. One study conjugated GAH and a collagen type II binding peptide to poly(ethylene glycol) (PEG) and slowed the degradation of articular cartilage following anterior cruciate ligament transection[15]. Other studies conjugated GAH to the sulfated GAG chondroitin sulfate (CS) to mimic aggrecan function. The GAH-CS bound to HA and restored compressive strength of AD cartilage[7,12–14]. Further, GAH-CS slowed the release of GAGs into the media in *ex vivo* cartilage explants and suppressed matrix metalloprotease activity[7,16]. We aimed to build upon previous GAH-CS conjugates by using an anionic, sulfated polymeric nanoparticle conjugated with GAH to inhibit the progression of OA.

In this study, we modified the recently developed anionic, polymeric hollow nanoparticle (hNP) composed of N-isopropyl acrylamide (NIPAm), 2-acrylamido-2-methyl-1-propanesulfonic

acid (AMPS), N,N′-Bis(acryloyl) cystamine (BAC), and acrylic acid (AAc)[17] with the HA-binding peptide GAH to mimic aggrecan function and generate a HA-binding nanoparticle (GAH-hNP). NIPAm is a thermoresponsive monomer with a lower critical solution temperature (LCST) of 32°C which, when polymerized into the particle, causes them to swell at temperatures below the LCST and constrict at temperatures above the LCST. AMPS is a highly sulfated, anionic monomer incorporated into the nanoparticles to mimic the charge provided by the GAGs attached to aggrecan. Moreover, the negative charge of AMPS maintains the colloidal stability of the nanoparticle. The incorporation of the homobifunctional degradable crosslinker BAC allows for particle degradation[17]. Finally, AAc serves as the carboxylate anchoring point within the hNP shell for peptide conjugation. These data presented here support the hypothesis that anionic hNP conjugated with GAH will restore the compressive strength of aggrecan-depleted cartilage and inhibit further degradation of its ECM. Further, nanoparticles are retained within the joint for at least 7 days. The detailed representation of the study is summarized in Figure 3.1.

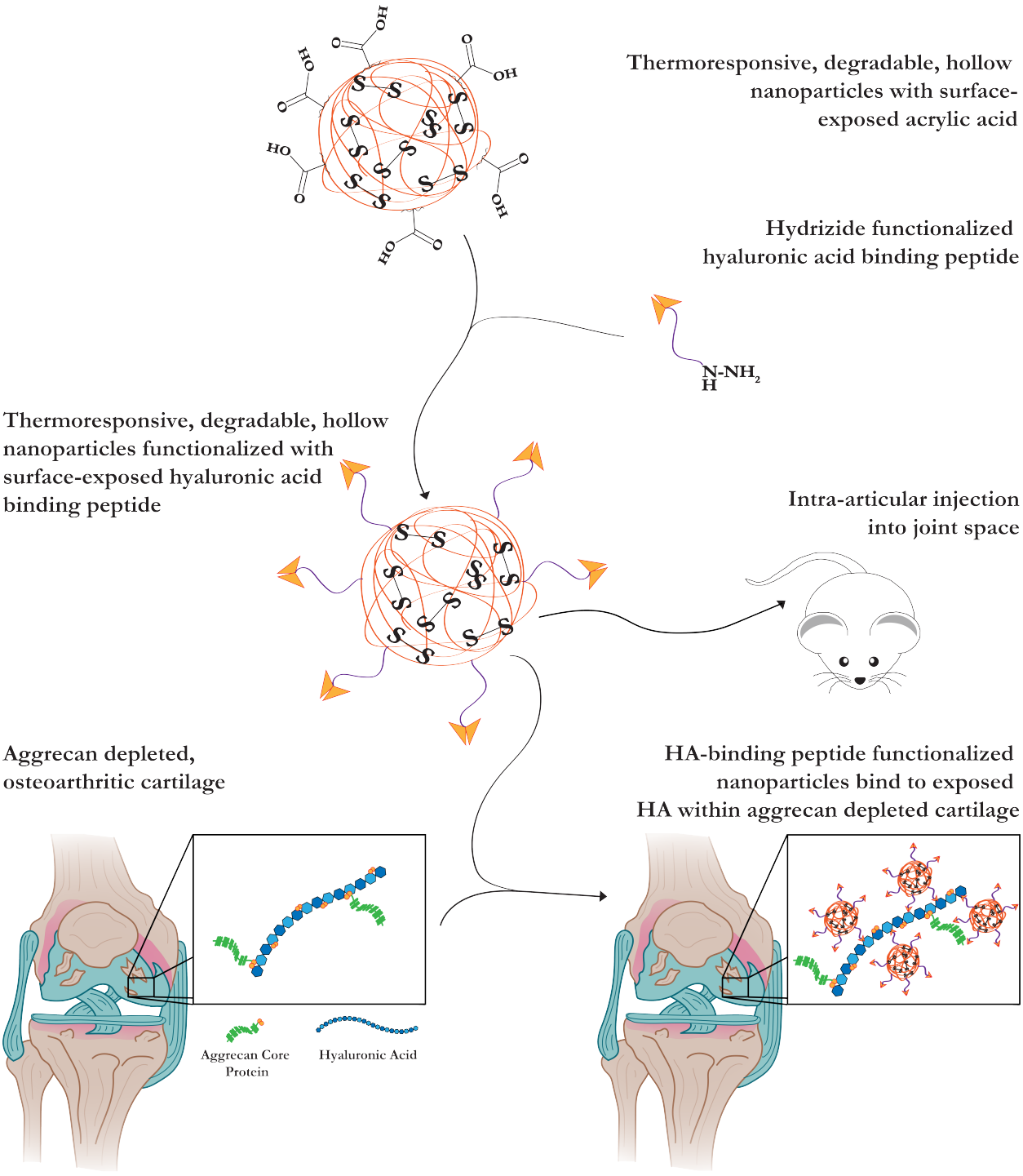

Figure 3.1: Schematic of the described studies. AAc polymerized into the nanoparticle shell served as the anchoring point of hyaluronic acid binding peptide (GAH) conjugation, termed GAH-hNP. The GAH-hNP therapeutic treated aggrecan-depleted (AD) cartilage explants and was retained within the joint space of rats. The image was created using BioRender.com.

3.3 Materials and Methods

3.3.1 Materials

N-isopropyl acrylamide (NIPAm, ≥98%), N,N'-Bis(acryloyl) cystamine (99%, BAC), N, N′-methylene-bis-diacrylaminde (MBA), sodium dodecyl sulfate (SDS; 20% w/v in water), 2-acrylamido-2-methyl-1-propanesulfonic acid (99%, AMPS), Rhodamine B isothiocyanate (98%, RBITC), N-diisopropylethylamine (99%, DIPEA), potassium persulfate (99%, KPS), trifluoroacetic acid (TFA), 4-(4,6-Dimethoxy-1,3,5-triazin-2-yl)-4-methylmorpholinium chloride (96% DMTMM), dimethyl sulfoxide (DMSO), and porcine trypsin were acquired from Sigma Aldrich (St. Louis, MO). Dimethylformamide (DMF), dichloromethane (DCM), acetonitrile (ACN), trifluoroacetic acid (TFA), triisopropylsilane (TIPS), and phenol were purchased from Thermo Fisher (Waltham, MA). Some GAHWQFNALTVRGSG-Hydrazide (GAH-Hyd) was purchased from the Chinese Peptide Company (CPC, Hangzhou, China). Dialysis membrane tubing and tangential flow filtration carbon tubing were purchased from Spectrum Laboratories (Dominguez, CA). NIPAm and BAC were stored under nitrogen at 4°C and −20°C, respectively. AMPS was stored at room temperature in a desiccator. All water used in synthesis, dialysis, and testing was treated by a Millipore milliQ system (Billerica, MA; 18.2 MΩ·cm resistivity).

3.3.2 Nanoparticle Synthesis

The nanoparticle (NP) core-shell complex was polymerized via precipitation reaction as previously described[17]. Briefly, the NP cores were synthesized by dissolving 394.5 mg NIPAm in 3 ml milliQ water and injecting it into a 100 ml three-neck flask under reflux and a nitrogen blanket with 35 ml milliQ water and 164 μl of a 20% SDS solution at 70°C. Following a 15 min equilibration time, 67.4 mg KPS dissolved in 2 ml milliQ water was injected into the reaction flask and continued for 2 h. NP cores were exposed to atmospheric oxygen for 45 min followed by a 15 min nitrogen purge. The NP shells were polymerized around the cores

by injection of 794.7 mg NIPAm, 78.0 mg AMPS, 48.2 mg BAC, 4.81 μl AAc, and 164 μl 20% SDS dissolved in 5 ml milliQ water into the reaction flask. After 15 min, 33.7 mg KPS dissolved in 2 ml milliQ water was injected into the reaction flask, and the mixture was refluxed at 70°C for 4 h. The nanoparticle solution was dialyzed in 10 kDa dialysis tubing (Spectrum Laboratories, Dominguez, CA) at 4°C for 14 days; milliQ water was changed daily. Following dialysis, the now hollow NPs (hNPs) were frozen and lyophilized.

3.3.2.1 Fluorophore Incorporation

For RBITC-shell NP batches, 0.1 mol% RBITC dissolved in 1 ml DMSO was injected following NIPAm, AMPS, BAC, AAc, and SDS addition and before shell polymerization initiation, resulting in fluorescently-labeled co-poly(NIPAm-AMPS-AAc-BAC-RBITC) (hNPsRBITC) shell. Each NP batch was synthesized three times for experimental replicates, and tested three times for technical replicates and placed in opaque coverings during dialysis and lyophilization to prevent photobleaching.

3.3.3 Peptide Synthesis

The majority of GAHWQFNALTVRGSG-Hydrazide (GAH-Hyd) was purchased from CPC while a portion was synthesized using the 2-Chlorotrityl Chloride (2-Cl-Trt) resin. Briefly, 2-Cl-Trt (1000 mg) was dissolved in DMF and washed in DMF, DCM, and DMF three times each. The hydrazide (0.5 ml) was dissolved with 100 μl DIPEA, and 4.5 ml DMF and reacted for 2 h. To maximize hydrazide conjugation, this process was repeated. Glycine was added to the hydrazide by dissolving 1848.6 mg FMOC-Glycine and 875.6 mg OymaPure (Sigma Aldrich, St. Louis, MO) in 5 ml DMF, added to the reaction vessel with 960 μl DIC plus 1060 μl DIPEA, and reacted overnight. This process was repeated to maximize glycine conjugation. The 2-Cl-Trt-Hyd-Gly resin was washed with DMF, DCM, and DMF three times each and then loaded into a CEM Liberty Blue Peptide Synthesizer (Matthews, NC) to complete the peptide synthesis. Briefly, FMOC protected L-amino acids were individually

dissolved in synthesis grade DMF to yield 0.2 M solutions. Synthesis occurred at 90°C for 4 – 30 min per amino acid, time varying for each amino acid. GAH-Hyd was cleaved from the 2-Cl-Trt resin using 2 ml of a cleavage cocktail (4.4 ml TFA, 0.25 ml phenol, 0.25 ml milliQ water, and 0.10 ml TIPS) for 3 h, precipitated with 0°C diethyl ether, centrifuged at 1,000 g for 5 min four times, and dried overnight at room temperature. GAH-Hyd was purified using reverse phase fast-protein liquid chromatography (FPLC). Quantification of molecular weight was assessed using Matrix Assisted Laser Desorption/Ionization – Time of Flight (MALDI-TOF) mass spectroscopy.

3.3.4 Peptide Conjugation

GAH-Hyd was conjugated to the surface of hNPs using DMTMM chemistries in MES buffer at pH 4.5. Briefly, 0.5 ml of DMTMM at 75 mg/ml was added to a solution of 1 mg/ml hNPs, titrated to pH 4.5, and allowed to activate carboxylate groups for 30 min. Following activation, GAH-Hyd was added to the solution on a 0, 0.5, 1, 2, 4, and 6 to 1 molar equivalent to AAc polymerized within the hNP shell and reacted while stirring for 60 h. Analogous chemistries were used for RBITC labeled hNPs, but extended to 0, 0.5, 1, 2, 4, 6, 8, 10, and 12-to-1 AAc molar equivalent within the hNPsRBITC shell. These chemistries were repeated using the 1:1 ratio of GAH to AAc within the hNPs in the absence of DMTMM and reacted for 60 h to quantify potential GAH adsorption to the particle. Following the reaction, all batches were purified using KR2i tangential flow filtration (TFF) from Spectrum Labs equipped with 10 kDa nanofiber filter.

Conjugation was quantified using the Pierce Quantitate Peptide Colorimetric Assay (Thermofischer, Waltham, MA) following manufacturer protocols. Briefly, 20 μl of each sample or standard was added to a 96-well clear bottom plate with 180 μl of the working reagent, incubated for 30 min at 25°C, then the absorbance of each well was read at 480 nm using Spectramax M5. A GAH peptide standard curve was used to calculate peptide concentration.

3.3.5 Nanoparticle Characterization

Following purification and lyophilization, hNPs were dissolved at 1 mg/ml in milliQ water and subjected to temperature sweeps from 18.0°C – 42.0°C, in 1.5°C increments, equilibrating for 3 min between each step, and measuring three times per step using dynamic light scattering (DLS) to assess diameter and polydispersity index (PDI). The same procedure was followed after peptide conjugation to obtain their physical characteristics. Zeta (ζ)-potential was obtained on a Nano-ZS90 Zetasizer at 1 mg/ml sample concentration in milliQ water at 18.0°C and 42.0°C using folded capillary cells. All temperature trends and ζ-potential measurements were run in experimental and technical triplicate. The mass of the nanoparticle was calculated using particle diameter assuming a density of 1 g/cm^3. The mass of the nanoparticle and GAH quantification were used to calculate the amount of peptide per particle.

3.3.6 Dynamic Viscosity

Dynamic viscosities were measured on the Discovery HR-3 rheometer (TA Instruments) set to a flow sweep equipped with a 20 mm stainless steel plate with constant angular momentum and the temperature set to 37°C. All therapeutics were dissolved in PBS then added to a solution of 700 kDA HA. Samples at 2.5 wt% HA were allowed to equilibrate to 37°C for 3 min prior to testing. All samples underwent shear sweep from 0.01 to 100 Hz. Dynamic viscosities were calculated using the slope of the shear rate values versus stress, based on a linear fit model.

3.3.7 Tissue Harvest

Fetal bovine knees were purchased from Animal Technologies (Tyler, TX) and cartilage explants were harvested 24 h after slaughter as previously described[18]. Briefly, using a cork borer, 3 mm diameter cartilage explants were taken from the load-bearing femoral condyle and washed three times with 1x PBS. Cartilage explants were then added to 25

ml of Dulbecco's Modified Eagle Media (FBS DMEM)/F12 containing 0.1% bovine serum albumin, 100 units/ml penicillin, 100 μg streptomycin, and 3% FBS), then incubated at 37°C for 10 min. Next, explants were washed three times with Serum Free DMEM/F12 then incubated in 10% FBS DMEM/F12 in a 48-well plate for 3 days.

3.3.8 Therapeutic Diffusion into Cartilage

Aggrecan was removed from cartilage explants using the previous described protocol[19]. Briefly, explants were washed three times with Hank's Balanced Salt Solution (HBSS) then treated with 0.5% (w/v) trypsin in HBSS for 3 h at 37°C. After treatment, explants were washed three times in HBSS and incubated within 20% FBS DMEM/F12 for 10 min to inactive any remaining trypsin activity. Explants were treated with 10% FBS DMEM/F12 (Healthy) or 20 ng/ml IL-1β dissolved in 10% FBS DMEM/F12 to perpetuate inflammation for aggrecan-depleted (AD) samples. Therapeutics were dissolved in PBS to create a 1.6 mg/ml solution and 10 μl was placed on the surface of cartilage explants every 10 min for 1 h at room temperature. For penetration studies: hNPsRBITC or 20 GAH-hNPsRBITC was added to the top of the explant at 10 μl every 10 min for 1 h. For diffusion studies 60 μl of a 1.6 mg/ml solution of 20 GAH-hNPsRBITC was placed on the top of the explant at time zero and at 10, 30, 60, 120, 240, and 1440 min following addition of the NP solution the explant was removed, rinsed and frozen in optimal cutting temperature (OCT) compound. Following, explants were cut in half, embedded in O.C.T. compound (Tissue Tek), sectioned at 5 μm thickness using a cryostat (Leica 3050S), and imaged on at 4x and/ or 60x magnification using a Keyence Digital Microscope.

3.3.9 Compression Testing

Cartilage explants were isolated and cultured as healthy (positive control), aggrecan-depleted (AD) (negative control), or AD and treated with unconjugated hNPs or 19 GAH-hNP. Explants were treated with 0.10 mg and 0.38 mg of unconjugated hNP or 19 GAH-hNP,

respectively. The media was changed every two days and compressive strength was analyzed on day 0 for healthy explants only, and day 6 and day 12 for all other groups. Displacement-controlled unconfined compression was performed using a Discovery HR-3 rheometer (TA Instruments). Explant height was measured (Duratool) and compressive loads were applied from 0 to 30% strain (at 5% intervals) with a 5 μm/s ramp and hold time of 30 s. Moduli were calculated with the slope of the linear fit equilibrium stress vs strain equation. Compression experiments were repeated twice with n = 5 – 7 per group per trial.

3.3.10 GAG Quantification

Glycosaminoglycan degradation was measured by chondroitin sulfate (CS) release from the explant every 2 days in cell culture media using a dimethyl methylene blue (DMMB) assay[20,21]. The weight of the cartilage explant was recorded and CS release was reported as μg of CS released per mg of cartilage explant

3.3.11 Histology & Immunohistochemistry Assessment

Cartilage explants were sectioned using Leica 3050s cryostat at 5 μm thickness. Sectioned and plated tissue samples were submitted to the UC Davis VMTH Anatomic Pathology Service - Histopathology Lab for all staining. Aggrecan depletion was assessed using Safranin O and counter stained with Fast Green. Immunohistochemistry (IHC) was performed to stain for collagen II using an anti-collagen II antibody (ab34712, Abcam, Cambridge, UK). Samples were imaged at 4x magnification using Keyence Digital Microscope. The staining was measured from tissue samples using the area coverage per sample with NIH ImageJ software. The average coverage area was quantified by converting fluorescent images to binary and extracting pixel counts at bins 0 and 255.

3.3.12 *In vivo* nanoparticle retention

Three month old Fischer 344 rats were purchased from Charles River (Wilmington, MA). Following accumulation, rats were anesthetized with isoflurane and the hair was removed from both rat knees. Rats were injected with 0.10 mg of 20 GAH-hNPsRBITC dissolved in PBS (n = 6) into their left joint space or PBS alone as negative control the right joint space as a non-fluorescent control (n = 6). Fluorescence was measured and quantified using the In Vivo Imaging System (IVIS) at the UC Davis Center for Molecular and Genomic Imaging (CMGI) at 557 nm excitation and 623 nm emission. Images were taken immediately prior to injection, post injection, daily for 7 days, then immediately following sacrifice and dissection. Rats were sacrificed using CO_2 euthanasia. Total radiance emission (TRE) fluorescence was collected and analyzed.

3.3.13 Statistical Analysis

Statistical differences of GAH conjugated particles, dynamic viscosity, zeta-potential, PDI, CS release, and histology and immunohistochemistry quantification were assessed using One-Way ANOVA. Two-Way paired ANOVA was used to assess statistical differences amongst compressive strength for cartilage explants, and Two-Way ANOVA for GAH retention *in vivo*. For all analysis, groups that share a letter are statistically analogous, and if the groups do not share a letter, this represents statistically significant differences from one another, with significance being $p < 0.05$.

3.4 Results

3.4.1 Peptide Conjugation & Characterization

The GAH-Hyd conjugation to the AAc polymerized into the hNPs and hNPsRBITCs was confirmed by the presence of peptide on the particle, Figure 3.2. The increase in GAH concentration per mass of hNP indicated GAH attachment to both the hNP and hNPsRBITC.

Nanoparticles incubated with GAH in the absence of DMTMM did not result in peptide conjugation to the nanoparticle as determined by results that showed only minor adsorption readings, indicative of the peptide, following NP purification. The number of GAH peptides per nanoparticle is summarized in Table 3.1. The nomenclature used subsequently to describe the various groups tested was based on the number of peptides added per hNP. For example, 0.5:1 GAH to hNP reaction yielded roughly 19 GAH per hNP and is termed 19 GAH-hNP.

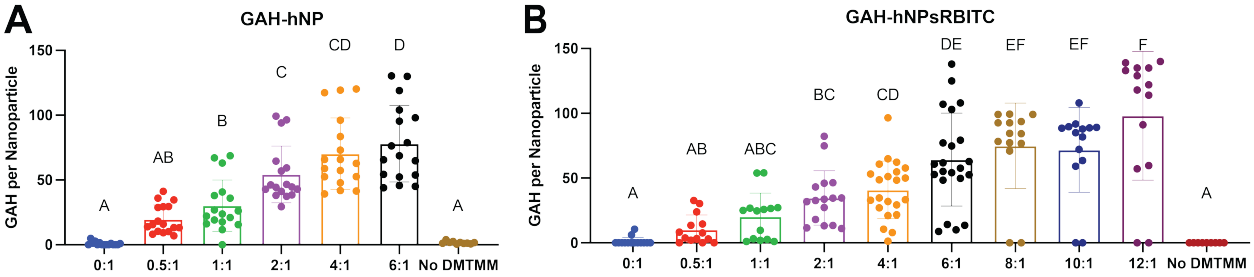

Figure 3.2: Increasing the molar ratio of GAH to AAc within hNP (A) or GAH to AAc within hNPsRBITC (B) increased the amount of GAH conjugated to the respective nanoparticles. Average values summarized in Supplemental Tables 3.2 & 3.3. Different letters denote statistically significant differences between groups while like letters represent groups that are statistically similar ($p < 0.05$).

Table 3.1: The average number of GAH peptides per nanoparticle

GAH to AAc Ratio	GAH/hNP	GAH/hNPsRBITC
0:1	0	0
0.5:1	19	10
1:1	30	20
2:1	54	35
4:1	70	41
6:1	78	64
8:1	N/A	75
10:1	N/A	71
12:1	N/A	98
No DMTMM	0	0

Dynamic light scattering (DLS) confirmed nanoparticle diameter and thermoresponsive behavior of hNP and hNPsRBITC with increasing GAH conjugation, Figure 3.3A and 3.3B

and Supplemental Figure S3.9. The unconjugated hNP and hNPs with $19-50$ GAH had analogous diameters, Figure 3.3A. The same trend was observed with unconjugated hNPsRBITCs and hNPsRBITC conjugated with $10-35$ GAH. The unconjugated hNPs, 70 GAH-hNP, and 78 GAH-hNPs had a diameter of 205.20 ± 8.83, 258.99 ± 69.16 and 986.36 ± 741.27 nm respectively at 18.0°C and 121.57 ± 6.71, 126.60 ± 12.27 and 182.38 ± 45.18 nm at 42.0°C, respectively, Figure 3.3A and Supplemental Table S 3.2. Notably, more than 41 GAH on the hNP and hNPsRBITC increased the polydispersity of the particles, Figure 3.3A and 3.3B and Supplemental Tables S 3.2 and 3.3. The 78 GAH-hNP had 4.58-times higher polydispersity index (PDI) than 19 GAH-hNP at 18.0°C, and 98 GAH-hNPsRBITC had a 10.63-times higher PDI than 10 GAH-hNPsRBITC at 18.0°C, Supplemental Figure S 3.10 and Supplemental Tables S 3.2 and 3.3.

Increasing the conjugation of GAH to both hNP and hNPsRBITC significantly increased the zeta-potential of the particles. At 18.0°C, unconjugated hNPs had a zeta-potential of -24.93 ± 2.53 mV, and the GAH conjugated hNPs had a 52.91 to 65.47% increase in surface charge in comparison, Figure 3.3C and Supplemental Tables S 3.2 and S 3.3. The unconjugated hNPsRBITCs at 18.0°C had a zeta-potential of -21.41 ± 1.26 mV at 18.0°C and GAH conjugation resulted in a 23.72 to 56.53% increase in surface charge, Figure 3.3E and upplemental Tables S 3.2 and S 3.3.

3.4.2 Hyaluronic Acid Binding and Diffusion into Cartilage Explants

The GAH-hNP and GAH-hNPsRBITC particles bind to HA as measured by the increase in dynamic viscosity (DV) of a free HA solution treated with GAH-hNP and GAH-hNPsRBITC particles, Figure 4A and 4C. The DV of the HA solution treated with unconjugated hNPs and hNPsRBITC was 3.2 ± 0.5 Pa.s and 3.3 ± 0.3 Pa.s, respectively, and 19 GAH-hNP and 20 GAH-hNPsRBITC had a DV of 6.2 ± 0.5 Pa.s and at 4.8 ± 0.6 Pa.s, respectively. In comparison, 10 GAH-hNPsRBITC had a 3.4% increase in DV compared to unconjugated hNPsRBITC and did not elicit significant HA binding, Figure 3.4C. All other groups had

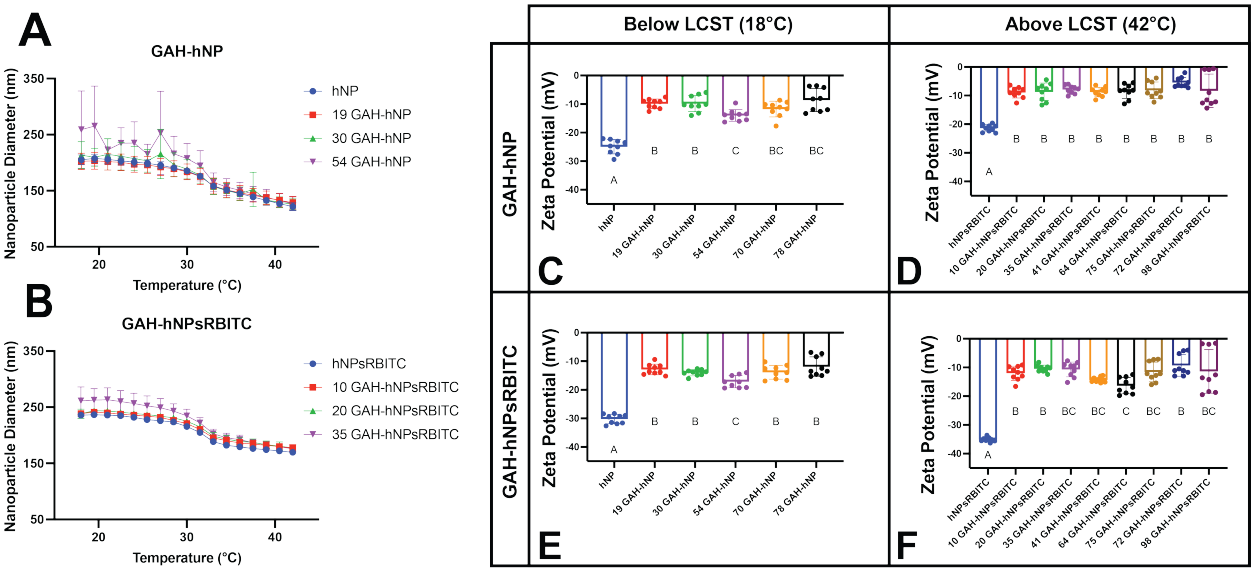

Figure 3.3: The diameter of the hNP (A) or hNPsRBITC (B) particles increased with increasing conjugation of GAH to the nanoparticle. Conjugating GAH to hNPs significantly increased the surface charge of the particles compared to unconjugated particles, below (C) and above (D) the LCST of pNIPAm. Conjugation of GAH to hNPsRBITC also increased the surface charge below (E) and above (F) the LCST of pNIPAm. Values listed in Supplemental Tables S 3.2 and S 3.3. Different letters denote statistically significant differences between groups while like letters represent grpups that are statistically similar ($p < 0.05$).

analogous increases in DV to the 19 GAH-hNP and 20 GAH-hNPsRBITC when compared to their unconjugated hNP or unconjugated hNPsRBITC, Figure 3.4A and 3.4C. hNPs and hNPsRBITCs conjugated with 19 – 35 GAH remained monodisperse and significantly bound to HA, Figure 3.4A, 3.4C, Supplemental Tables S 3.2 and S 3.3. We subsequently proceeded with particles conjugated with 19 GAH-hNP and 20 GAH-hNPsRBITC since they elicited statistically similar increases in DV compared to respective unconjugated nanoparticles and were monodisperse.

As determined by DV measurements, all concentrations of 19 GAH-hNP and 20 GAH-hNPsRBITC significantly bound to HA, Figure 3.4B and 3.4D. Notably, treatment with 60 μl of 3.2, 6.4, 12.8 and 25.6 mg/ml of 19 GAH-hNP and of 20 GAH-hNPsRBITC showed similar HA binding and had at least a 54.6% increase in DV compared to their respective

controls, Figure 3.4B and 3.4D. The treatment with 60 μl of 0.08 mg/ml 19 GAH-hNP and 20 GAH-hNPsRBITC had a 28.2% and 31.8% increase in DV compared to control, respectively. Treatment with 1.6 mg/ml of 19 GAH-hNP and 20 GAH-hNPsRBITC had a 54.6% and 45.6% increase in DV compared to the PBS control, respectively, Figure 3.4B and 3.4D. The subsequent *ex vivo* cartilage explant studies proceeded with treatment with 0.10 mg of 19 GAH-hNP or 0.10 mg of 20 GAH-hNPsRBITC as the lower mass per cartilage plus, and 0.38 mg of 19 GAH-hNP or 0.38 mg of 20 GAH-hNPsRBITC as the higher mass per cartilage plug.

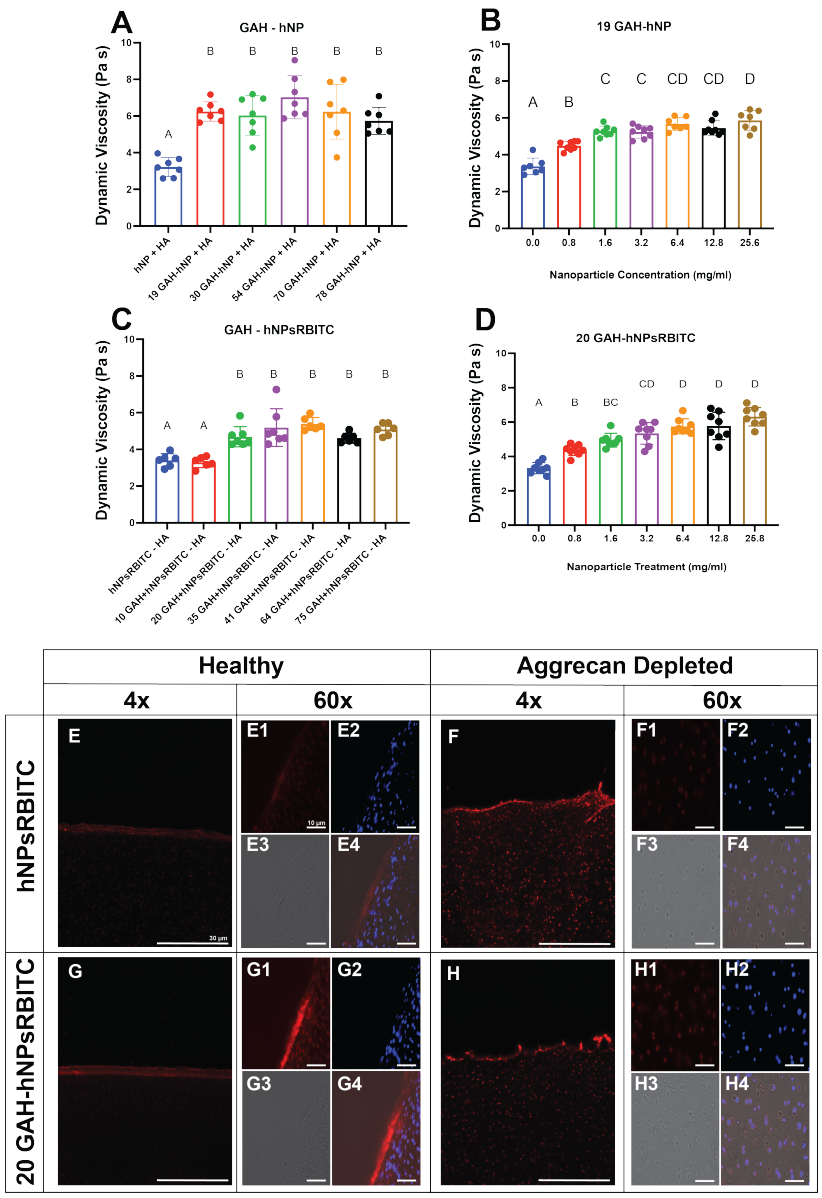

Figure 3.4: (A - D) Dynamic viscosity (DV) of the HA solution by GAH-hNP or GAH-hNPsRBITC and (E - H) diffusion of unconjugated hNPsRBITC or 20 GAH-hNPsRBITC into (E & G) healthy or (F & H) aggrecan-depleted cartilage explants. (A & C) GAH-hNP and GAH-hNPsRBITC with greater than 19 GAH per nanoparticle significantly increased DV. (B & D) Increasing the concentration of 19 GAH-hNP and 20 GAH-hNPsRBITC within the HA solution increased DV. (E - H) Sagittal cross section of load bearing fetal bovine articular cartilage. Healthy (E & G) and aggrecan depleted (F & H) ex vivo cartilage plugs treated with unconjugated hNPsRBITC (E & F) and 20 GAH-hNPsRBITC (G & H). Unconjugated hNPsRBITC and 20 GAH-hNPsRBITC significantly penetrated into aggrecan-depleted cartilage. E - H1: RBITC; E - H2: Hoechst (Nuclei); E - H3: Brightfield; E-H4: Overlay. Scale bar for A - H: 30 μm; E-H1 - E-H4: 10 μm. Different letters denote statistically significant differences between groups while like letters represent grpups that are statistically similar ($p < 0.05$).

3.4.3 Diffusion into Aggrecan Depleted Cartilage Explants

After 48 h of incubation with unconjugated hNPsRBITC and 20 GAH-hNPsRBITC, fluorescent images of cryosectioned tissue showed that hNPsRBITC and 20 GAH-hNPsRBITC remained on the surface of healthy articular cartilage, Figure 3.4E & 3.4G, while hNPsRBITC and 20 GAH-hNPsRBITC permeated into AD cartilage explants, Figure 3.4F & 3.4H. Figure 3.4F4 and 3.4H4 show the overlay of hNPsRBITC and 20 GAH-hNPsRBITC, respectively, with nuclei of chondrocytes within the explants suggesting localization of the particles near chondrocytes. Moreover, roughly 4 h was required for unconjugated hNPsRBITC and 20 GAH-hNPsRBITC to significantly diffuse into the AD explant, Supplemental Figure S 3.11.

3.4.4 Compression Testing

The untreated-healthy explants and untreated-AD cartilage explants had a compressive strength of 123.7 ± 26.5 kPa and 31.9 ± 11.8 kPa on day 6, and 130.5 ± 29.7 kPa and 34.9 ± 9.8 kPa on day 12, respectively. The AD explants showed a 74.2% and 73.2% loss in compressive strength on day 6 and 12, respectively, compared to untreated-healthy controls on the same day, Figure 3.5. The AD explants treated with 0.10 mg of 19 GAH-hNP had a compressive strength of 95.68 ± 16.22 kPa on day 6 and were statistically analogous to untreated-healthy explants, Figure 3.5. The AD explants treated with 0.10 mg of 19 GAH-hNP on day 12 had a compressive strength of 79.7 ± 21.9 kPa and were statistically similar to explants treated with 0.10 mg of 19 GAH-hNP on day 6, but had a 63.8% loss in compressive strength compared to untreated-healthy explants on the same day, Figure 3.5. The untreated-AD explants and explants treated with 0.10 mg of hNP had statistically analogous compressive strength on day 6 and day 12. However, they had a compressive strength of 63.8 ± 10.0 kPa and 58.9 ± 21.1 kPa on day 6 and day 12, respectively – a 200.1% and 168.9% increase in compressive strength compared to untreated-AD explants on the same day, Figure 3.5. The AD explants treated with 0.38 mg of hNP and 0.38 mg of 19 GAH-hNP had similar

compressive strengths, 27.0 ± 9.4 kPa and 30.6 ± 10.6 kPa on day 6 and 26.6 ± 8.0 kPa and 34.8 ± 8.9 kPa on day 12, respectively, to untreated-AD explants, Figure 3.5.

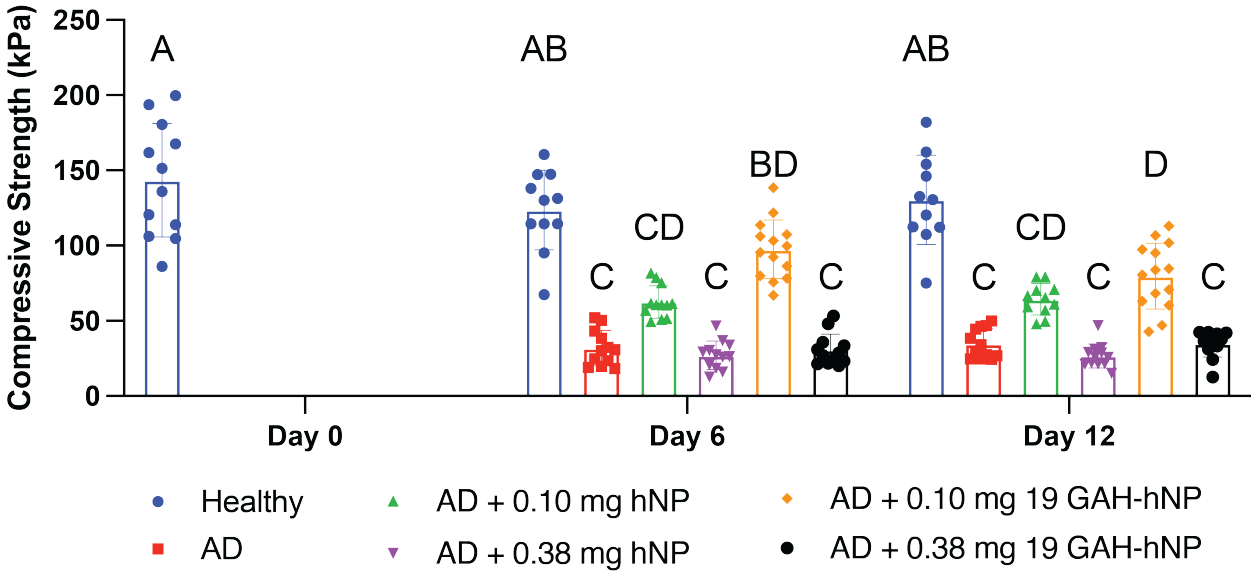

Figure 3.5: Treatment with 0.10 mg of 19 GAH-hNPs significantly restored the compressive strength of osteoarthritic *ex vivo* cartilage explants at day 6 and day 12. Data is represented as mean ± StDev (n = 10 – 12 per treatment per timepoint). Different letters denote statistically significant differences between groups while like letters represent grpups that are statistically similar ($p < 0.05$).

3.4.5 ECM Degradation

The amount of CS released from explants treated with 0.10 mg of 19 GAH-hNP was statistically analogous to healthy cartilage, Figure 3.6. The explants treated with 0.38 mg of 19 GAH-hNP released 18.19% more CS than explants treated with 0.10 mg of 19 GAH-hNP. Untreated-AD explants and explants treated with 0.10 mg and 0.38 mg of hNPs had a 53.94%, 43.96% and 47.81% increase in CS release, respectively, compared to untreated-healthy explants, Figure 3.6. However, explants treated with 0.10 mg of hNP had 17.78% decrease in CS release compared to untreated-AD explants. There was no significant difference in CS release of the explants treated with 0.38 mg of hNP compared to untreated-AD explants, Figure 3.6. Notably, the DMMB assay did not react with the sulfated hNPs demon-

strating that the DMMB signal is associated with GAGs, Supplemental Figure S 3.13.

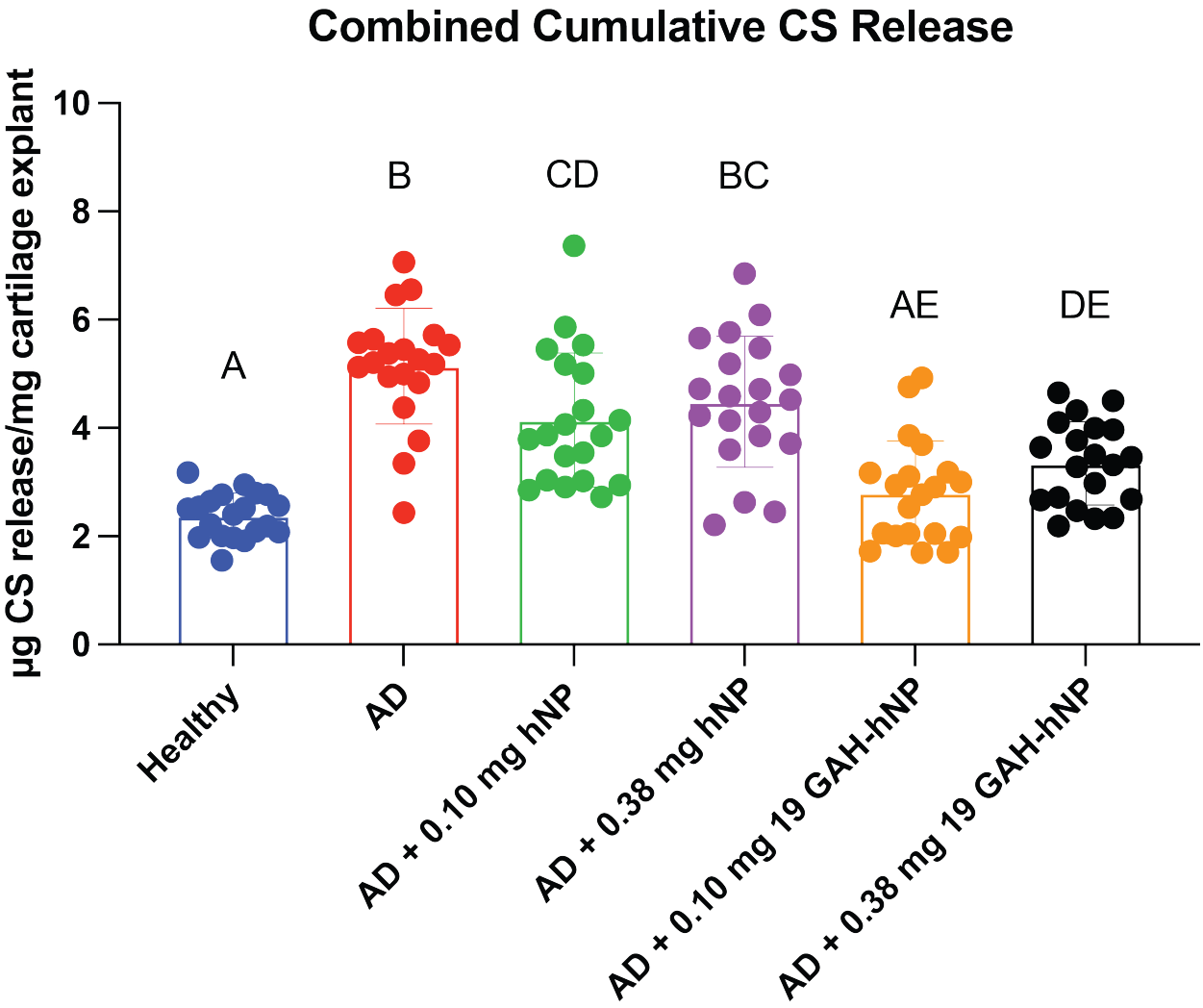

Figure 3.6: Treatment with 0.10 mg of 19 GAH-hNP inhibited further degradation of the ECM of AD cartilage as quantified by accumulative CS release. Different letters denote statistically significant differences between groups while like letters represent grpups that are statistically similar ($p < 0.05$).

3.4.6 Histology and Immunohistochemistry

Positive Safranin O staining showed the presence of GAGs in untreated-healthy explants and AD explants treated with 0.10 mg of 19 GAH-hNP, with some expression in explants treated with 0.38 mg of 19 GAH-hNP, Figure3.7A, 3.7E, 3.7F, and 3.7M. The explants

treated with 0.10 mg of 19 GAH-hNP had a 44.95% decreases in GAG content, compared to untreated-healthy explants. However, AD-explants treated with 0.10 mg of 19 GAH-hNP had 5.99-times more GAG content than untreated-AD explants, Figure 3.7A, 3.7B, 3.7E, and 3.7M. The untreated-AD explants and explants treated with 0.10 mg and 0.38 mg of hNP showed a significant loss of GAGs and were all statistically similar with respect to GAG content, Figure 3.7B-D, and 3.7M. Notably, Safranin O and Fast Green does not stain the sulfated hNPsRBITC, shown in Supplemental Figure S 3.12.

The untreated-AD explants had a 87.58% loss in collagen type II, compared to untreated-healthy explants, Figure 3.7H, 3.7G, and 3.7N, respectively. The explants treated with 0.10 mg of 19 GAH-hNP has 409.1% more collagen type II than untreated-AD explants, Figure 3.7K, 3.7H, and 3.7N. However, the explants treated with 0.10 mg of 19 GAH-hNP had 49.19% less collagen type II than the untreated-healthy explants, Figure 3.7G, 3.7K, and 3.7N. The explants treated with 0.10 mg and 0.38 mg of hNP showed a 92.39% and 86.15% loss of collagen type II compared to untreated-healthy explants, Figure 3.7I, 3.7J, and 3.7N. The explants treated with 0.38 mg of 19 GAH-hNP showed 73.25% loss in collagen type II compared to untreated-healthy explants, Figure 3.7H, 3.7L, and 3.7N.

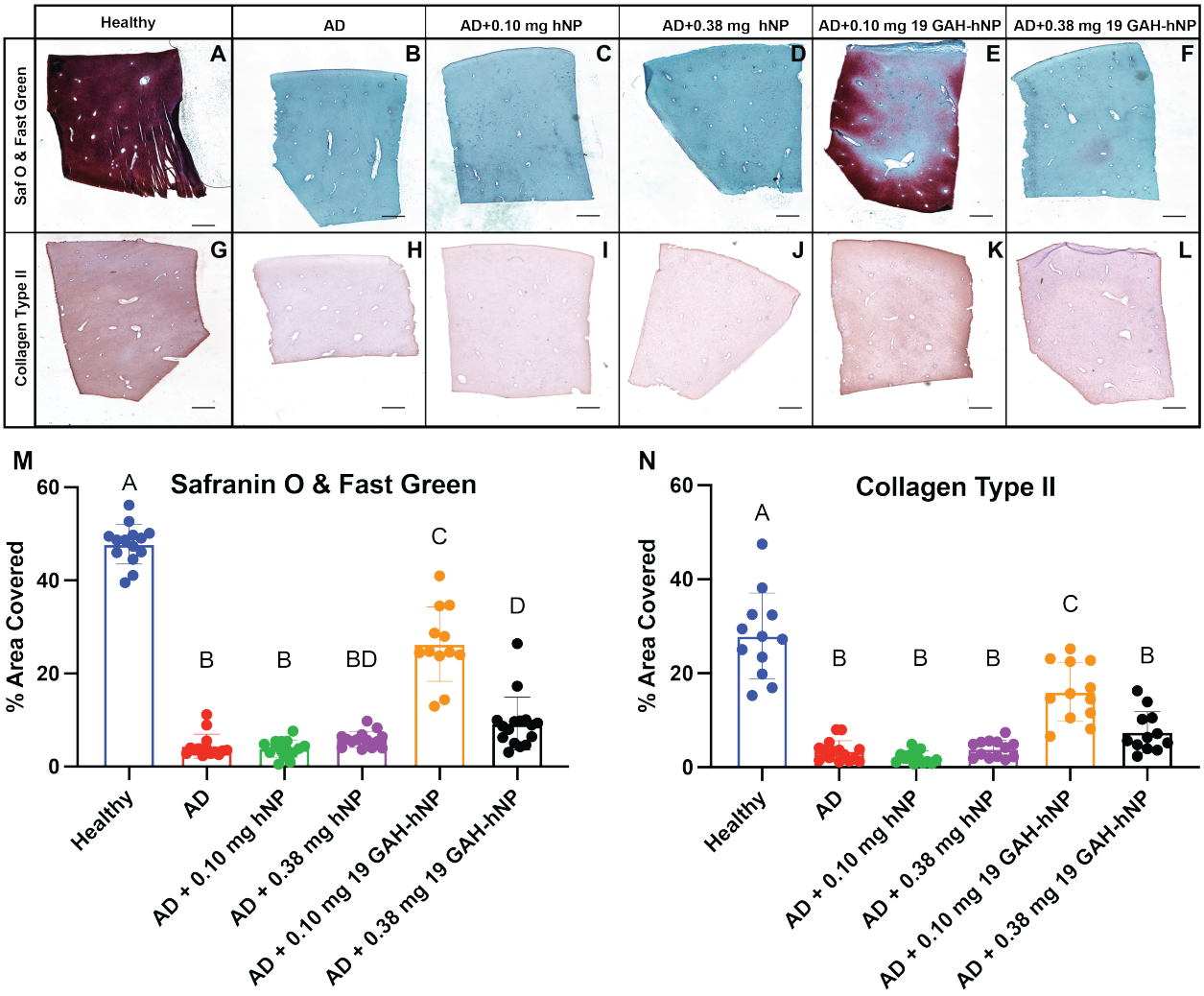

Figure 3.7: Safranin O & Fast Green staining of cartilage explants to quantify GAG content. IHC using anti-collagen II antibody. The explants treated with 0.10 mg of 25 GAH-hNP (E & K) inhibited the degradation of the ECM. Scale bar 100 μm. Different letters denote statistically significant differences between groups ($p < 0.05$).

3.4.7 Retention of GAH-hNPsRBITC within Joint Space

20 GAH-hNPsRBITC was injected into and retained within the joint space of rats for at least 7 days as confirmed by the 400.1% increase in total radiant efficiency (TRE) of the injected knee compared to the same knee before injection, Figure 3.8. Moreover, 24 h following the injection the 20 GAH-hNPsRBITC injected knee had 327.1% increase in TRE

compared to the PBS injected knee. After dissection, the 20 GAH-hNPsRBITC injected knee had a 958.9% increase in TRE compared to the PBS injected knee, Figure 3.8.

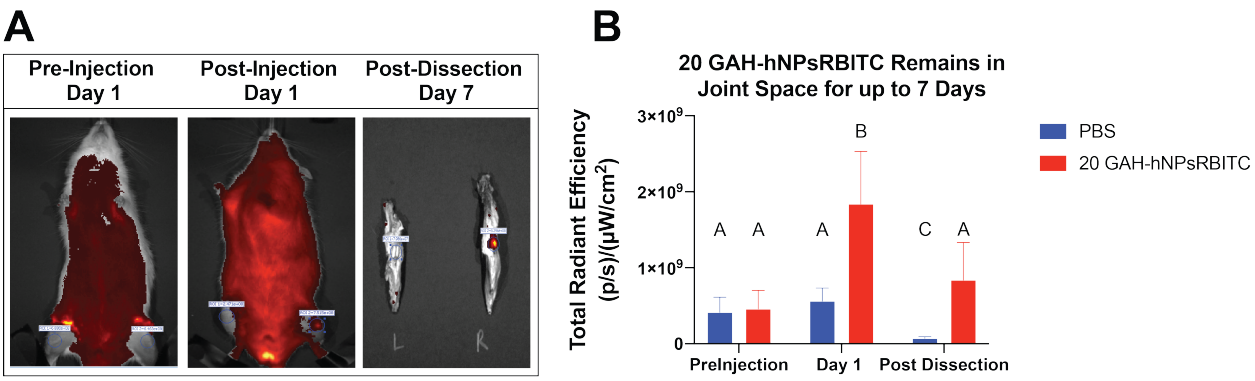

Figure 3.8: 20 GAH-hNPsRBITC remain in the joint space for at least 7 days following injection. Different letters denote statistically significant differences between groups while like letters represent grpups that are statistically similar ($p < 0.05$).

3.5 Discussion

Nanomedicine offers a potential solution to halt the progression of PTOA. There are several polymeric[22–26], lipid[27–31], and metallic[32,33] nanotherapeutics currently being studied to treat osteoarthritis. However, many emerging osteoarthritis nanotherapeutics do not specifically target osteoarthritic cartilage nor do they inhibit the degradation of its ECM. They instead focus on inflammation and/ or joint pain[24,26–36]. Modifying nanoparticles to bind to and treat damaged osteoarthritic cartilage offers a solution to this current limitation. Recent advances within nanomedicine have resulted in modified nanoparticles functionalized with antibodies for cell targeting[35], poly(ethylene glycol)(PEG) for increased biocompatibility[36,37], and peptides for cell targeting and as therapeutics[38]. Antibody-NPs are used therapeutically for drug delivery[39,40], gene delivery[41], and radio therapy[42], and diagnostically for MRI[43], bioseparation[44], and immunoassays[45]. PEG conjugated to metallic NPs decreased particle aggregation[36] and PEG conjugated to polymeric NPs to increase the particles half-life[37]. Peptide-NPs are primarily used for biomarker detection and molecular imaging probes, with the nanoparticles used being overwhelmingly metallic. New studies are emerging using peptides conjugated to polymeric nanoparticles for imaging and detec-

tion[46,47], breast[48] and lung[49] cancer treatment, gene delivery[50], as well as multiple sclerosis treatment[51]. Here, we build upon the targeting success of peptide-NPs wherethe HA-binding peptide GAH was conjugated to an anionic hNPs to target damaged cartilage and support nanoparticle therapeutic function to inhibit the progression of OA.

Preventing aggrecan degradation within osteoarthritic cartilage is difficult since it happens quickly following joint trauma and inflammation. Therefore, we aimed to mimic aggrecan function using an anionic nanoparticle conjugated with the peptide GAH. CS and keratin sulfate (KS) compose the anionic GAGs component of aggrecan and provide it with a net negative charge, thus allowing the aggrecan to generate an osmotic gradient that supports water retention and provides articular cartilage with its compressive strength[5]. To mimic the protective effects of aggrecan, we used our previously described anionic, degradable, poly(NIPAM-co-AMPS-AAc-BAC) hollow nanoparticles (hNPs)[17] and functionalized them with GAH to support HA-binding.

DMTMM carboxylic acid activation chemistry was used to conjugate GAH-hydrazide to the anionic hNPs; this chemistry avoids potential covalent attachment of ECD to the hNP due to conversion from the N- to O-acylurea[52]. Functionalization of the hNPs with GAH was confirmed using a peptide colorimetric assay, Figure 3.2. An increase in peptide number conjugated per hNP was achieved by increasing the molar equivalent of GAH to the molar equivalent AAc polymerized within the shell of the nanoparticle during the conjugation reaction, Figure 3.2. Notably, when GAH and hNP or hNPsRBITC were reacted without DMTMM, no significant peptide conjugation was recorded. Similar conjugation of GAH was achieved to both hNPs and nanoparticles with RBITC polymerized into the shell (hNPsRBITC). Similar GAH binding to hNPsRBITC compared to hNP was achieved by allowing the hNPsRBITC particles to dissolve for 24 h, rather than the 3 h used for hNP, and increasing the molar ratio of GAH to AAc to 12:1 in the reaction mixture as compared to 6:1 used for hNP, Figure 3.2. GAH conjugation to hNPsRBITCs was likely hindered by the large, hydrophobic RBITC monomer sterically limited access to AAc within the nanoparti-

cle nanoparticle leading to the requirement of increased particle swelling time and increased GAH:AAc as compared to that used for GAH hNP conjugation.

The anionic charge of the hNPs provided colloidal stability, and was hypothesized to mimic the anionic charge of GAGs in order to treat aggrecan-depleted cartilage[17,23,53]. Any addition of GAH to the particle resulted in a significant increase in surface charge. However, the magnitude of increase in the zeta-potential did not increase with additional GAH conjugation. The GAH-hNP retained an anionic charge at all tested concentrations of GAH conjugation, Figure 3.3D & 3.3F, and Supplemental Tables S 3.2 and S 3.3.

The incorporation of NIPAm within the poly(NIPAm-co-AMPS-AAc-BAC) shell gives the particles their thermoresponsive behavior, Figure 3.3A & 3.3B and Supplemental Tables S 3.2 and 3.3, with an LCST near 32°C. The particles swell below the LCST, and have a 284.87% larger surface area when swollen compared to when collapsed at temperatures above the LCST. This trait was exploited to promote particle swelling and thereby decrease potential steric hindrance that may lower the GAH conjugation to AAc within the particles. The addition of 19 to 35 GAH to the nanoparticles did not significantly alter final nanoparticle diameter either below or above the LCST. However, more than 41 GAH on the nanoparticle resulted in a significant increase in diameter compared to particles with 19 – 35 GAH conjugated to them, Figure 3.3A & 3.3B and Supplemental Tables S 3.2 and S 3.3. These data suggest that there is a maximum concentration of peptide that can be conjugated to the particle before agglomeration occurs and causes variability in the measured diameter due to the presence of nanoparticle clusters. This insight is critical since nanoparticles with a diameter over 200 nm are known to initiate an inflammatory response *in vivo*[54]. Therefore, we aimed to develop a peptide-nanoparticle system that was under 200 nm when administrated at physiological temperatures. Notably, the 19 GAH-hNP had a diameter of 128.58 ± 11.34 nm above its LCST at physiological temperatures, and should not elicit an immune response due to size *in vivo*[54].

PDI is crucial for the quality control of nanotherapies and the FDA recently published

guidelines for liposome (lipid-based nanoparticle) drug products emphasizing the importance of size and size distribution as "critical quality attributes (CQAs)"[55]. Additionally, Danaei et al published a review article further emphasizing the importance of monodisperse nanocarriers for medical applications[56]. A PDI of less than 0.2 signifies monodispersion of particles in solution[56]. The nanoparticles with 19 to 35 GAH were monodisperse while the nanoparticles with more than 41 GAH were polydisperse. The conjugation of molecules to pNIPAm-based nanoparticles shifts the LCST of the polymer making them more hydrophobic[57]. Conjugating molecules to the pNIAPm nanoparticles inhibited its ability to form hydrogen bonds with water and swell, causing the particle to lose its thermoresponsive behavior and be more hydrophobic[57]. Hydrophobic pNIPAm agglomerate to form stabilized particles[17]. Agglomerating into larger hydrophobically stabilized particles may explain why the particles with more than 41 GAH conjugated to them had a significant increase in diameter, loss of thermoresponsive behavior, and increased PDI. Supplemental Figure S 3.9 and Supplemental Figure S 3.10.

Previously GAH was conjugated to anionic CS and was shown to restore the compressive strength of aggrecan-depleted cartilage[7]. Here, we show that synthetic nanoparticles with a high anionic character can also improve the compressive strength of damaged cartilage. To show that the GAH-hNPs bound to HA, we used dynamic viscosity, a value that increases with apparent polymer molecular weight. The 19 GAH-hNPs and 20 GAH-hNPsRBITC bound to HA and had a 94.0% and 39.7% increase in DV compared to an HA solution treated with unconjugated particles. Initially, it was hypothesized that increasing GAH conjugation to the particle would lead to increased HA binding. This, however, was not observed. This unexpected outcome may be due to particle aggregation at high peptide conjugation density. Examining the DLS and DV data together to find peptide conjugation densities that supported HA binding without inducing particle aggregation led to the use of 19 GAH-hNP and 20 GAH-hNPsRBITC Figure 3.4A & 3.4C, Supplemental Figure S 3.10, and Supplemental Tables S 3.2 and S 3.3. Further studies examined the concentration of

19 GAH-hNP and 20 GAH-hNPsRBITC necessary to significantly increase the DV. All concentrations of 19 GAH-hNP and 20 GAH-hNPsRBITC tested increased DV by binding to HA. These data showed a lower and higher range where binding to HA was statistically similar. The increase in viscosity was mostly linear between treatment with 0.8 mg/ml and 3.2 mg/ml of 19 GAH-hNP and 20 GAH-hNPsRBITC. Above treatment with 6.4 mg/ml of GAH-particle the there was no significant increase in DV between the treatments groups. These data suggest there is a maximum amount of HA to which the GAH conjugated particles can bind. The subsequent *ex vivo* cartilage explant studies proceeded with treatment of 60 μ of 1.6 mg/ml (0.10 mg) of 19 GAH-hNP as the lower concentration since it had higher increase in DV compared to the 0.8 mg/ml treatment and had analogous DV to treatment with 3.2 mg/ml of 19 GAH-hNP. Treatment with 60 μ of 6.4 mg/ml (0.38 mg) of 19 GAH-hNP was chosen has the higher concentration as it had analogous DV as treatment with 12.5 mg/ml and 25.8 mg/ml of GAH conjugated nanoparticles.

Treating cartilage explants with trypsin has been shown to strip aggrecan from the explant without damaging chondrocytes, HA, or collagen, and serves as an *ex vivo* model for osteoarthritis[7,18,58,59]. Unconjugated hNPsRBITC and 20 GAH-hNPsRBITC permeated into aggrecan-depleted explants while they remained at the surface of the healthy explants. These data agreed with previous studies where anionic bottle brush polymers and pNIAPm-based nanoparticles diffused into damaged cartilage[23,60], while pNIPAm-based nanoparticles remained on the surface of healthy cartilage[23]. The 20 GAH-hNPsRBITC diffused slower than the compared to unconjugated hNPsRBITC, potentially due to differences in HA binding within the explant, though both unconjugated and conjugated particle types significantly permeated into AD cartilage after 4 h.

The ability of 19 GAH-hNP to restore compressive strength and inhibit further ECM degradation was tested using cultured bovine explants. In other studies, healthy cartilage explants tested under unconfined compression had stiffness of 100 - 500 kPa, and damaged untreated cartilage had stiffness of 40 - 60 kPa, matching our data[7,61,62]. Untreated-healthy

explants were examined on day 0, 6, and 12 to serve as a baseline time point comparison to account for the potential effects that *ex vivo* culturing might have on cartilage compressive strength, Figure 3.5; however, no statistically significant changes occurred. Stripping the explants of aggrecan greater than 70% loss in compressive strength on days 6 and day 12, respectively, compared to the same day untreated-healthy controls, highlighting the importance of aggrecan to maintain the compressive strength within joint[4]. The compressive strength of AD explants treated with unconjugated hNPs was examined to assess the therapeutic effect of nanoparticle HA binding when treating damaged cartilage. The unconjugated hNP treated AD explants had a slightly increase in compressive strength, but the increase was not statistically different from the compressive strength of untreated-AD explants. The explants treated with 0.10 mg of 19 GAH-hNP significantly restored the compressive strength of AD cartilage to healthy levels 6 days after single treatment. The observed improvement in compressive strength is likely due largely to retention of the 19 GAH-hNP within the cartilage ECM as a results of interactions with HA, and thus its ionic charge. It is also likely that the 19 GAH-hNP serves as transient crosslinks within the damaged tissue that may also contribute to the compressive strength. The decrease in compressive strength observed between days 6 and 12 in GAH-hNP treated cartilage suggests that some of the particles are lost from the tissue either via diffusion out of the tissue or by degradation of the particles over time. The colocalization of 20 GAH-hNPsRBITC with chondrocytes, shown using immunofluorescent imaging in Figure 3.5, suggests some particle endocytosis. Previously, the poly(NIPAm-co-AMPS-AAc-BAC) hNPs were shown to be endocytosed, degraded, and cleared from chondrocytes in 5 – 7 days in vitro[17]. Interactions with HA may dampen the uptake of 19 GAH-hNP by chondrocytes and slow their endosomal degradation, but it is unlikely that cell uptake is not eliminated. Further, glutathione (GSH) is also present in the ECM, although at lower concentrations than that within the cells[63,64], and can degrade the disulfate crosslinked GAH-hNPs even in the ECM. Therefore the 19 GAH-hNP that remained in the tissue can also be slowly degraded by GSH. The unconjugated hNPs can

both be more readily endocytosed and degraded and diffuse from the tissue, which would both account for their loss and a decrease in the restored compressive strength. Together, these data suggest that some nanoparticle degradation and/or diffusion from the tissue is occurring and this loss of particles from the tissue happens more quickly than the deposition of new aggrecan; the loss of nanoparticles and subsequent decrease in compressive strength happens quicker for hNP than for 19 GAH-hNP. Overall, NP loss accounts for the decline in compressive strength between day 6 and 12. Notably, the explants treated with the 0.38 mg of unconjugated hNP and 19 GAH-hNP exhibited a loss in compressive strength compared to the respective explants treated with the lower concentration. This is believed to be due to a rapid buildup of the particles on the surface of the cartilage, which formed an anionic particle layer that inhibited therapeutic diffusion into the AD explant. This has been similarly observed and noted in a previous study using anionic polymer treated AD explants[58]. These data show the AD-explants treated with 0.10 mg of 19 GAH-hNP restored compressive strength to that of untreated-healthy cartilage on day 6.

Aggregation of aggrecan on HA and the charge of aggrecan have been shown to lower catabolic enzyme expression and protect collagen type II from degradation[5–7]. Mimicking aggrecan-HA binding and charge using sulfate polymers may elicit the same protection. To test this, CS release from cartilage explants was studied. Nominal CS release is normal from healthy cartilage, while excess CS release leads to increased catabolic enzyme expression and the irreparable degradation of collagen type II – resulting in OA[7,13]. Treatment of AD explants with 0.10 mg and 0.38 mg of unconjugated hNPs did not protect the ECM from degradation as determined by a significant release of CS into the media compared to that seen with untreated-healthy explants. However, explants treated 19 GAH-hNP resulted in significantly less CS release into the media than untreated-AD explants. Because the hNPs are sulfated and DMMB was used to assess CS release, we examined whether DMMB also detected the hNP. Although, DMMB binds to a sulfated tetrasaccharide sequence in GAGs, so it is likely that the dye would bind to the hNPs[21]. To test DMMB-hNP binding/detection,

serial dilutions of the hNPs were created and reacted with the DMMB. However, no signal was detected at any hNP concentration, Supplemental Figure S 3.13. Therefore, the DMMB signal detected in our cartilage explant studies was not from released hNPs, but from released CS throughout the culture time. The DMMB data support the hypothesis that 19 GAH-hNPs slowed the ECM degradation of articular cartilage that is associated with OA.

Further examination into the ECM composition of the AD explants demonstrated that treatment with 0.10 mg of 19 GAH-hNP was able to slow ECM degradation, Figure 3.7. The AD explants treated with the 0.10 mg of 19 GAH-hNP had 5.99 times more GAGs and 4.09 times more collagen type II than untreated-AD explants. Both fragmented HA and collagen are known catabolic stimulants[65]. The GAH-hNPs may sterically hinder catabolic enzyme diffusion into the matrix and inhibit HA and collagen degradation, thus protecting the ECM. While there was a loss of GAGs and collagen type II compared to untreated-healthy explants, these data show the 19 GAH-hNP slowed the degradation of the ECM of articular cartilage in AD cartilage explants and suggest that the chondrocytes are synthesizing new CS.

Current intra-articular delivery of free therapeutics have less than a 3 day retention time within the joint[66,67]. We examined the retention of 19 GAH-hNP in a rat joint. HA is a major component of the synovial fluid and is turned over roughly every 13 h[68], binding to HA could reduce GAH conjugated nanoparticles joint retention time. Rats injected with 20 GAH-hNPsRBITC had a 400.1% increase in the total radiant efficiency (TRE) compared to before injection, Figure 3.8. The GAH conjugated particle remained in the joint for up to 7 days as confirmed by the 958.9% increase in TRE of the 20 GAH-hNPsRBITC injected joint compared to the contralateral following dissection, Figure 3.8. Other studies showed that charged nanoparticles increase the retention time of therapeutics within the joint following intra-articular injection[17,26]. Previously we showed that unconjugated hNPsRBITC injected into the joint space had no loss of TRE between initial injection and at the conclusion of 7 days[17]. However, the 20 GAH-hNPsRBITC injected rats had a 45.58% reduction in TRE between day 1 and after hindlimb dissection. This decreased retention could be due to

interactions with the HA in the synovial fluid and potential increased nanoparticle clearance due to the continual replenishment of synovial fluid within articular joints. Nonetheless the 20 GAH-hNPsRBITC therapeutic was retained to a significant level within the joint for 7 days. Future studies will investigate the dosage of nanoparticles needed to observe a therapeutic effect *in vivo*. In addition, the unconjugated poly(NIPAM-co-AMPS-BAC-AAc) hNP have been shown previously to load and release therapeutic doses of an MAPKAP Kinase 2 (MK2) inhibitor peptide[17]. Future studies will investigate the potential therapeutic benefit of combining the protective effects conferred by these anionic, HA-binding particles with the controlled release of anti-inflammatory, MK2 inhibitor peptides.

3.6 Conclusion

Here we highlight the ability of hollow, degradable nanoparticles to be functionalized with ECM-binding peptides using DMTMM peptide coupling chemistry. Increasing the molar equivalent of GAH-peptide to AAc polymerized into the shell of the poly(NIPAM-co-AMPS-AAc-BAC) and poly(NIPAM-co-AMPS-AAc-BAC-RBITC) particles led to increased peptide concentration on the hNPs and hNPsRBITCs, respectively. Notably, increasing the peptide amount to more than 41 GAH per particle led to increased polydispersity. The PDI and DV data together resulted in the use of 19 GAH-hNP and 20 GAH-hNPsRBITC, in all *ex vivo* studies as they were able to bind to HA and increase DV while resisting aggregation. In *ex vivo* cartilage studies, AD explants treated with 0.10 mg of 19 GAH-hNP showed restored compressive strength and inhibited ECM degradation. Finally, the 19 GAH-hNP therapeutic was retained within the joint space of rats for 7 days. Treatment with 0.10 mg of 19 GAH-hNP slowed ECM degradation and restored the compressive strength in AD cartilage and showed promise in inhibiting the degradation of cartilage associated with OA.

3.7 Conflicts of Interest

The authors declare no conflicts of interest.

3.8 Acknowledgements

The authors would like to thank Dr. David Cameron for cryotome training and help in sectioning cartilage plugs. Additional thanks to Dr. Michele Marcolongo, Evan Phillips, and Dr. Tomas Gonzalez-Fernandez for their advice and recommendations with IHC. Thank you to Alena Casella in her training using ImageJ to analyze histology and IHC staining.

3.9 Supplemental Material

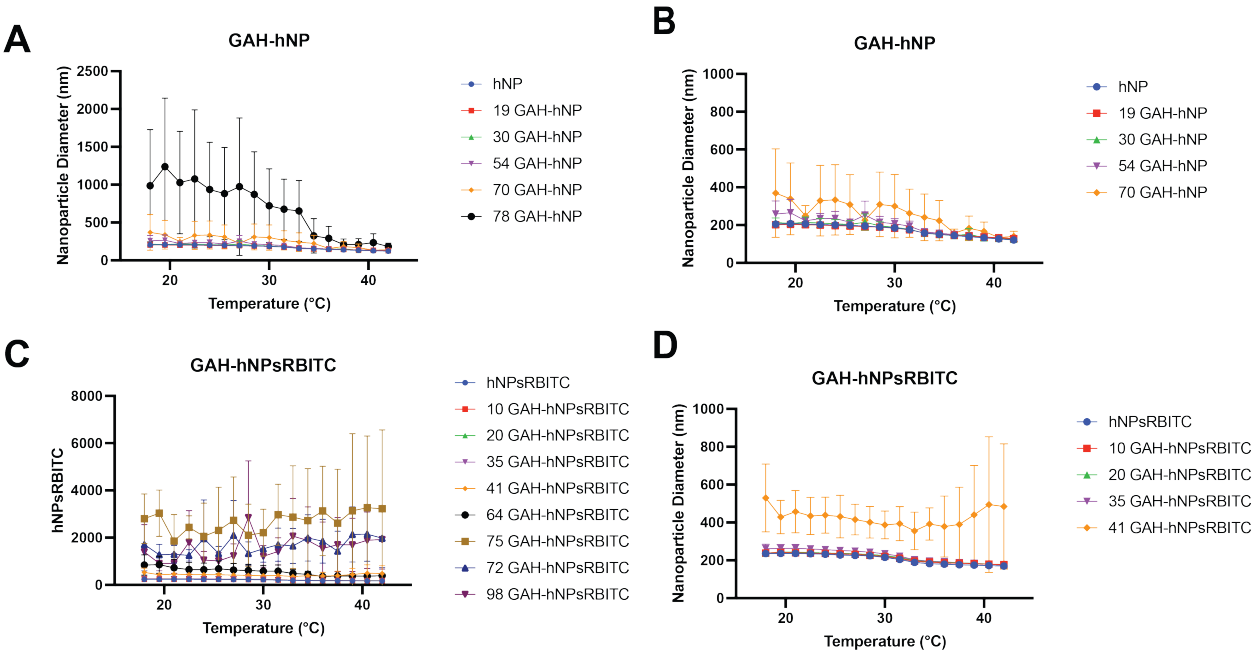

Figure S 3.9: Increasing peptide concentration on the surface of hNP and hNPsRBITC significantly increases the variation in nanoparticle diameter.

Table S 3.2: GAH-hNP diameter, PDI, and Zeta-Potential at increasing GAH concentration to the hNP

GAH:hNP Conjugation	**Diameter (nm) ± STDEV 18.0°C**	**Diameter ± STDEV 42.0°C**	**Zeta Potential (mV) ± STDEV 18.0°C**	**Zeta Potential ± STDEV 42.0°C**	**PDI ± STDEV 18.0°C**	**PDI ± STDEV 42.0°C**
0:1 (hNP)	205.20 ± 8.83	121.57 ± 6.71	-24.93 ± 2.53	-30.22 ± 1.65	0.13 ± 0.03	0.11 ± 0.03
0.5:1 (19 GAH-hNP)	202.46 ± 14.69	128.68 ± 11.34	-9.89 ± 1.66	-12.89 ± 1.87	0.11 ± 0.00	0.09 ± 0.02
1:1 (30 GAH-hNP)	213.43 ± 24.12	125.54 ± 10.03	-9.85 ± 2.82	-14.03 ± 1.08	0.17 ± 0.09	0.14 ± 0.06
2:1 (54 GAH-hNP)	258.99 ± 69.16	126.60 ± 12.27	-13.99 ± 2.04	-17.13 ± 2.15	0.25 ± 0.14	0.18 ± 0.05
4:1 (70 GAH-hNP)	369.84 ± 234.59	140.57 ± 27.98	-11.74 ± 2.77	-13.87 ± 2.40	0.34 ± 0.30	0.23 ± 0.15
6:1 (78 GAH-hNP)	986.36 ± 741.27	182.38 ± 45.18	-8.61 ± 4.03	-11.89 ± 3.39	0.52 ± 0.29	0.30 ± 0.07

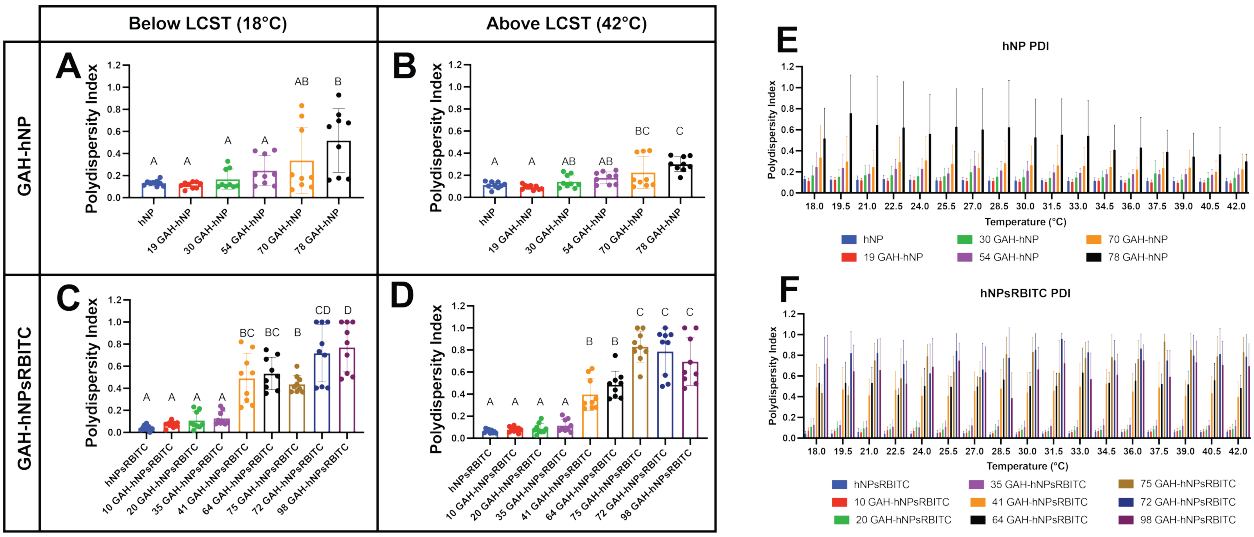

Figure S 3.10: Increasing GAH concentration to the hNP and hNPsRBITC increasing polydispersity of particles in solution. Direct values listed in Supplemental Tables 3.2 and 3.3.

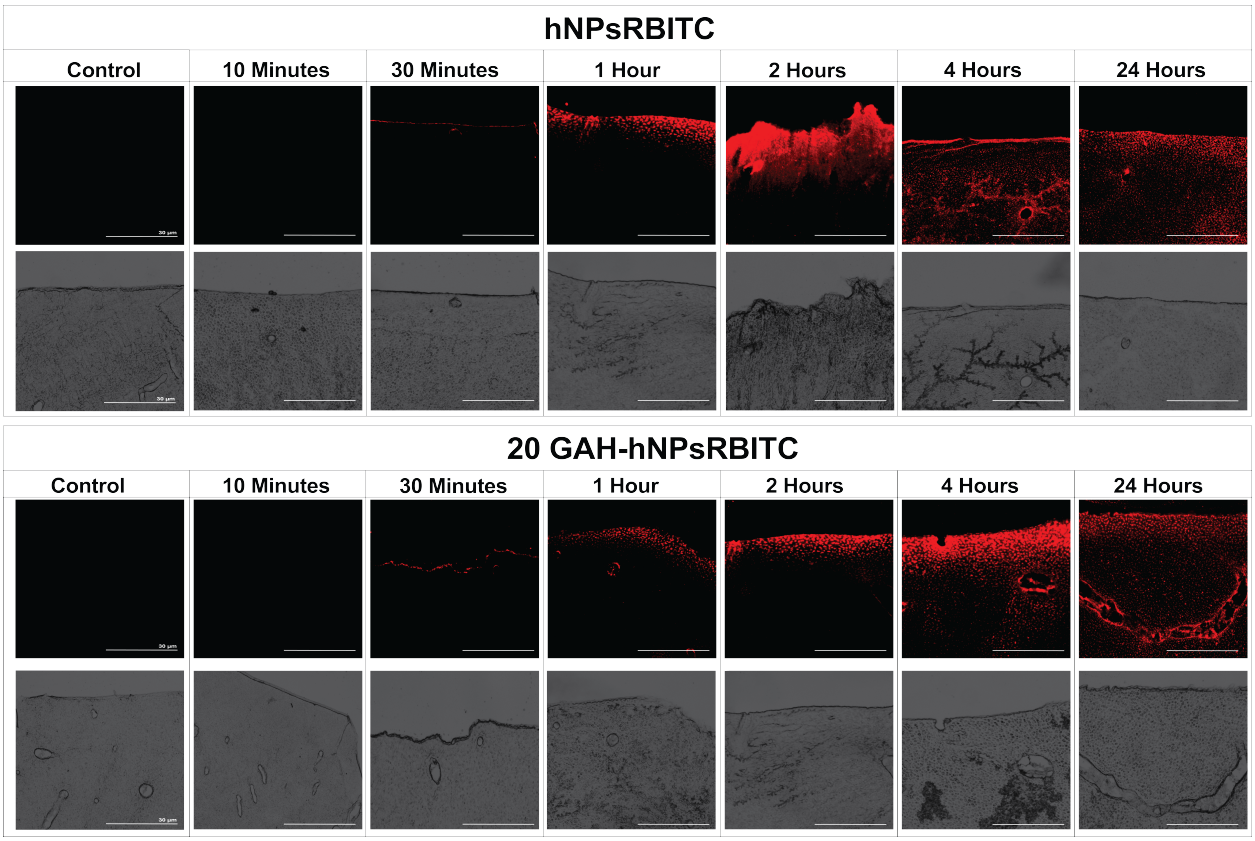

Figure S 3.11: Timed diffusion of 20 GAH-hNPsRBITC into AD cartilage explants.

Table S 3.3: GAH-hNPsRBITC diameter, PDI, and Zeta-Potential at increasing GAH concentration to the hNPsRBITC

GAH:hNPsRBITC Conjugation	**Diameter (nm) ± STDEV 18.0°C**	**Diameter ± STDEV 42.0°C**	**Zeta Potential (mV) ± STDEV 18.0°C**	**Zeta Potential ± STDEV 42.0°C**	**PDI ± STDEV 18.0°C**	**PDI ± STDEV 42.0°C**
0:1 (hNPsRBITC)	235.75 ± 3.63	169.60 ± 3.96	-21.41 ± 1.26	-35.11 ± 0.77	0.04 ± 0.02	0.06 ± 0.02
0.5:1 (10 GAH-hNPsRBITC)	238.73 ± 5.33	177.52 ± 5.99	-8.94 ± 1.92	-12.01 ± 2.46	0.07 ± 0.03	0.08 ± 0.02
1:1 (20 GAH-hNPsRBITC)	238.25 ± 8.37	177.52 ± 5.44	-8.69 ± 3.06	-10.44 ± 1.23	0.11 ± 0.08	0.09 ± 0.05
2:1 (35 GAH-hNPsRBITC)	261.41 ± 24.73	175.80 ± 1.69	-7.90 ± 1.43	-10.71 ± 2.57	0.13 ± 0.06	0.12 ± 0.06
4:1 (41 GAH-hNPsRBITC)	529.92 ± 179.80	484.56 ± 330.96	-8.75 ± 1.64	-14.33 ± 0.94	0.49 ± 0.22	0.40 ± 0.15
6:1 (64 GAH-hNPsRBITC)	844.35 ± 424.90	393.14 ± 25.43	-8.45 ± 2.53	-16.33 ± 2.85	0.53 ± 0.15	0.48 ± 0.12
8:1 (75 GAH-hNPsRBITC)	2081.00 ± 1047.58	3223.51 ± 3341.12	-8.18 ± 2.91	-11.57 ± 3.41	0.44 ± 0.08	0.83 ± 0.14
10:1 (72 GAH-hNPsRBITC)	1709.23 ± 1112.62	1975.47 ± 126.464	-5.44 ± 1.78	-9.31 ± 3.75	0.72 ± 0.26	0.79 ± 0.21
12:1 (98 GAH-hNPsRBITC)	1394.99 ± 1151.76	1926.57 ± 1254.16	-8.31 ± 5.81	-11.37 ± 7.59	0.77 ± 0.22	0.70 ± 0.15

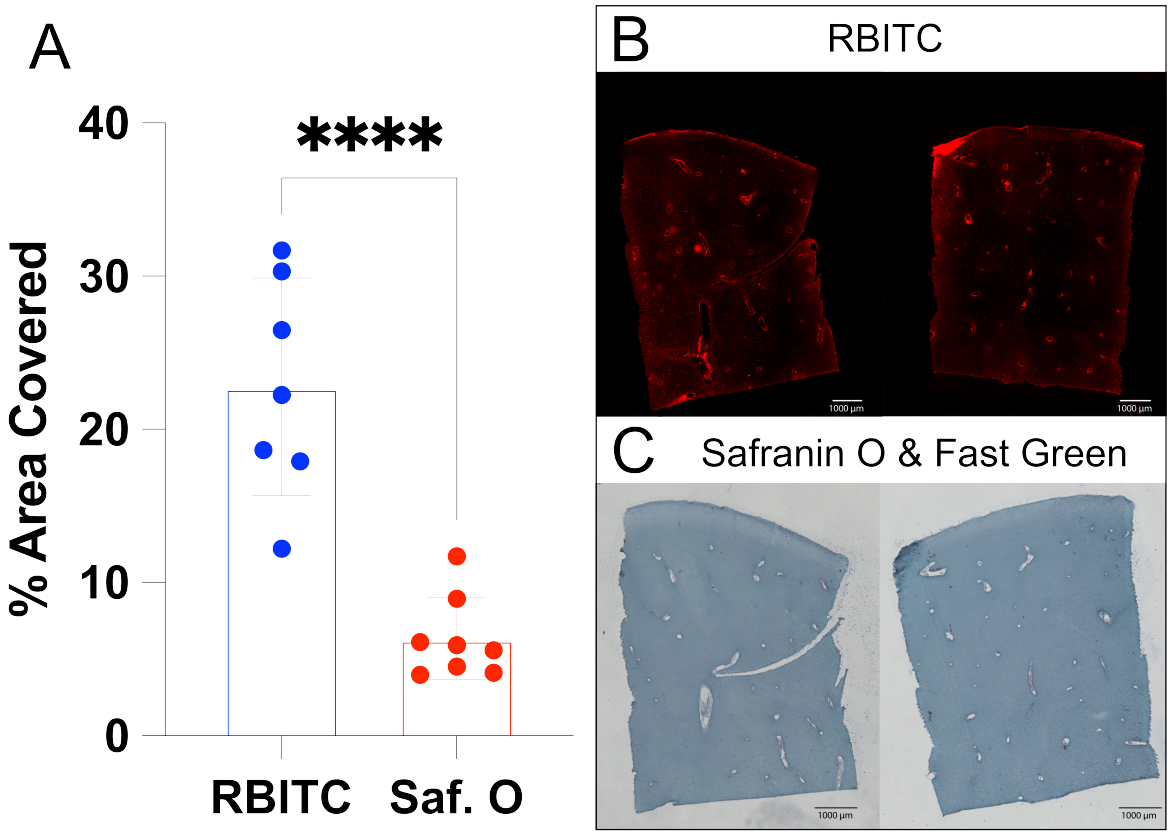

Figure S 3.12: Aggrecan-depleted explants treated with 0.10 mg unconjugated hNPsRBITC, frozen in OCT, and sectioned. The explants were quantified for hNPsRBITC (A) and were stained with Safranin O and Fast Green (B) to assess whether the sulfated AMPS within the hNPsRBITC were stained as well. The Safranin O and Fast Green stain does not stain the hNPsRBITC. Scale bars are 1000 μm.

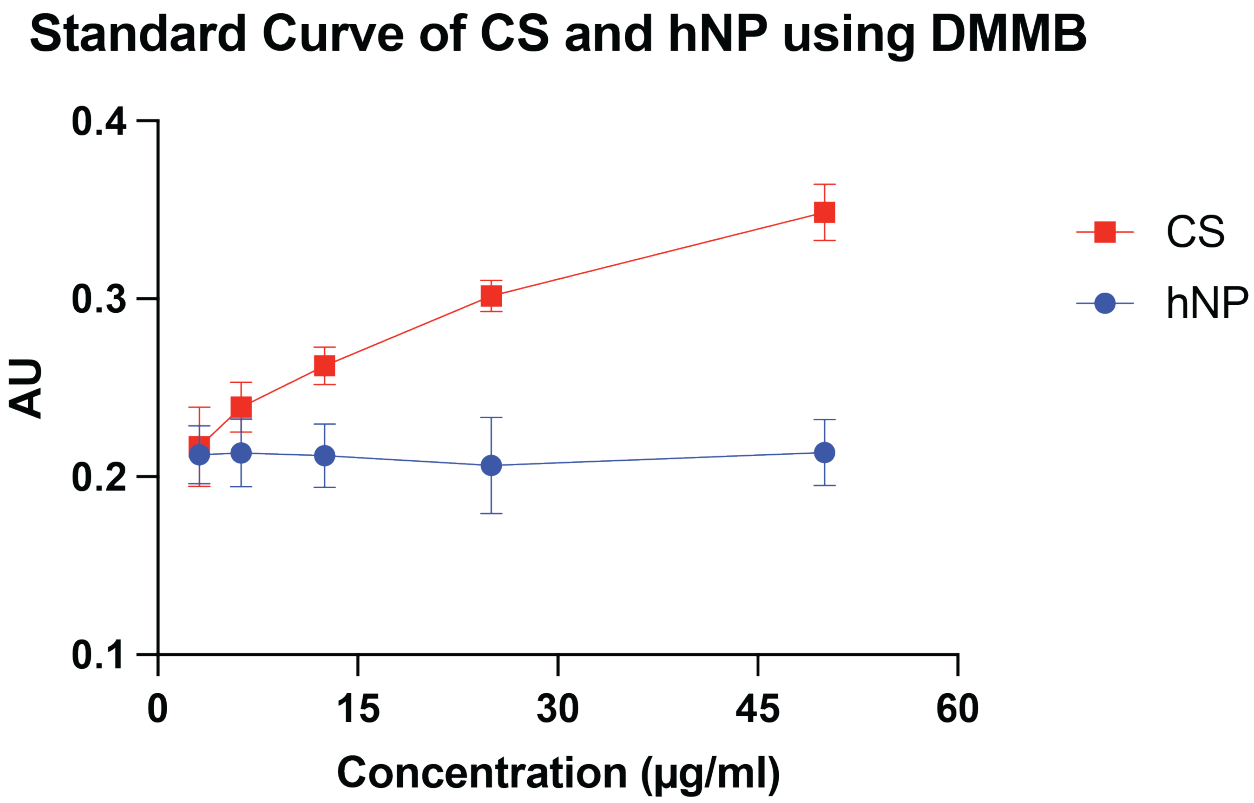

Figure S 3.13: : Standard curves of chondroitin sulfate (CS) (red) and hNP (blue) using DMMB assay. CS SC: y = 0.0028x + 0.2171 R2 = 0.9661; hNP SC: 0.0002x + 0.2106 R2 = 0.7512.

References

1. Brown, T. D., Johnston, R. C., Saltzman, C. L., Marsh, J. L. & Buckwalter, J. A. Posttraumatic Osteoarthritis : A First Estimate of Incidence , Prevalence , and Burden of Disease. **20,** 739–744 (2006).

2. Dare, D. & Rodeo, S. Mechanisms of Post-traumatic Osteoarthritis After ACL Injury. *Current Rheumatology Reports* **16,** 1–5. ISSN: 15346307 (2014).

3. Muir, H. The chondrocyte, architect of cartilage. *BioEssays* **17,** 1039–1048 (1995).

4. Roughley, P. J. & Mort, J. S. The role of aggrecan in normal and osteoarthritic cartilage. *Journal of Experimental Orthopaedics* **1,** 1–11. ISSN: 21971153 (2014).

5. Pratta, M. A. *et al.* Aggrecan Protects Cartilage Collagen from Proteolytic Cleavage. *Journal of Biological Chemistry* **278,** 45539–45545. ISSN: 00219258 (2003).

6. Little, C. B. *et al.* Blocking aggrecanase cleavage in the aggrecan interglobular domain abrogates cartilage erosion and promotes cartilage repair (Journal of Clinical Investigation (2008) 117, (1627-1636) DOI: 10.1172/JCI30765). *Journal of Clinical Investigation* **118,** 3813. ISSN: 00219738 (2008).

7. Sharma, S., Vazquez-Portalatin, N., Calve, S. & Panitch, A. Biomimetic Molecules Lower Catabolic Expression and Prevent Chondroitin Sulfate Degradation in an Osteoarthritic ex Vivo Model. *ACS Biomaterials Science & Engineering* **2,** 241–250. ISSN: 2373-9878. `http://pubs.acs.org/doi/abs/10.1021/acsbiomaterials.5b00458` (2016).

8. Crofford, L. J. Use of NSAIDs in treating patients with arthritis. *Arthritis Research and Therapy* **15.** ISSN: 14786354 (2013).

9. Mora, J. C., Przkora, R. & Cruz-almeida, Y. Knee osteoarthritis : pathophysiology and current treatment modalities, 2189–2196 (2018).

10. Katz, J. N., Arant, K. R. & Loeser, R. F. Diagnosis and Treatment of Hip and Knee Osteoarthritis: A Review. *JAMA - Journal of the American Medical Association* **325,** 568–578. ISSN: 15383598 (2021).

11. Webb, D. & Naidoo, P. Viscosupplementation for knee osteoarthritis: A focus on hylan G-F 20. *Orthopedic Research and Reviews* **10,** 73–81. ISSN: 11791462 (2018).

12. Bernhard, J. C. & Panitch, A. Synthesis and characterization of an aggrecan mimic. *Acta Biomaterialia* **8,** 1543–1550. ISSN: 17427061. http://dx.doi.org/10.1016/j.actbio.2011.12.029 (2012).

13. Sharma, S., Panitch, A. & Neu, C. P. Incorporation of an aggrecan mimic prevents proteolytic degradation of anisotropic cartilage analogs. *Acta Biomaterialia* **9,** 4618–4625. ISSN: 17427061. http://dx.doi.org/10.1016/j.actbio.2012.08.041 (2013).

14. Stuart, K., Sharma, S. & Panitch, A. *Development of an aggrecan mimic to halt osteoarthritis progression* 2014. http://linkinghub.elsevier.com/retrieve/pii/S1063458414009406.

15. Faust, H. J. *et al.* A hyaluronic acid binding peptide-polymer system for treating osteoarthritis. *Biomaterials* **183,** 93–101. ISSN: 18785905 (2018).

16. Sharma, S., Panitch, A. & Neu, C. P. Incorporation of an aggrecan mimic prevents proteolytic degradation of anisotropic cartilage analogs. *Acta Biomaterialia* **9,** 4618–4625. ISSN: 17427061. http://dx.doi.org/10.1016/j.actbio.2012.08.041 (2013).

17. Deloney, M., Smart, K., Christiansen, B. A. & Panitch, A. Thermoresponsive, hollow, degradable core-shell nanoparticles for intra-articular delivery of anti-inflammatory peptide. *Journal of Controlled Release* **323,** 47–58. ISSN: 18734995. https://doi.org/10.1016/j.jconrel.2020.04.007 (2020).

18. Bartlett, R. L., Sharma, S. & Panitch, A. Cell-penetrating peptides released from thermosensitive nanoparticles suppress pro-inflammatory cytokine response by specif-

ically targeting inflamed cartilage explants. *Nanomedicine: Nanotechnology, Biology, and Medicine* **9,** 419–427. ISSN: 15499634 (2013).

19. Poole, A. *et al.* Localization of proteoglycan monomer and link protein in the matrix of bovine articular cartilage: An immunohistochemical study. *Journal of Histochemistry & Cytochemistry* **28,** 621–635 (1980).

20. Farndale, R. W., Buttle, D. J. & Barrett, A. J. Improved quantitation and discrimination of sulphated glycosaminoglycans by use of dimethylmethylene blue. *BBA - General Subjects* **883,** 173–177. ISSN: 03044165 (1986).

21. Coulson-Thomas, V. J. G. T. F. Dimethylmethylene Blue Assay (DMMB). *Bio-protocol* **4,** 18–21 (2014).

22. Poh, S., Lin, J. B. & Panitch, A. Release of Anti-inflammatory Peptides from Thermosensitive Nanoparticles with Degradable Cross-Links Suppresses Pro-inflammatory Cytokine Production. *Biomacromolecules* **16,** 1191–1200. ISSN: 15264602 (2015).

23. McMasters, J., Poh, S., Lin, J. B. & Panitch, A. Delivery of anti-inflammatory peptides from hollow PEGylated poly(NIPAM) nanoparticles reduces inflammation in an ex vivo osteoarthritis model. *Journal of Controlled Release* **258,** 161–170. ISSN: 18734995. http://dx.doi.org/10.1016/j.jconrel.2017.05.008 (2017).

24. Lin, J. B., Poh, S. & Panitch, A. Controlled release of anti-inflammatory peptides from reducible thermosensitive nanoparticles suppresses cartilage inflammation. *Nanomedicine: Nanotechnology, Biology and Medicine* **12,** 2095–2100. ISSN: 15499634. http://linkinghub.elsevier.com/retrieve/pii/S1549963416300570 (2016).

25. She, P. *et al.* Dextran sulfate-triamcinolone acetonide conjugate nanoparticles for targeted treatment of osteoarthritis. *International Journal of Biological Macromolecules* **158,** 1082–1089. ISSN: 18790003. https://doi.org/10.1016/j.ijbiomac.2020.05.013 (2020).

26. Morgen, M. *et al.* Nanoparticles for improved local retention after intra-articular injection into the knee joint. *Pharmaceutical Research* **30,** 257–268. ISSN: 07248741 (2013).

27. Cipollaro, L. *et al.* Liposomes for intra-articular analgesic drug delivery in orthopedics: State-of-art and future perspectives. insights from a systematic mini-review of the literature. *Medicina (Lithuania)* **56,** 1–17. ISSN: 16489144 (2020).

28. Corciulo, C. *et al.* Intraarticular injection of liposomal adenosine reduces cartilage damage in established murine and rat models of osteoarthritis. *Scientific Reports* **10,** 1–16. ISSN: 20452322. https://doi.org/10.1038/s41598-020-68302-w (2020).

29. Koning, G. A. *et al.* Targeting of angiogenic endothelial cells at sites of inflammation by dexamethasone phosphate-containing RGD peptide liposomes inhibits experimental arthritis. *Arthritis and Rheumatism* **54,** 1198–1208. ISSN: 00043591 (2006).

30. Dong, J. *et al.* Intra-articular delivery of liposomal celecoxib-hyaluronate combination for the treatment of osteoarthritis in rabbit model. *International Journal of Pharmaceutics* **441,** 285–290. ISSN: 03785173. http://dx.doi.org/10.1016/j.ijpharm.2012.11.031 (2013).

31. Maudens, P., Jordan, O. & Allémann, E. Recent advances in intra-articular drug delivery systems for osteoarthritis therapy. *Drug Discovery Today* **23,** 1761–1775. ISSN: 18785832. https://doi.org/10.1016/j.drudis.2018.05.023 (2018).

32. Wang, J. X., Fan, Y. B., Gao, Y., Hu, Q. H. & Wang, T. C. TiO2 nanoparticles translocation and potential toxicological effect in rats after intraarticular injection. *Biomaterials* **30,** 4590–4600. ISSN: 01429612. http://dx.doi.org/10.1016/j.biomaterials.2009.05.008 (2009).

33. Kumar, S., Adjei, I. M., Brown, S. B., Liseth, O. & Sharma, B. Manganese dioxide nanoparticles protect cartilage from inflammation-induced oxidative stress. *Biomaterials* **224,** 119467. ISSN: 18785905. https://doi.org/10.1016/j.biomaterials.2019.119467 (2019).

34. Poh, S., Lin, J. B. & Panitch, A. Release of Anti-inflammatory Peptides from Thermosensitive Nanoparticles with Degradable Cross-Links Suppresses Pro-inflammatory Cytokine Production. *Biomacromolecules* **16,** 1191–1200. ISSN: 15264602 (2015).

35. Arruebo, M., Valladares, M. & González-Fernández, Á. Antibody-conjugated nanoparticles for biomedical applications. *Journal of Nanomaterials* **2009.** ISSN: 16874110 (2009).

36. Cheraghipour, E., Tamaddon, A. M., Javadpour, S. & Bruce, I. J. PEG conjugated citrate-capped magnetite nanoparticles for biomedical applications. *Journal of Magnetism and Magnetic Materials* **328,** 91–95. ISSN: 03048853. `http://dx.doi.org/10.1016/j.jmmm.2012.09.042` (2013).

37. Froiio, F. *et al. Polymer-based nanocontainers for drug delivery* 271–285. ISBN: 9780128167700. `http://dx.doi.org/10.1016/B978-0-12-816770-0.00016-2` (Elsevier Inc., 2019).

38. Jin Jeong, W. *et al.* Peptide–nanoparticle conjugates: a next generation of diagnostic and therapeutic platforms? *Nano Convergence* **5,** 1–18. ISSN: 21965404. `https://doi.org/10.1186/s40580-018-0170-1` (2018).

39. Steinhauser, I., Spänkuch, B., Strebhardt, K. & Langer, K. Trastuzumab-modified nanoparticles: Optimisation of preparation and uptake in cancer cells. *Biomaterials* **27,** 4975–4983. ISSN: 01429612 (2006).

40. Kou, G. *et al.* Preparation and characterization of paclitaxel-loaded PLGA nanoparticles coated with cationic SM5-1 single-chain antibody. *Journal of Biochemistry and Molecular Biology* **40,** 731–739. ISSN: 02191024 (2007).

41. Heidel, J. D. *et al.* Administration in non-human primates of escalating intravenous doses of targeted nanoparticles containing ribonucleotide reductase subunit M2 siRNA. *Proceedings of the National Academy of Sciences of the United States of America* **104,** 5715–5721. ISSN: 00278424 (2007).

42. Ogino, C., Kanehira, K., Sasai, R., Sonezaki, S. & Shimizu, N. Recognition and effective degradation of 17β-estradiol by anti-estradiol-antibody-immobilized TiO2 nanoparticles. *Journal of Bioscience and Bioengineering* **104,** 339–342. ISSN: 13891723 (2007).

43. Richardson, J. C., Bowtell, R. W., Mäder, K. & Melia, C. D. Pharmaceutical applications of magnetic resonance imaging (MRI). *Advanced Drug Delivery Reviews* **57,** 1191–1209. ISSN: 0169409X (2005).

44. Kemmner, W., Moldenhauer, G., Schlag, P. & Brossmer, R. Separation of tumor cells from a suspension of dissociated human colorectal carcinoma tissue by means of monoclonal antibody-coated magnetic beads. *Journal of Immunological Methods* **147,** 197–200. ISSN: 00221759. http://dx.doi.org/10.1016/S0022-1759(12)80008-1 (1992).

45. Liu, X. *et al.* A one-step homogeneous immunoassay for cancer biomarker detection using gold nanoparticle probes coupled with dynamic light scattering. *Journal of the American Chemical Society* **130,** 2780–2782. ISSN: 00027863 (2008).

46. Xia, B. *et al.* Activatable Cell-Penetrating Peptide Conjugated Polymeric Nanoparticles with Gd-Chelation and Aggregation-Induced Emission for Bimodal MR and Fluorescence Imaging of Tumors. *ACS Applied Bio Materials* **3,** 1394–1405. ISSN: 25766422 (2020).

47. Choi, K. M. *et al.* A monitoring method for Atg4 activation in living cells using peptide-conjugated polymeric nanoparticles. *Autophagy* **7,** 1052–1062. ISSN: 15548635 (2011).

48. Kulhari, H., Pooja, D., Shrivastava, S., V.G.M, N. & Sistla, R. *Peptide conjugated polymeric nanoparticles as a carrier for targeted delivery of docetaxel* 2014.

49. Wang, R. T., Zhi, X. Y., Yao, S. Y. & Zhang, Y. LFC131 peptide-conjugated polymeric nanoparticles for the effective delivery of docetaxel in CXCR4 overexpressed lung cancer cells. *Colloids and Surfaces B: Biointerfaces* **133,** 43–50. ISSN: 18734367 (2015).

50. Yang, D. C., Eldredge, A. C., Hickey, J. C., Muradyan, H. & Guan, Z. Multivalent Peptide-Functionalized Bioreducible Polymers for Cellular Delivery of Various RNAs. *Biomacromolecules* **21,** 1613–1624. ISSN: 15264602 (2020).

51. Kuo, R., Saito, E., Miller, S. D. & Shea, L. D. Peptide-Conjugated Nanoparticles Reduce Positive Co-stimulatory Expression and T Cell Activity to Induce Tolerance. *Molecular Therapy* **25,** 1676–1685. ISSN: 15250024. http://dx.doi.org/10.1016/j.ymthe.2017.03.032 (2017).

52. D'Este, M., Eglin, D. & Alini, M. A systematic analysis of DMTMM vs EDC/NHS for ligation of amines to Hyaluronan in water. *Carbohydrate Polymers* **108,** 239–246. ISSN: 01448617. http://dx.doi.org/10.1016/j.carbpol.2014.02.070 (2014).

53. McMasters, J. & Panitch, A. Prevention of Collagen-Induced Platelet Binding and Activation by Thermosensitive Nanoparticles. *The AAPS Journal* **17,** 1117–1125. ISSN: 1550-7416. http://link.springer.com/10.1208/s12248-015-9794-9 (2015).

54. García-Couce, J. *et al.* Targeting Polymeric Nanobiomaterials as a Platform for Cartilage Tissue Engineering. *Current Pharmaceutical Design* **25,** 1–18. ISSN: 13816128. http://www.eurekaselect.com/173321/article (2019).

55. Zhou, Y., Gong, X. J. & Yang, J. B. Introduction to the guidance for industry on liposome drug products: chemistry, manufacturing, and controls; human pharmacokinetics and bioavailability; and labeling documentation issued by FDA. *Chinese Journal of New Drugs* **27,** 1835–1840. ISSN: 10033734 (2018).

56. Danaei, M. *et al.* Impact of particle size and polydispersity index on the clinical applications of lipidic nanocarrier systems. *Pharmaceutics* **10,** 1–17. ISSN: 19994923 (2018).

57. García-Peñas, A. *et al.* Effect of hydrophobic interactions on lower critical solution temperature for poly (N-isopropylacrylamide-co-dopamine Methacrylamide) copolymers. *Polymers* **11,** 991 (2019).

58. Lawrence, A. *et al.* Synthesis and characterization of a lubricin mimic (mLub) to reduce friction and adhesion on the articular cartilage surface. *Biomaterials* **73,** 42–50. ISSN: 18785905. http://dx.doi.org/10.1016/j.biomaterials.2015.09.012 (2015).

59. Lee, J. I., Sato, M., Ushida, K. & Mochida, J. Measurement of diffusion in articular cartilage using fluorescence correlation spectroscopy. *BMC Biotechnology* **11,** 19. ISSN: 14726750. http://www.biomedcentral.com/1472-6750/11/19 (2011).

60. Phillips, E. R. *et al.* Biomimetic proteoglycans diffuse throughout articular cartilage and localize within the pericellular matrix. *Journal of Biomedical Materials Research - Part A* **107,** 1977–1987. ISSN: 15524965 (2019).

61. Fischenich, K. M., Lewis, J., Kindsfater, K. A., Bailey, T. S. & Donahue, T. L. H. Effects of degeneration on the compressive and tensile properties of human meniscus. *Journal of biomechanics* **48,** 1407–1411 (2015).

62. Korhonen, R., Laasanen, M., Toyras, J., Helminen, H. & Jurvelin, J. *Superficial collagen network modifies differently equilibrium response of articular cartilage in unconfined compression and indentation* in *TRANSACTIONS OF THE ANNUAL MEETING-ORTHOPAEDIC RESEARCH SOCIETY* (2002), 79–79.

63. Estrela, J. M., Ortega, A. & Obrador, E. *Glutathione in cancer biology and therapy* **2,** 143–181. ISBN: 1040836050052 (2006).

64. Griffith, O. W. Determination of glutathione and glutathione disulfide using glutathione reductase and 2-vinylpyridine. *Analytical Biochemistry* **106,** 207–212. ISSN: 00032697 (1980).

65. Man, G. S. & Mologhianu, G. Osteoarthritis pathogenesis - a complex process that involves the entire joint. *Journal of medicine and life* **7,** 37–41. ISSN: 18443117 (2014).

66. Gerwin, N., Hops, C. & Lucke, A. Intraarticular drug delivery in osteoarthritis. *Advanced Drug Delivery Reviews* **58,** 226–242. ISSN: 0169409X (2006).

67. Owen, S., Francis, H. & Roberts, M. Disappearance kinetics of solutes from synovial fluid after intra- articular injection. *British Journal of Clinical Pharmacology* **38,** 349–355. ISSN: 13652125 (1994).

68. Brown, T. & Laurent, U. Turnover of hyaluronan in synovial joints: elimination of labelled hyaluronan from the knee joint of the rabbit. *Experimental Physiology: Translation and Integration* **76,** 125–134 (1991).

CHAPTER IV

Peptide-Nanoparticle Therapeutic to Halt the Progression of PTOA in Non-Invasively Ruptured ACL in Rat Model

4.1 Abstract

Inflammation following joint trauma causes the expression of inflammatory cytokines, e.g. IL-6 and TNF-α, and stimulates the secretion of catabolic enzymes that cause the degradation of articular cartilage. The degraded cartilage further stimulates inflammatory cytokine expression and leads to the progression of post traumatic osteoarthritis (PTOA). Inhibiting inflammation following joint trauma may halt PTOA progression. The objective of this study was to examine the efficacy of a peptide-nanoparticle therapeutic to prevent the progression of PTOA in a physiologically relevant small animal model. We encapsulated the anti-inflammatory MK2 inhibiting (MK2i) peptide YARAAARQARAKALARQLGVAA (YARA) within hollow nanoparticles (hNP) composed of N-isopropyl acrylamide (NIPAm), N, N'-bis (acryloyl) cystamine (BAC), 2-acrylamido-2-methyl-1-propanesulfonic acid (AMPS), and acrylic acid (AAc) (poly(NIPAm-co-AMPS-BAC-AAc)). The poly(NIPAm-co-AMPS-BAC-AAc) hNPs encapsulated 75.07 $\pm$ 7.19% (mg MK2i/mg hNP) and released 43.00 $\pm$ 4.20% after 5 days *ex situ*. The MK2i loaded hNPs were tested *in vivo* using a non-invasive anterior cruciate ligament (ACL) rupture (NIACLR) model that causes PTOA. However, only 9 of the 28 rats that underwent NIACLR resulted in complete ACL tears, as confirmed by a veterinary pathologist. Future work will further develop the NIACLR model and confirm ACL tear by assessing joint range of motion. Once injury is confirmed, future work will also include a new study to assess therapeutic efficacy of the MK2i loaded hNPs.

4.2 Introduction

Post traumatic osteoarthritis (PTOA) is the result of a joint trauma or injury and leads to inflammation within the joint. PTOA affects roughly 2.7 million people within the United States and is estimated to cost the healthcare system upwards of $3 billion annually[1]. Anterior cruciate ligament (ACL) tears are the most common knee injury that results in PTOA, and is most prominent in younger, more active persons[2,3]. Unlike most osteoarthritis cases, patients that suffer from PTOA are acutely aware of the joint trauma and this "genesis point" presents a unique opportunity for early stage treatment.

During the progression of PTOA, loss of aggrecan from articular cartilage happens first and is considered reversible if caught early enough[4,5]. Aggrecan is a prominent component within cartilage and is composed of three globular domains and contains anionic sulfated glycosaminoglycans (GAGs). Following joint trauma, inflammatory cytokines (e.g. IL-6 and TNF-α) are expressed and stimulate the secretion of catabolic enzymes, such as aggrecanases and matrix metalloproteases (MMPs), by chondrocytes[6]. Aggrecanases irreparably cleave aggrecan in its interglobular domain and its degradation results in the loss of the compressive strength of cartilage[7–9]. Aggrecan loss exposes hyaluronic acid (HA) to degradation by hyaluronidases[10], and the degraded articular cartilage further upregulates cytokine and MMP activity[6,11]. This results in the cyclic progression of PTOA that damages remaining healthy cartilage and impacts overall joint architecture. Inhibiting the expression of inflammatory cytokines may halt the degradation of cartilage, and slow the advancement of PTOA[12–14].

Current animal models used to induce PTOA include: injection of iodoacetate into the joint to inhibit glycolysis and cause chondrocyte death[15,16], meniscal destabilization[17], and surgical transection of ACL[18–22]. ACL transection is the most common technique to induce PTOA due to its high degree of reproducibility and relevance since 50 — 90% of ACL tears result in PTOA[18–22]. Transecting the ACL causes the destabilization of the knee, proteoglycan loss, thinning of articular cartilage, and osteophyte formation[18,20]. However, surgical transection is not physiologically relevant. Previous work developed a non-invasive method to

induce PTOA using tibial compressions to tear the ACL of rats[3,23–25]. These models showed tibial compressions resulted in complete ACL tears, epiphyseal bone remodeling, cartilage degradation, and proteoglycan loss[3,23–25]. The non-invasive ACL rupture (NIACLR) model was directly compared to the surgical transection model, and showed both models result in PTOA, and concluded that the NIACLR model was more physiologically relevant[25].

Non-surgical PTOA treatments are divided into supplements and injections. Supplements to treat PTOA include lifestyle adaptations, exercise, physical therapy, topical creams and the systemic delivery of non-steroidal anti-inflammatory drugs (NSAIDs) and painkillers. Since most patients who suffer from PTOA are active individuals who exercise regularly, NSAIDs, painkillers, and topical creams are primarily used. However, systemic delivery of NSAIDs leads to increased cardovascular[26], kidney[27], and gastrointestinal tract complications[28–30]. Opioids, as well as topical creams, do not treat the underlying causes of inflammation, and opioids are linked to severe cases of addiction[30,31]. Injections to treat PTOA primarily consist of corticosteroids and glucosteroids to address inflammation. However, corticosteroid and glucosteroid injections result in chondrocyte death[31]. Localized delivery of a biocompatible therapeutic able to inhibit inflammation and treat damaged cartilage following joint trauma may prevent the progression of PTOA.

Early-stage treatment of PTOA may be possible by inhibiting inflammatory cytokine production and ECM degradation using a peptide-nanoparticle therapeutic. Peptide therapeutics are advantageous due to their high biological activity, specificity, and low toxicity[32]. However, using peptides as therapeutics has its challenges since they are susceptible to enzymatic breakdown and low stability. Nanoparticles present a solution to this problem by protecting peptides from extracellular degradation. Combining peptides with nanoparticles has been shown to improve their solubility and extend therapeutic half-life *in vivo*[33,34]. While nanoparticle-peptide therapeutics have their limitations, such as potentially altered therapeutic efficacy and the possibility of toxic degradation products, their ability to improve peptide solubility, sustained release, and extended half-life *in vivo* make them advantageous

for drug delivery[35]. Here, we encapsulated an anti-inflammatory MK2 inhibiting (MK2i) peptide within hollow polymeric nanoparticles to protect them from enzymatic degradation and allow for controlled release within the joint to inhibit the progression of PTOA.

MK2 (mitogen activated protein kinase activated protein kinase 2) is part of the p38 pathway and acts downstream of p38 MAPK. When MK2 is phosphorylated it stabilizes the mRNA responsible for the production of inflammatory cytokines, e.g. IL-6 and TNF-α. Ward et al. tested a series of MK2i peptides and found YARAAARQARAKALARQLGVAA (YARA) to be the most specific to MK2 and the least toxic of the variants[36]. Hollow nanoparticles (hNPs) composed of N-isopropyl acrylamide (NIPAm), N, N'-bis (acryloyl) cystamine (BAC), 2-acrylamido-2-methyl-1-propanesulfonic acid (AMPS), and acrylic acid (AAc) (poly(NIPAm-co-AMPS-BAC-AAc)) were shown to encapsulate the MK2i peptide and inhibited IL-6 production *in vitro*[37]. Moreover, the hNPs were retained within the joint space of rats for 7 days[37]. Here, we used the NIACLR rat model to induce PTOA and aimed to examine the efficacy of MK2i loaded poly(NIPAm-co-AMPS-BAC-AAc) hNP to inhibit the progression of PTOA. However, our data was inconclusive since not all rats that underwent NIACLR resulted in a complete ACL tear.

4.3 Materials and Methods

4.3.1 Animal Procurement

Thirty-eight 10-week old Fisher 344 rats were purchased from Charles River Laboratories (Wilmington, MA) and acclimated for 2 weeks. In all but sham control animals, the right knee underwent NIACLR and the left served as contralateral control. Both the knees received the same treatment, allowing the contralateral knee to serve as an internal control and reduce the number of animal used. Treatments included: Group A: right and left uninjured injected with PBS (n = 5, 10 total knees), Group B: NIACLR right and contralateral left injected with PBS (n = 10), Group C: NIACLR right and (5) contralateral left injected with hNP

only (n = 10), and Group D: NIACLR right and contralateral left injected with hNP+MK2i (n = 10). Rats were euthanized at 4 weeks following injury. Three rats were used to evaluate the retention of the particles in the joint following NIACRL and were euthanized 7 days after injury and injection. Rats were maintained and used in accordance with National Institutes of Health guidelines on the care and use of laboratory animals. All procedures were approved by the UC Davis Institutional Animal Care and Use Committee.

4.3.2 Materials

N-isopropyl acrylamide (NIPAm, $\geq$ 98%), N,N'-Bis(acryloyl) cystamine (99%, BAC), N, N'-methylene-bis-diacrylaminde (MBA), sodium dodecyl sulfate (SDS; 20% w/v in water), 2-acrylamido-2-methyl-1-propanesulfonic acid (99%, AMPS), N-diisopropyl ethylamine (99%, DIPEA), Rhodamine B isothiocyanate (98%, RBITC), potassium persulfate (99%, KPS), trifluoroacetic acid (TFA), 4-(4,6-Dimethoxy-1,3,5-triazin-2-yl)-4-methyl morpholinium chloride (96% DMTMM), and dimethyl sulfoxide (DMSO) were acquired from Sigma Aldrich (St. Louis, MO). Dimethylformamide (DMF), dichloromethane (DCM), acetonitrile (ACN), trifluoroacetic acid (TFA), triisopropylsilane (TIPS), and phenol were purchased from Thermo Fisher (Waltham, MA). Dialysis membrane tubing and tangential flow filtration carbon tubing were purchased from Spectrum Laboratories (Dominguez, CA). NIPAm and BAC were stored under nitrogen at 4°C and −20°C, respectively. AMPS was stored at room temperature in a desiccator. All water used in synthesis, dialysis, and testing was treated by a Millipore milliQ system (Billerica, MA; 18.2 MΩ:cm resistivity).

4.3.3 Nanoparticle Synthesis

Nanoparticles were synthesized as described previously[37]. Briefly, cores were synthesized by dissolving 394.5 mg NIPAm and injecting it into a 100 ml three-neck flask under reflux and a nitrogen blanket with 35 ml milliQ water and 164 μl of a 20% SDS solution at 70°C. Following a 15 min equilibration time, 67.4 mg KPS was dissolved and injected into the

reaction flask and continued for 2 h. NP cores were exposed to atmospheric oxygen for 45 min, followed by a 15 min nitrogen purge. The NP shells were polymerized around the cores by injection of 794.7 mg NIPAm, 78.0 mg AMPS, 48.2 mg BAC, 4.81 μl AAc, and 164 μl 20% SDS into the reaction flask. After 15 min, 33.7 mg KPS was dissolved and was injected into the reaction flask, and reacted for 4 hours at 37°C. The nanoparticle solution was dialyzed in 10 kDa dialysis tubing (Spectrum Laboratories, Dominguez, CA) at 4°C for 14 days; milliQ water was changed daily. Following dialysis, the now hollow NPs (hNPs) were frozen and lyophilized.

4.3.3.1 Fluorophore Incorporation

For RBITC-shell NP batches, 0.1 mol% RBITC dissolved in 1 ml DMSO was injected following NIPAm, AMPS, BAC, AAc, and SDS addition and before shell polymerization initiation. These produced fluorescently-labeled co-poly(NIPAm-AMPS-AAc-BAC-RBITC) (hNPsRBITC) nanoparticles.

4.3.4 Peptide Synthesis and Purification

YARAAARQARAKALARQLGVAA (YARA) was synthesized as previously described using a CEM Liberty Blue Peptide Synthesizer (Matthews, NC)[37]. Briefly, FMOC protected L-amino acids were individually dissolved in synthesis grade DMF to yield 0.2 M solutions. Rink-Amide (Sigma Aldrich, St. Louis, MO) resin was added to the reaction vessel of the CEM Liberty Blue peptide synthesizer. Synthesis occurred at 90°C for 4 — 30 min per amino acid, time varying for each amino acid. YARA was cleaved from the Rink-Amide resin using 2 ml of a cleavage cocktail (4.4 ml TFA, 0.25 ml phenol, 0.25 ml milliQ water, and 0.10 ml TIPS) for 3 h, precipitated with 0°C diethyl ether, centrifuged at 1,000 g for 5 min four times, and dried overnight at room temperature. YARA was purified using reverse phase fast-protein liquid chromatography (FPLC). Quantification of molecular weight was assessed using Matrix Assisted Laser Desorption/Ionization - Time of Flight (MALDI-TOF)

mass spectroscopy.

4.3.5 Drug Loading

One mg of hNPs were dissolved with 2 mg YARA in 1 ml ethanol (EtOH), incubated for 24 h at 4°C. Following incubation, YARA-loaded hNPs were centrifuged at 17,000 g for 30 min and 500 μl of the supernatant was collected, centrifuged again for 30 min at 17,000 g, then 300 μl of that supernatant was collected for post-load analysis to quantify remaining unloaded peptide using a C18 reverse phase column on a high-performance liquid chromatography (HPLC). Respectively, 1 ml of milliQ water was added to loaded hNP to resuspend them prior to freezing and lyophilizing.

4.3.6 Nanoparticle Characterization

Following purification and lyophilization, hNPs were dissolved at 1 mg/ml in milliQ water, and subjected to temperature sweeps from 18.0°C — 42.0°C, in 1.5°C increments, equilibrating for 3 min between each step, and measuring three times per step using dynamic light scattering (DLS) to assess diameter and polydispersity index (PDI). Zeta (ζ)-potential was obtained on a Nano-ZS90 Zetasizer at 1 mg/ml sample concentration in milliQ water at 18.0°C and 42.0°C using folded capillary cells.

4.3.7 Treatments & NIACLR

Rats were anesthetized via isoflurane inhalation and a depilatory was used to remove hair from both hindlimbs. Following hair removal, animals were injected with respective treatments: Group A (n = 5), left and right hindlimb were uninjured and injected with 150 μl of 1x PBS; Groups B (n = 10) both hindlimbs were injected with 150 μl of PBS; Groups C (n = 10), both hindlimbs were injected with 150 μl of 2 mg/ml hNP; Groups D (n = 10), both hindlimbs were injected with 150 μl of 2 mg/ml hNP+MK2i. Following injection, rats from Groups B, C, and D were placed in a prone position with right tibias vertically aligned

between two platens for tibial compression and underwent NIACLR. A 0 to 45 N preload was oscillated for 10 cycles. Then 0 to 55 N was then applied increasing by 5 N per cycle until 75 N until the ACL popped (ElectroForce 3200, TAInstruments, New Castle, DE). In two cases, 0 to 80 N load was used with both rats weighing more than 280 g. Two indices of tibial fractures occurred following NIACLR and were immediately sacrificed using carbon dioxide asphyxiation. All left hindlimbs were left uninjured. Buprenorphine analgesia was administered immediately post-injury (0.3 mg/kg) and 12 h post injury. Rats from Group A-D were weighed 3 days after injury, then weekly until sacrifice. Whole hindlimbs were removed for analysis at the end of 4 weeks and fixed in 4% paraformaldehyde (PFA) for 7 days followed by preservation in 70% ethanol (EtOH).

For the retention study, rats were allowed to acclimate for 2 weeks, then were anesthetized with isoflurane and the hair was removed from both rat knees. Rats were injected with 150 μl of 2 mg/ml hNPsRBITC dissolved in PBS (n = 3) into their left and right joint space. Their right knee underwent NIACLR and the left served as contralateral control. Images were taken by the Davis Center for Molecular and Genomic Imaging (CMGI) core and fluorescence was measured and quantified using the In Vivo Imaging System (IVIS) at 557 nm excitation and 623 nm emission. Images were taken on day 1, 3, and 7 after injection, then immediately following sacrifice and dissection. Rats were sacrificed using CO_2 euthanasia. Total radiance emission (TRE) fluorescence was collected and analyzed.

4.3.8 Micro-Computed Tomography (μCT)

Immediately following dissection, rats joints were fully immersed in 4% paraformaldehyde solution for 7 days. Knees were scanned using micro-computed tomography (SCANCO, mCT 35, Brüttisellen, Switzerland) to quantify osteophyte volume around the knee joint. μCT scans were performed according to guidelines for rodent bone structure analysis (X-ray tube potential ¼ 55 kVp, intensity ¼ 114 mA,10 mm isotropic nominal voxel size, integration time ¼ 900 ms). The global threshold for "bone" will be set equivalent to 567

mg HA/cm3. Trabecular bone analysis of the epiphysis was performed starting at the distal growth plate through the femoral condyles. Trabecular bone volume fraction (BV/TV), trabecular number (Tb. N), trabecular thickness (Tb. Th.) and trabecular separation (Tb. Sp.) and were calculated using the manufacturer's 3D analysis software. Following scans, joints were emersed in 70% ethanol.

4.3.9 Histology & ORASI Scoring

Whole joint histology was performed to visualize cartilage composition and joint deterioration following NIACLR and injection. Knees were submitted to Inotiv and decalcified in formic acid, sectioned, stained using T-Blue and Safranin O and Fast Green (SafO/FG), and ORASI graded by a DVM trained pathologist. Knees were embedded in paraffin blocks in the frontal plane, sectioned at the anterior and approximate mid-point of the knee, and stained. Six sections were taken per knee at 6 μm at 250 μm steps, and the best section, as determined by the pathologist, was graded. Grades 0 to 6 were assigned for osteoarthritic cartilage damage, with 0 indicating normal and 6 indicating severe degeneration and calcified cartilage extending greater than 75% of the articular surface. Osteophyte thickness was measured with an ocular micrometer. Osteophyte score was assigned to the largest osteophyte area and ranged from 0 to 5, with 0 being less than 50 μm and 5 being greater than 600 μm. The total joint score was calculated by adding the medial and lateral osteophyte scores to the total joint cartilage degeneration sum with maximum value being 29. Synovial inflammation was scored from 0 to 4, with 0 being no fibrosis and 4 being severe fibrosis. Extent of ACL rupture was detailed by the pathologist as no tear (N), partial tear (P) or complete tear (Y).

4.4 Results

4.4.1 Drug Loading and Release

The hNPs were able to load 75.07 ± 7.19% (mg MK2i/mg hNP) and released 43.00 ± 4.20% of MK2i *ex situ* at the end of 5 days, Figure 4.1A and 4.1B. hNPs were thermoresponsive and swelled to a diameter of 252.33 ± 11.73 nm at 18.0°C and constricted to 165.13 ± 21.97 nm at 42.0°C, Figure 4.1C. The particles were monodisperse at all temperatures, and were colloidally stable with zeta potential of -29.91 ± 5.33 mV at 18.0°C and -32.91 ± 1.87 mV at 42.0°C.

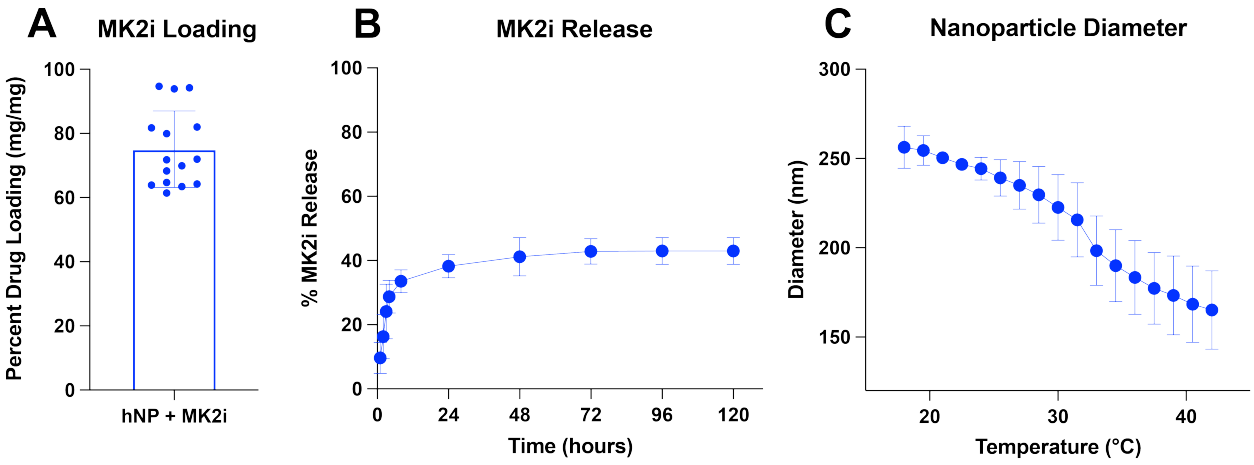

Figure 4.1: (A) MK2i loading into hNP when loaded at 4°C, (B) release ex situ, and (C) DLS of nanoparticle diameter.

4.4.2 Rat Weight

Rats from all groups lost weight between Day 0 and Day 3. Group A, B, C, and D lost 6.6%, 7.2%, 6.0%, and 7.1% mass on Day 3 compared to Day 0, respectively, Figure 4.2. After Day 3, rats steadily increased their weight until sacrifice. There was not a significant weight change between groups.

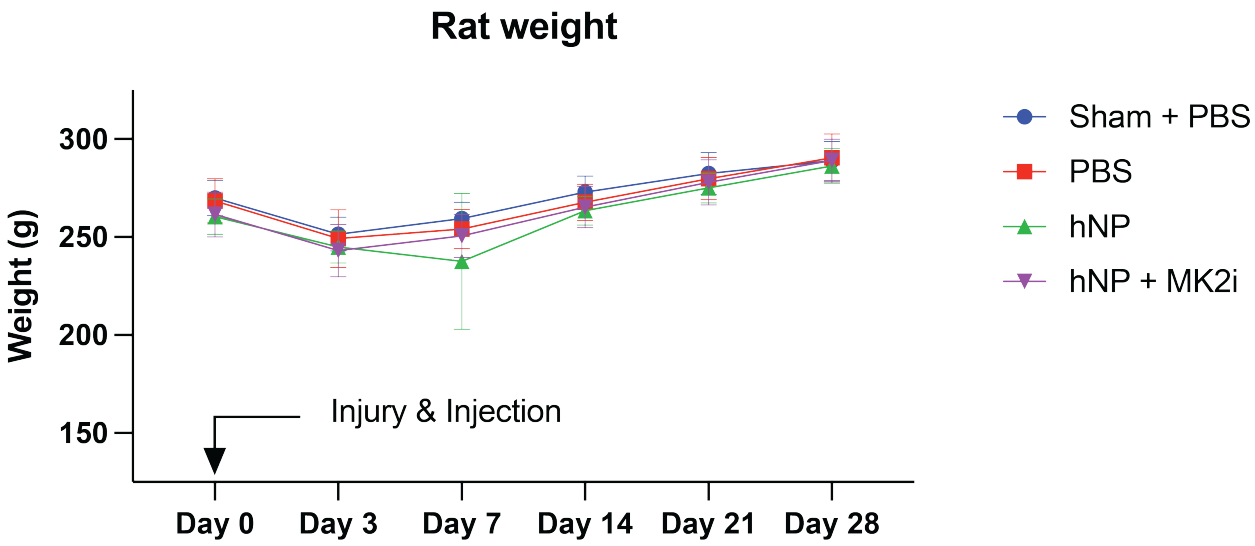

Figure 4.2: Rats lost weight 3 days following injection and/ or injury.

4.4.3 Complete Injury, Fracture Incidences, and Particle Retention

Successful ACL tears in PBS (4/9), hNP (3/10) and hNP+MK2i (2/9) treated rats were confirmed by a veterinary pathologist. All histology and µCT data presented here only included rats with confirmed ACL tears. Tibial fractures occurred in two rats over 280 g when compression reached over 80 N of force. These rats were immediately sacrificed using carbon dioxide asphyxiation. hNPsRBITC was retained in the contralateral knees for 7 days. However, there was a 85.97% loss in TRE between the contralateral and NIACLR joints 7 days after dissection. These data showed hNPsRBITC cleared the NIACLR joint 4-7 days following tibial compression while remaining in uninjured joints, Figure 4.3.

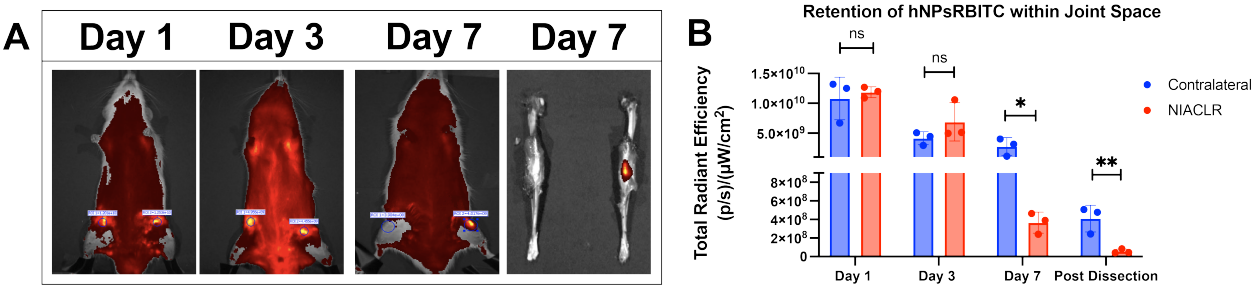

Figure 4.3: hNPsRBITC was cleared from NIACLR injured rats 4-7 days following injury.

4.4.4 Histology and OARSI Scoring

Histological scoring indicated changes in the structure and morphology of articular cartilage following successful ACL tear. However, there is no apparent difference between NIACLR injured rats injected with PBS, hNP, nor hNP+MK2i. Since not all tibial compressions resulted in a complete ACL tear, these results were not conclusive as to the effect of the therapeutic due to small sample sizes. The NIACLR showed that the medial femoral condyle (MFC) and lateral femoral condyle (LFC) were more damaged than the medial tibial plateau (MTP) and lateral tibial plateau (LTP), Figure 4.4. Of the joints with confirmed ACL tears, there was a drastic increase in articular cartilage degradation compared to the contralateral, though the sample numbers are too low to draw statistical conclusions.

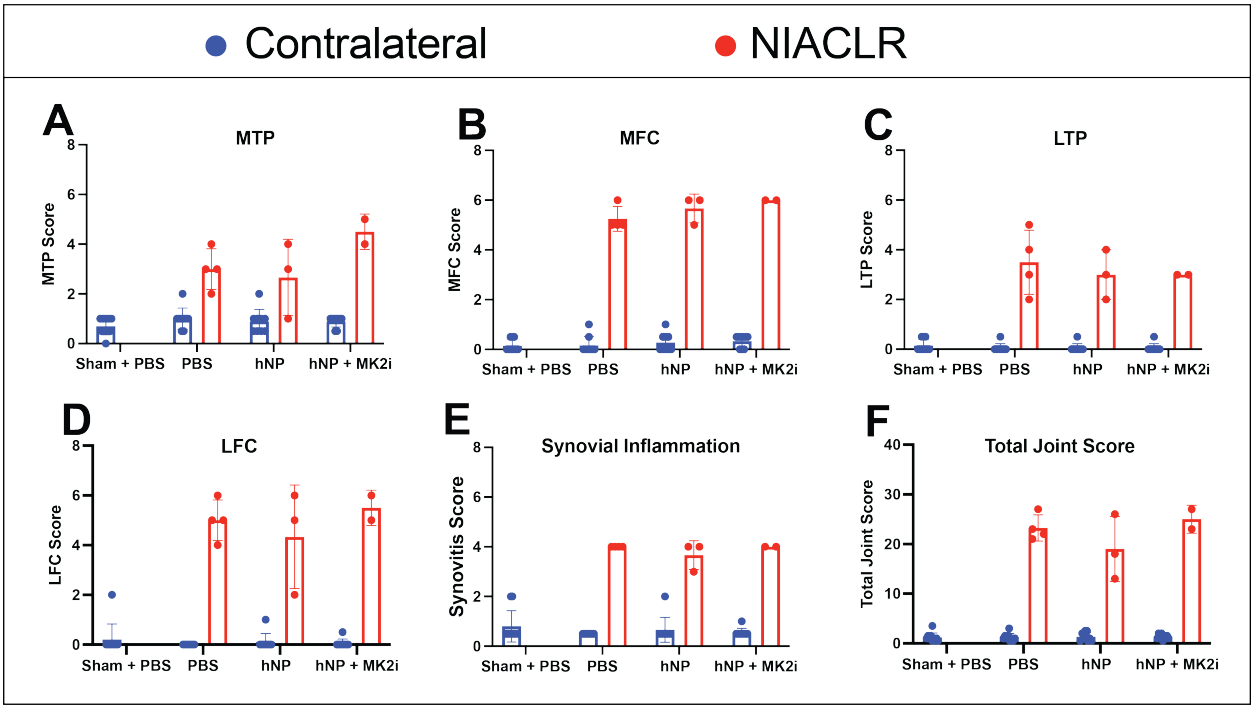

Figure 4.4: Histological results of (blue) contralateral and (red) NIACLR rats 4 weeks after injury and injection. (A) MTP, (B) MFC, (C) synovial inflammation, (D) LTP, (E) LFC, and (F) total joint score. Data from confirmed ACL tears only. Complete ACL tears resulted in articular cartilage damage.

4.4.5 Micro-computed Topography

There was no apparent difference in trabecular bone remodeling between contralateral and NIACRL groups. No difference was observed in BT/TV, Tb. N, and Tb. Sp. between NIACLR and contralateral joints nor treatment groups, Figure 4.5. However, there was a trend in decrease in BV/TV in NIACLR joints compared to contralateral, Figure 4.5C.

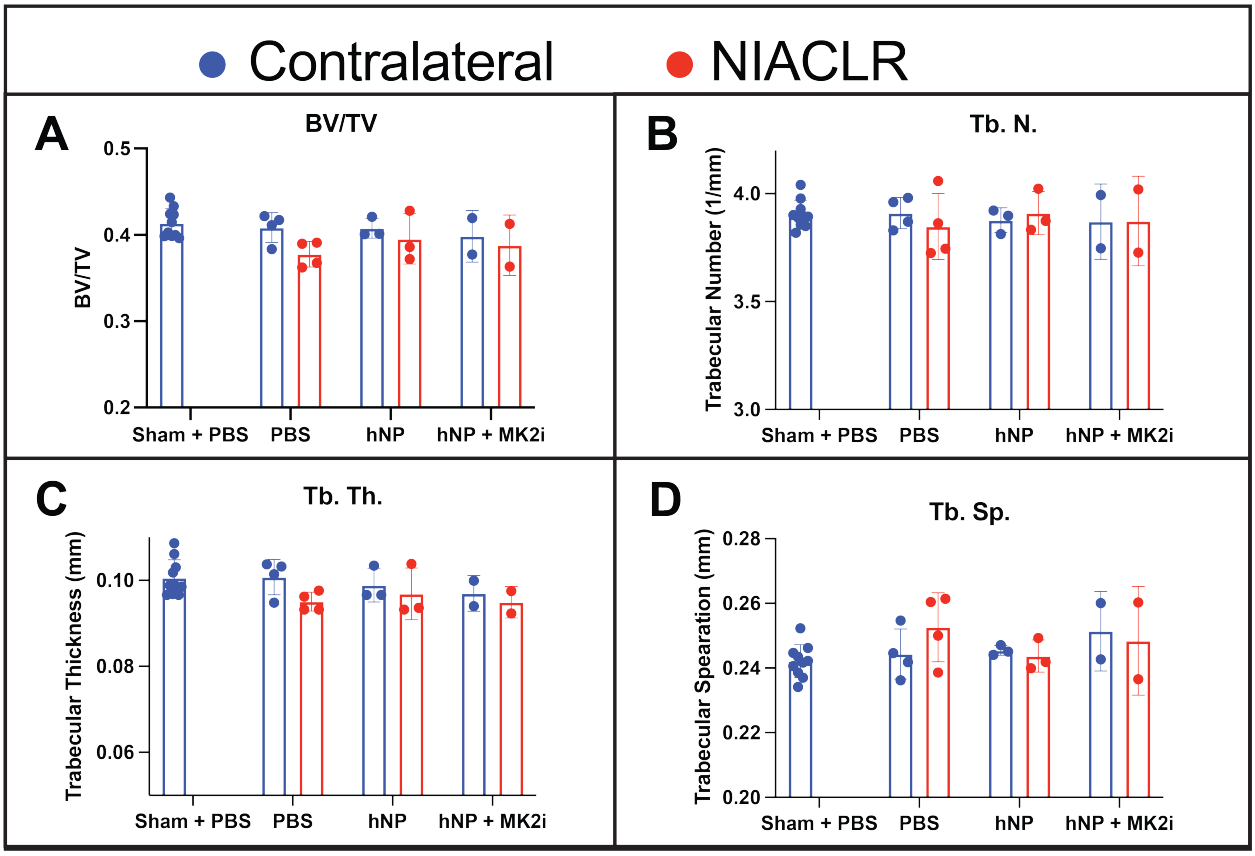

Figure 4.5: μCT of the femoral condyles follow NIACLR and intra-articular injection. Data from confirmed ACL tears only. There are no significant differences between the contralateral and NIACLR knees.

4.5 Discussion

Localized delivery of biocompatible therapeutics into damaged joints could inhibit inflammation without causing chondrocyte death, and prevent the progression of PTOA. The

MK2i peptide was shown to inhibit MK2 phosphorylation downstream of MAPK p38 and reduce inflammatory cytokine expression[36]. However, peptides are susceptible to proteolytic degradation and low stability. Poly(NIPAm-co-AMPS-BAC-AAc) nanoparticles were able to encapsulate MK2i and allowed for its sustained release *ex situ*, and previous studies showed the ability of MK2i to inhibit IL-6 production *in vitro* using bovine derived chondrocytes[37]. NIPAm has a lower critical solution temperature (LCST) of 32°C. Below the LCST of NIPAm, the particle swells, and above the LCST it constricts, giving it thermoresponsive behavior. Loading MK2i below the LCST of NIPAm led to 2.5 times more drug loading than when loaded above the LCST[37]. Furthermore, nanoparticles over 200 nm have been shown to initiate an immune response[38]. When the particles were at physiological temperatures, above the LCST of NIPAm, they were below 200 nm and should not initiate an immune response due to size. Here, we aimed to examine the efficacy of MK2i loaded hNPs for inhibiting the progression of PTOA using an *in vivo* small animal model.

The use of charged nanoparticles has been shown to increase the residence time of therapeutics in cartilage[39]. The anionic hNPsRBITC intra-articularly injected into non-injured knees remained in the joint for 7 days and showed the ability of our therapeutics to be accurately injected into the joint, and agreed with previous studies[37]. The injury itself and potential disruption to the joint capsule did not appear to contribute to loss of hNPsRBITC since contralateral and NIACRL retention were similar through Day 3. However, tibial compression of the joint caused the hNPsRBITC particles to be cleared 4 — 7 days after the procedure. Joint matrix turnover is increased following acute injury[40], and may be responsible for the decreased retention time of hNPsRBITC injected into the knees that underwent tibial compression.

The development of PTOA may be as high as 90% following an ACL tear[23]. Rupturing the ACL using a tibial compression was found to be physiological relevant and significantly induce PTOA compared to surgical transection of the ACL[3,25]. Previous work showed the NIACLR and the ACL transection model had analogous trabecular bone remodeling and

proteoglycan loss, as well as more observed damage to the MFC and LFC compared to the MTP and LTP[23–25]. Brown et al noted medial osteophyte formation following NIACLR was less severe than the surgical transection model, and argued they were more similar in size to typical human osteophytes relative to the size of the joint[3,41]. While the NIACLR model has been proven to induce PTOA, our model needs to be further developed to consistently result in complete ACL tears.

The histology and μCT data presented only consisted of rats where a complete ACL tear was confirmed by a trained veterinary pathologist. Here, we saw a trend of increased cartilage damage and synovial inflammation following complete ACL tear. These data suggested tibial compressions resulted in the development of PTOA when a complete tear occurs. Notably, the joints that underwent NIACLR resulted in more cartilage damage on the MFC and LFC compared to the MTP and LTP, and is consistent with other NIACLR and ACL transection models[25]. The μCT data did not show any differences between the contralateral and NIACLR joints. Previous studies showed no significant change in BV/TV nor Tb.Sp. for the epiphysis 4 weeks after injury compared to the control. However, the other models showed had a significant decrease in Tb.N. and a significant increase in Tb.Th. 4 weeks after injury[24]. Here we saw no change in Tb.Sp. 4 weeks after injury. Moreover, the BV/TV and Tb.Th. slightly decreased in the injured knee compared to the contralateral. Loss in BV/TV was expected and shows bone loss following injury. However, there wasn't a change with Tb.N. between NIACLR and contralateral joints, Figure 4.5B. Further work is needed to develop our NIACLR model to consistently tear the ACL of rats.

The results of the study with respect to treatment efficacy were inconclusive as not all rats that underwent tibial compression resulted in a complete ACL tear, which led to low sample numbers per group. Due to the lack of successful ACL tears, we were not able to determine the efficacy of the MK2i loaded hNP for inhibiting the progression of PTOA.

Previous studies using mice that underwent NIACLR showed a 11.7% increase in range of motion (ROM) compared to contralateral limb after tibial compressions that resulted in an

ACL tear. Future research will examine the joint ROM following tibial compression to assess ACL tear, and rats will undergo subsequent tibial compressions until a successful ACL tear is confirmed. Studies have shown that not all ACLs rupture after a single tibial compression and multiple compressions may be necessary to successful tear the ACL[3]. No significant difference was reported between ACLs torn with single tibial compressions and ACLs torn with multiple tibial compressions3. Multiple tibial compressions may be required in future studies to successfully tear the ACL using the NIACLR model.

4.6 Conclusion

In this study we aimed to assess the efficacy of MK2i loaded hNPs to inhibit the progression of PTOA. However, these data are inconclusive since not all rats had a complete ACL tear following tibial compression. Of the successful injuries, our data closely aligned with trends previously published where the MFC and LFC had a greater degree of cartilage damage than the MTP and LTP following NIACLR[24,25]. Future studies will require a developed NIACLR model to produce complete ACL tears and be confirmed by increased joint ROM. After the model is confirmed, the study would need to be repeated to assess the ability of MK2i loaded hNPs to inhibit the development of PTOA following ACL tear.

4.7 Acknowledgements

Thank you to Dr. Tristian Maerz and Dr. Kevin Baker for their help with NIACLR work.

References

1. Brown, T. D., Johnston, R. C., Saltzman, C. L., Marsh, J. L. & Buckwalter, J. A. Posttraumatic osteoarthritis: a first estimate of incidence, prevalence, and burden of disease. *Journal of orthopaedic trauma* **20,** 739–744 (2006).

2. Carbone, A. & Rodeo, S. Review of current understanding of post-traumatic osteoarthritis resulting from sports injuries. *Journal of orthopaedic research* **35,** 397–405 (2017).

3. Brown, S. B. *et al.* Characterization of post-traumatic osteoarthritis in rats following anterior cruciate ligament rupture by non-invasive knee injury (NIKI). *Journal of Orthopaedic Research®* **38,** 356–367 (2020).

4. Mort, J. S. & Billington, C. J. Articular cartilage and changes in arthritis matrix degradation. *Arthritis Research* **3,** 337–341. ISSN: 14659905 (2001).

5. Bondeson, J., Wainwright, S., Hughes, C. & Caterson, B. The regulation of the ADAMTS4 and ADAMTS5 aggrecanases in osteoarthritis: A review. *Clinical and Experimental Rheumatology* **26,** 139–145. ISSN: 0392856X (2008).

6. Klatt, A. R. *et al.* A critical role for collagen II in cartilage matrix degradation: collagen II induces pro-inflammatory cytokines and MMPs in primary human chondrocytes. *Journal of orthopaedic research* **27,** 65–70 (2009).

7. Troeberg, L. & Nagase, H. Proteases involved in cartilage matrix degradation in osteoarthritis. *Biochimica et Biophysica Acta (BBA)-Proteins and Proteomics* **1824,** 133–145 (2012).

8. Tortorella, M. D. *et al.* Sites of aggrecan cleavage by recombinant human aggrecanase-1 (ADAMTS-4). *Journal of Biological Chemistry* **275,** 18566–18573 (2000).

9. Roughley, P. J. & Mort, J. S. The role of aggrecan in normal and osteoarthritic cartilage. *Journal of experimental orthopaedics* **1,** 1–11 (2014).

10. Yamamoto, K., Wilkinson, D. & Bou-Gharios, G. Targeting dysregulation of metalloproteinase activity in osteoarthritis. *Calcified Tissue International,* 1–14 (2020).

11. Ohno, S., Im, H.-J., Knudson, C. B. & Knudson, W. Hyaluronan oligosaccharide–induced activation of transcription factors in bovine articular chondrocytes. *Arthritis & Rheumatism* **52,** 800–809 (2005).

12. Man, G. & Mologhianu, G. Osteoarthritis pathogenesis–a complex process that involves the entire joint. *Journal of medicine and life* **7,** 37 (2014).

13. Xia, B. *et al.* Activatable Cell-Penetrating Peptide Conjugated Polymeric Nanoparticles with Gd-Chelation and Aggregation-Induced Emission for Bimodal MR and Fluorescence Imaging of Tumors. *ACS Applied Bio Materials* **3,** 1394–1405. ISSN: 25766422 (2020).

14. Dare, D. & Rodeo, S. Mechanisms of post-traumatic osteoarthritis after ACL injury. *Current rheumatology reports* **16,** 1–5 (2014).

15. Janusz, M. J. *et al.* Moderation of iodoacetate-induced experimental osteoarthritis in rats by matrix metalloproteinase inhibitors. *Osteoarthritis and Cartilage* **9,** 751–760. ISSN: 10634584 (2001).

16. Guzman, R. E., Evans, M. G., Bove, S., Morenko, B. & Kilgore, K. Mono-Iodoacetate-Induced Histologic Changes in Subchondral Bone and Articular Cartilage of Rat Femorotibial Joints: AN Animal Model of Osteoarthritis. *Toxicologic Pathology* **31,** 619–624. ISSN: 01926233 (2003).

17. Daans, M., Luyten, F. P. & Lories, R. J. GDF5 deficiency in mice is associated with instability-driven joint damage, gait and subchondral bone changes. *Annals of the Rheumatic Diseases* **70,** 208–213. ISSN: 00034967 (2011).

18. Guilak, F., Ratcliffe, A., Lane, N., Rosenwasser, M. P. & Mow, V. C. Mechanical and biochemical changes in the superficial zone of articular cartilage in canine experimental osteoarthritis. *Journal of Orthopaedic Research* **12,** 474–484. ISSN: 1554527X (1994).

19. Faust, H. J. *et al.* A hyaluronic acid binding peptide-polymer system for treating osteoarthritis. *Biomaterials* **183,** 93–101. ISSN: 18785905 (2018).

20. Hashimoto, S. *et al.* Development and regulation of osteophyte formation during experimental osteoarthritis. *Osteoarthritis and Cartilage* **10,** 180–187. ISSN: 10634584 (2002).

21. Gregory, M. H. *et al.* A Review of Translational Animal Models for Knee Osteoarthritis. *Arthritis* **2012,** 1–14. ISSN: 2090-1984 (2012).

22. Kapoor, M., Martel-Pelletier, J., Lajeunesse, D., Pelletier, J. P. & Fahmi, H. Role of proinflammatory cytokines in the pathophysiology of osteoarthritis. *Nature Reviews Rheumatology* **7,** 33–42. ISSN: 17594790 (2011).

23. Maerz, T. *et al.* Biomechanical Characterization of a Model of Noninvasive, Traumatic Anterior Cruciate Ligament Injury in the Rat. *Annals of Biomedical Engineering* **43,** 2467–2476. ISSN: 15739686 (2015).

24. Maerz, T. *et al.* Subchondral and epiphyseal bone remodeling following surgical transection and noninvasive rupture of the anterior cruciate ligament as models of post-traumatic osteoarthritis. *Osteoarthritis and Cartilage* **24,** 698–708. ISSN: 15229653. http://dx.doi.org/10.1016/j.joca.2015.11.005 (2016).

25. Maerz, T. *et al.* Articular cartilage degeneration following anterior cruciate ligament injury: a comparison of surgical transection and noninvasive rupture as preclinical models of post-traumatic osteoarthritis. *Osteoarthritis and Cartilage* **24,** 1918–1927. ISSN: 15229653. http://dx.doi.org/10.1016/j.joca.2016.06.013 (2016).

26. Gislason, G. H. *et al.* Increased Mortality and Cardiovascular Morbidity Associated With Use of Nonsteroidal Anti-inflammatory Drugs in Chronic Heart Failure. *Arch. Intern Med.* **169,** 141–149 (2009).

27. Lee, A., Mg, C., Jc, C., Jf, K. & Jp, K. Effects of nonsteroidal anti-inflammatory drugs on postoperative renal function in adults with normal renal function (Review) (2007).

28. Rostom, A. *et al.* Prevention of NSAID-induced gastroduodenal ulcers (Review) (2011).

29. Bhala, N. *et al.* Vascular and upper gastrointestinal effects of non-steroidal anti-infl ammatory drugs : meta-analyses of individual. *The Lancet* **382,** 769–779. ISSN: 0140-6736 (2013).

30. Katz, J. N., Arant, K. R. & Loeser, R. F. Diagnosis and Treatment of Hip and Knee Osteoarthritis: A Review. *JAMA - Journal of the American Medical Association* **325,** 568–578. ISSN: 15383598 (2021).

31. Mora, J. C., Przkora, R. & Cruz-almeida, Y. Knee osteoarthritis : pathophysiology and current treatment modalities, 2189–2196 (2018).

32. Zompra, A. A., Galanis, A. S., Werbitzky, O. & Albericio, F. Manufacturing peptides as active pharmaceutical ingredients. *Future Medicinal Chemistry* **1,** 361–377. ISSN: 17568919 (2009).

33. Lalatsa, A., Schatzlein, A. G. & Uchegbu, I. F. Strategies to deliver peptide drugs to the brain. *Molecular Pharmaceutics* **11,** 1081–1093. ISSN: 15438392 (2014).

34. Lau, J. L. & Dunn, M. K. Therapeutic peptides: Historical perspectives, current development trends, and future directions. *Bioorganic and Medicinal Chemistry* **26,** 2700–2707. ISSN: 14643391. https://doi.org/10.1016/j.bmc.2017.06.052 (2018).

35. Jin Jeong, W. *et al.* Peptide–nanoparticle conjugates: a next generation of diagnostic and therapeutic platforms? *Nano Convergence* **5,** 1–18. ISSN: 21965404. https://doi.org/10.1186/s40580-018-0170-1 (2018).

36. Ward, B., Seal, B. L., Brophy, C. M. & Panitch, A. Design of a bioactive cell-penetrating peptide: When a transduction domain does more than transduce. *Journal of Peptide Science* **15,** 668–674. ISSN: 10752617. arXiv: NIHMS150003 (2009).

37. Deloney, M., Smart, K., Christiansen, B. A. & Panitch, A. Thermoresponsive, hollow, degradable core-shell nanoparticles for intra-articular delivery of anti-inflammatory peptide. *Journal of Controlled Release* **323,** 47–58. ISSN: 18734995. https://doi.org/10.1016/j.jconrel.2020.04.007 (2020).

38. García-Couce, J. *et al.* Targeting Polymeric Nanobiomaterials as a Platform for Cartilage Tissue Engineering. *Current Pharmaceutical Design* **25,** 1–18. ISSN: 13816128. http://www.eurekaselect.com/173321/article (2019).

39. Morgen, M. *et al.* Nanoparticles for improved local retention after intra-articular injection into the knee joint. *Pharmaceutical Research* **30,** 257–268. ISSN: 07248741 (2013).

40. Catterall, J. B., Stabler, T. V., Flannery, C. R. & Kraus, V. B. Changes in serum and synovial fluid biomarkers after acute injury (NCT00332254). *Arthritis Research and Therapy* **12,** R229. ISSN: 14786354. http://arthritis-research.com/content/12/6/R229 (2010).

41. Lützner, J., Kasten, P., Günther, K.-P. & Kirschner, S. Surgical options for patients with osteoarthritis of the knee. *Nature Reviews Rheumatology* **5,** 309–316 (2009).

CHAPTER V

Summary & Future Directions

5.1 Conclusion

The collection of data within this dissertation represents work aimed to develop therapeutics to prevent the progression of post traumatic osteoarthritis (PTOA) by inhibiting inflammation and treating damaged articular cartilage. This work resulted in a degradable hollow nanoparticle (hNP) capable of being modified into two nanoparticle-peptide therapeutics. The first loaded an anti-inflammatory MK2 inhibiting (MK2i) peptide shown to reduce inflammatory cytokine expression *in vitro*. The second utilized the hyaluronic acid (HA)-binding peptide, GAH, conjugated to the hNP and restored the compressive strength of articular cartilage while also inhibiting further ECM degradation. Finally, the efficacy of the MK2i loaded hNPs were assessed in a pilot small animal *in vivo* PTOA model. The results of the *in vivo* study were inconclusive and it showed our non-invasive anterior cruciate ligament (ACL) rupture (NIACLR) model needed to be further developed. However, it also showed that when ACL rupture occurred did result in the generation of PTOA.

Nanoparticles to treat OA are a growing field of study within nanomedicine. Nanoparticles made from lipids, metals, and polymers used in OA research have varying degrees of utility, each with specific benefits compared to others. Lipid-based nanoparticles are used in the delivery of small molecule drugs into the joint to inhibit inflammation[1–5]. Metal nanoparticles are used to diagnose OA[6–8], image the joint[7], and counteract reactive oxidative species produced during OA[9,10]. Polymeric nanoparticles (PNPs) have been used to load nucleic acids[11,12], plasmid DNA-cytokine modifiers[13–15], and peptides[16–18] to inhibit inflammation and slow the progression of OA. Here, we developed degradable, polymeric, hollow nanoparticles (hNPs) to encapsulate the MK2i peptide YARA (Chapter 2) and conjugated

the HA-binding peptide GAH to the hNP (Chapter 3). Finally, the MK2i loaded hNP (MK2i + hNP) was tested in a small animal *in vivo* study (Chapter 4).

Chapter 2 detailed the synthesis and development of thermoresponsive, degradable hNPs and examined the relationship between crosslink density and the ability of hNPs to load and release the MK2i peptide YARA. The physical characteristics, such as diameter, zeta-potential, and polydispersity of the hNPs with varying crosslinked density were also measured. Increasing the crosslink density in hNPs decreased the diameter of the particle. The hNPs displayed a greater degree of swelling below the lower critical solution temperature (LCST) of poly(N-isopropyl acrylamide) (pNIPAm) than analogously crosslinked solid nanoparticles (sNPs). Both hNPs and sNPs loaded roughly 2.5 times more MK2i when swollen below the LCST than when constricted above the LCST, and demonstrated the benefit of using pNIPAm based NPs. Furthermore, the hNPs released significantly more MK2i than the analogously crosslinked sNPs after 5 days. The hNPs were endocytosed and degraded from primary derived bovine chondrocytes in 5 - 7 days *in vitro*. As shown by *in vivo* imaging, hNPs were accurately injected into the joint and remained there for 7 days. Finally, all MK2i loaded hNPs inhibited inflammation, as measured by normalized IL-6 expression two days after treatment. Notably, only the 1x crosslinked hNP loaded with MK2i reduced IL-6 production four days after a single treatment. The MK2i-loaded hNPs were able to inhibit inflammation *in vitro* and showed promise in preventing the progression of PTOA.

Chapter 3 showed the ability of the hNPs to be functionalized with tissue-specific peptides using the acrylic acid (AAc) monomer polymerized within the shell of the particles. Increasing the molar ratio of peptide to AAc increased peptide conjugation to the hNP. Specifically, we used the HA-binding peptide GAH to generate the GAH-hNP therapeutic. The 19 GAH-hNP therapeutic was able to significantly bind to HA, as measured by changes in dynamic viscosity upon its addition. Both the unconjugated hNP and GAH conjugated hNP penetrated into aggrecan-depleted cartilage explants, while they remained on the sur-

face of healthy articular cartilage. The 19 GAH-hNP significantly restored the compressive strength of aggrecan-depleted cartilage to healthy levels for at least 6 days after treatment. Moreover, Safranin O and Fast Green staining and immunohistochemistry for collagen type II showed 19 GAH-hNP inhibited further ECM degradation and may support cartilage regeneration. Treatment with 19 GAH-hNP is a promising therapeutic to inhibit the progression of PTOA.

The efficacy of MK2i loaded hNPs and unloaded hNPs were tested in a small animal PTOA model detailed in Chapter 4. Rats underwent tibial compressions to non-invasively rupture their ACL. Previously, the NIACLR model was characterized in rats as a reproducible and physiologically relevant method that resulted in PTOA[19,20]. However, our results were inconclusive as not all injuries resulted in complete ACL tears. Furthermore, hNPsRBITC injected into the joint space of NIACLR rats remained within the knee 3 days following injury rather than 7 days in non-injured knees. While our results were inconclusive due to low sample numbers, the injuries with successful ACL tears closely aligned trends of previously developed models[20,21]. These results suggest further work is needed to develop our NIACLR model, and that a second dose of therapeutic may inhibit the progression of PTOA.

The work described within this dissertation shows the promise in using MK2i loaded degradable hNPs to inhibit inflammation and GAH conjugated hNPs to restore the compressive strength to aggrecan-depleted cartilage and inhibit the progression of PTOA.

5.2 Future Directions

The hNPs developed here could be transitioned to treat other diseases and conditions. In addition to inhibiting inflammation, MK2i previously demonstrated the ability to prevent abdominal adhesion[22], inhibit pulmonary fibrosis[23], and limit intimal hyperplasia after vein graft bypass[24]; future work using MK2i loaded hNPs could be used to treat these conditions. The efficacy of the therapeutics could also be examined to treat OA, as the GAH-hNPs may

restore functionality to damaged cartilage and allow for ECM repair. The release of MK2i from hNPs in this study was limited to a non-degrading environment and future research will characterize the release of MK2i from hNPs in a degrading model, and will assess the size of the hNP fragments using size exclusion chromatography. Additionally, the ability of the hNPs to be functionalized with peptides is not limited to HA-binding peptides. These chemistries could be used to conjugate peptides to the surface of the hNP that are specific to other ECM components and further translated to numerous disease models without altering the nanoparticle synthesis.

Future work will continue the small animal study to generate a model to reproducibly induce an ALC rupture in rats, and treat the joint with the dual 19 GAH-hNP loaded with MK2i (19 GAH-hNP + MK2i). Preliminary work combined the GAH conjugated hNPs with MK2i, which had analogous MK2i loading and release profiles as the unconjugated hNP. Treatment of NIACLR rats with the 19 GAH-hNP + MK2i could inhibit inflammation following injury and treat the damaged cartilage. Additionally, treating the injured joint with a second dose of MK2i loaded hNP (hNP + MK2i) or 19 GAH-hNP + MK2i could be advantageous as the particles were shown to be cleared from the joint 4-7 days following the injury. This study would also benefit from examining inflammation 24-36 hours after joint injury to assess the utility of MK2i to inhibit inflammatory cytokine production.

The hNPs described here are anionic and currently proven to load cationic peptides. Future iterations of these particles will explore altering the synthesis and replacing the anionic sulfated monomer, 2-acrylamido-2-methyl-1-propanesulfonic acid (AMPS) polymerized within the polymer shell with a cationic monomer, such as (3-Acrylamidopropyl)trimethylammonium chloride (APTMA), 2-Aminoethylmethacrylamide hydrochloride (AEMAAHCl), N-[3-(Dimethylamino)pro (DMAPMAm), or 2-(Dimethylamino)ethyl methacrylate (DMAEMA). Incorporating a cationic monomer within the shell of the nanoparticle could enable anionic therapeutics to be loaded and released from the hNPs.

References

1. Koning, G. A. *et al.* Targeting of angiogenic endothelial cells at sites of inflammation by dexamethasone phosphate-containing RGD peptide liposomes inhibits experimental arthritis. *Arthritis and Rheumatism* **54,** 1198–1208. ISSN: 00043591 (2006).

2. Vanniasinghe, A. S., Bender, V. & Manolios, N. The Potential of Liposomal Drug Delivery for the Treatment of Inflammatory Arthritis. *Seminars in Arthritis and Rheumatism* **39,** 182–196. ISSN: 00490172. http://dx.doi.org/10.1016/j.semarthrit.2008.08.004 (2009).

3. Dong, J. *et al.* Intra-articular delivery of liposomal celecoxib-hyaluronate combination for the treatment of osteoarthritis in rabbit model. *International Journal of Pharmaceutics* **441,** 285–290. ISSN: 03785173. http://dx.doi.org/10.1016/j.ijpharm.2012.11.031 (2013).

4. Cipollaro, L. *et al.* Liposomes for intra-articular analgesic drug delivery in orthopedics: State-of-art and future perspectives. insights from a systematic mini-review of the literature. *Medicina (Lithuania)* **56,** 1–17. ISSN: 16489144 (2020).

5. Corciulo, C. *et al.* Intraarticular injection of liposomal adenosine reduces cartilage damage in established murine and rat models of osteoarthritis. *Scientific Reports* **10,** 1–16. ISSN: 20452322. https://doi.org/10.1038/s41598-020-68302-w (2020).

6. Eichaker, L. R., Cho, H., Duvall, C. L., Werfel, T. A. & Hasty, K. A. Future nanomedicine for the diagnosis and treatment of osteoarthritis. *Nanomedicine* **9,** 2203–2215. ISSN: 17486963 (2014).

7. Xie, M. *et al.* Intra-articular tracking of adipose-derived stem cells by chitosan-conjugated iron oxide nanoparticles in a rat osteoarthritis model. *RSC Advances* **9,** 12010–12019. ISSN: 20462069 (2019).

8. Peng, S. *et al.* Detection of ADAMTS-4 activity using a fluorogenic peptide-conjugated Au nanoparticle probe in human knee synovial fluid. *ACS Applied Materials and Interfaces* **5,** 6089–6096. ISSN: 19448244 (2013).

9. Kumar, S., Adjei, I. M., Brown, S. B., Liseth, O. & Sharma, B. Manganese dioxide nanoparticles protect cartilage from inflammation-induced oxidative stress. *Biomaterials* **224,** 119467. ISSN: 18785905. `https://doi.org/10.1016/j.biomaterials.2019.119467` (2019).

10. Leonavičiene, L. *et al.* Effect of gold nanoparticles in the treatment of established collagen arthritis in rats. *Medicina (Lithuania)* **48,** 91–101. ISSN: 1010660X (2012).

11. Shin, H. J. *et al.* p47phox siRNA-loaded PLGA nanoparticles suppress ROS/oxidative stress-induced chondrocyte damage in osteoarthritis. *Polymers* **12,** 1–14. ISSN: 20734360 (2020).

12. Shin, H. J. *et al.* p66shc siRNA nanoparticles ameliorate chondrocytic mitochondrial dysfunction in osteoarthritis. *International Journal of Nanomedicine* **15,** 2379–2390. ISSN: 11782013 (2020).

13. Zhou, P. H. *et al.* Chondroprotective effects of hyaluronic acid-chitosan nanoparticles containing plasmid DNA encoding cytokine response modifier A in a rat knee osteoarthritis model. *Cellular Physiology and Biochemistry* **47,** 1207–1216. ISSN: 14219778 (2018).

14. Jin, G. Z. Current nanoparticle-based technologies for osteoarthritis therapy. *Nanomaterials* **10,** 1–20. ISSN: 20794991 (2020).

15. Viral inhibition of inflammation: Cowpox virus encodes an inhibitor of the interleukin-1β converting enzyme. *Cell* **69,** 597–604. ISSN: 00928674 (1992).

16. McMasters, J., Poh, S., Lin, J. & Panitch, A. Delivery of anti-inflammatory peptides from hollow PEGylated poly (NIPAM) nanoparticles reduces inflammation in an ex vivo osteoarthritis model. *Journal of Controlled Release* **258,** 161–170. ISSN: 23265205.

arXiv: NIHMS150003. http://dx.doi.org/10.1016/j.joca.2009.10.007%20http://dx.doi.org/10.1016/j.jconrel.2017.05.008%20http://dx.doi.org/10.1016/j.joca.2010.12.013%20http://www.nature.com/doifinder/10.1038/nprot.2013.152 (2011).

17. Poh, S., Lin, J. B. & Panitch, A. Release of Anti-inflammatory Peptides from Thermosensitive Nanoparticles with Degradable Cross-Links Suppresses Pro-inflammatory Cytokine Production. *Biomacromolecules* **16,** 1191–1200. ISSN: 15264602 (2015).

18. Lin, J. B., Poh, S. & Panitch, A. Controlled release of anti-inflammatory peptides from reducible thermosensitive nanoparticles suppresses cartilage inflammation. *Nanomedicine: Nanotechnology, Biology and Medicine* **12,** 2095–2100. ISSN: 15499634. http://linkinghub.elsevier.com/retrieve/pii/S1549963416300570 (2016).

19. Maerz, T. *et al.* Biomechanical Characterization of a Model of Noninvasive, Traumatic Anterior Cruciate Ligament Injury in the Rat. *Annals of Biomedical Engineering* **43,** 2467–2476. ISSN: 15739686 (2015).

20. Brown, S. B. *et al.* Characterization of Post-Traumatic Osteoarthritis in Rats Following Anterior Cruciate Ligament Rupture by Non-Invasive Knee Injury (NIKI). *Journal of Orthopaedic Research* **38,** 356–367. ISSN: 1554527X. http://dx.doi.org/10.1002/jor.24470 (2020).

21. Maerz, T. *et al.* Subchondral and epiphyseal bone remodeling following surgical transection and noninvasive rupture of the anterior cruciate ligament as models of post-traumatic osteoarthritis. *Osteoarthritis and Cartilage* **24,** 698–708. ISSN: 15229653. http://dx.doi.org/10.1016/j.joca.2015.11.005 (2016).

22. Ward, B. C., Kavalukas, S., Brugnano, J., Barbul, A. & Panitch, A. Peptide inhibitors of MK2 show promise for inhibition of abdominal adhesions. *Journal of Surgical Research* **169,** e27–e36. ISSN: 00224804. http://dx.doi.org/10.1016/j.jss.2011.01.043 (2011).

23. Vittal, R. *et al.* Peptide-mediated inhibition of mitogen-activated protein kinase-activated protein kinase-2 ameliorates bleomycin-induced pulmonary fibrosis. *American Journal of Respiratory Cell and Molecular Biology* **49,** 47–57. ISSN: 10441549 (2013).

24. Muto, A. *et al.* Inhibition of Mitogen Activated Protein Kinase Activated Protein Kinase II with MMI-0100 reduces intimal hyperplasia ex vivo and in vivo. *Vascular pharmacology* **56,** 47–55 (2012).